

**Development of Glass Ionomer Cements with  
Improved Mechanical and Remineralizing Properties  
by Incorporation of 45S5 Bioglass<sup>®</sup>-Ceramic**

Alireza Zandi Karimi

A Thesis

In the Department

of

Mechanical, Industrial and Aerospace Engineering

Presented in Partial Fulfillment of the Requirements

For the Degree of

Doctor of Philosophy (Mechanical Engineering) at

Concordia University

Montreal, Quebec, Canada

November 2019

© Alireza Zandi Karimi, 2019

**CONCORDIA UNIVERSITY**  
**SCHOOL OF GRADUATE STUDIES**

This is to certify that the thesis prepared

By:                   Alireza Zandi Karimi

Entitled:           Development of glass ionomer cements with improved mechanical and remineralizing properties by incorporation of 45S5 Bioglass<sup>®</sup>-ceramic

and submitted in partial fulfillment of the requirements for the degree of

Doctor Of Philosophy (Mechanical Engineering)

complies with the regulations of the University and meets the accepted standards with respect to originality and quality.

Signed by the final examining committee:

_____	Chair
Dr. Catherine Mulligan	
_____	External Examiner
Dr. Mohammad Jahazi	
_____	External to Program
Dr. Michelle Nokken	
_____	Examiner
Dr. Martin Pugh	
_____	Examiner
Dr. Mamoun Medraj	
_____	Thesis Supervisor
Dr. Robin Drew	

Approved by \_\_\_\_\_  
Dr. Ivan Contreras, Graduate Program Director

December 19, 2019

\_\_\_\_\_  
Dr. Amir Asif, Dean  
Gina Cody School of Engineering & Computer Science

## **ABSTRACT**

### **Development of Glass Ionomer Cements with Improved Mechanical and Remineralizing Properties by Incorporation of 45S5 Bioglass<sup>®</sup>-Ceramic**

**Alireza Zandi Karimi, Ph.D.**

**Concordia University, 2019**

Despite significant efforts to improve the clinical performance (e.g. mechanical and remineralizing properties) of glass ionomer cements (GICs), their essential characteristics such as proper translucency, adhesion to enamel and dentine, and fluoride-releasing capability cannot yet be fully exploited in load-bearing areas in restorative dentistry. The aim of this study is to introduce a functional approach to improve not only the mechanical properties of GICs, but also to enhance their biomineralizing capacity.

In the first stage of this study, a series of versatile heat treatment profiles are used to tailor the crystallinity of 45S5 Bioglass<sup>®</sup> within a wide range of 5% to 100% via the formation of solely combeite as a mechanically competent yet bioactive phase. The resulting 45S5 glass-ceramics containing combeite not only are expected to retain beneficial levels of bioactivity, but also show improved mechanical properties compared to those of the amorphous 45S5 Bioglass<sup>®</sup>. By choosing the proper heat treatment from the proposed profiles in this study, different levels of mechanical properties and bioactivity in Bioglass<sup>®</sup> can be achieved according to the target application(s).

In the second stage of this study, hybrid GICs with enhanced mechanical and remineralizing properties were developed via incorporation of an optimum amount (5 wt%) of 45S5 Bioglass<sup>®</sup>-ceramic particles with a certain degree of crystallinity. The effect of the degree of crystallinity of additives, which is completely overlooked in the current literature, was also addressed in this study. Mechanical properties testing, in vitro studies and microstructural analysis

revealed that the Bioglass<sup>®</sup>-ceramic particles with 74% crystallinity best act as both remineralizing and reinforcing agents. Enhanced remineralizing and mechanical properties may not only broaden the hybrid GICs' clinical applications but also can potentially enhance their in vivo performance.

In the last stage of this study, a novel aluminum-free, 45S5 Bioglass<sup>®</sup>-based GIC with standard mechanical properties was produced. For the first time, 45S5 Bioglass<sup>®</sup> and its Bioglass<sup>®</sup>-ceramic were used as the GIC solid component. The Bioglass<sup>®</sup>-ceramic particles with 74% crystallinity was used as they favorably act as both remineralizing and reinforcing agents. The early stage progression of setting reaction was monitored. Bimodal particle size distribution was shown to improve the packing density and integrity of the set cement. In such GICs, not only the neurotoxicity of Al is eliminated, but chemical bond formation at cement/hard tissue(s) interface through interfacial biomineralization and adhesion is expected.

## Acknowledgements

I would like to express the deepest appreciation and respect to my supervisor Dr. Robin Drew for his continuous trust, support and patience. He open-mindedly supervised me throughout my research with an encouraging attitude. His constant incentive and sincerity taught me to survive in the academic world and to remain authentic.

I would like to thank Dr. Robert Hill from Barts and The London School of Medicine and Dentistry for his generous donation of the Bioglass<sup>®</sup> powder used in this work. His insightful comments on the core idea behind this research are highly appreciated.


In the Mechanical, Industrial and Aerospace Engineering department I had great support. I would particularly like to thank Leslie Hosein and Arlene Zimmerman. I also want to thank Robert Oliver, Henry Szczawinski, Ahmad Omar Mostafa and Mazen Samara for their technical assistance.

I wish to thank my friends Ali Alem and Mohammad Sadegh Mahdipoor for their heartwarming and constant support.

In particular I owe my deepest gratitude to a great friend, a good mentor, and wonderful human being, Ehsan Rezabeigi. I cannot imagine finishing this journey without his encouragement and mentorship. He always believed in me and showed me that I can fly higher.

I am deeply grateful to my family for their unconditional support. I want to thank my mother, Marzieh, whose warmth always makes me feel comfortable and loved. I want to thank my father, Mehdi, who is my guide in the value of hard work and principled way of living. I want to thank my sister, Atieh, for blessing me with her kindness and gentle spirit. I want to thank my brother, Mohammadreza, who to me, is simply the embodiment of “hope”.

Above all, I would like to thank my better half, Leila; the one who understands and shares my “chaotic” side better than anyone else; the one who gave birth to my beautiful Jana and made this world a better place for me; the one who never gave up on me; and the one who made me realize that love is imperfect, raw, and real.

Dedicated to  
my mother,  
*Marzieh*,  
and all the  
courageous  
women of  
my country,  
  
Iran.

## Contributions of Authors

The main body of this thesis is composed of two articles which have already been published as well as one manuscript that is currently under review for publication. The already published journal articles are presented in their original format. The list of articles is provided below.

**Chapter 3:** A. Zandi Karimi, E. Rezabeigi, and R. A. L. Drew, “Crystallization behavior of combeite in 45S5 Bioglass<sup>®</sup> via controlled heat treatment,” *J. Non. Cryst. Solids*, vol. 502, pp. 176–183, 2018.

**Chapter 4:** A. Zandi Karimi, E. Rezabeigi, and R. A. L. Drew, “Glass ionomer cements with enhanced mechanical and remineralizing properties containing 45S5 bioglass-ceramic particles,” *J. Mech. Behav. Biomed. Mater.*, vol. 97, pp. 396–405, 2019.

**Chapter 5:** A. Zandi Karimi, E. Rezabeigi, and R. A. L. Drew, “Development of aluminum-free glass ionomer cements using 45S5 Bioglass<sup>®</sup> and its Bioglass<sup>®</sup>-ceramic”, *J. Adv. Eng. Mat.*, currently under review.

The experimental work of all these articles was performed by the author Alireza Zandi Karimi as a part of this PhD program. The first drafts of all articles were written by Alireza Zandi Karimi which was then reviewed and revised by Dr. Robin Drew and Dr. Ehsan Rezabeigi prior to submission. Dr. Robin Drew supervised this work during the entire research.

Also, parts of the preliminary results of this research have been accepted and orally presented in two conferences. They are not presented in this thesis as chapters, but mentioned in Appendix A.

# TABLE OF CONTENTS

List of Figures .....	xi
List of Tables.....	xvi
Abbreviations .....	xvii
<b>1 Chapter 1 .....</b>	<b>1</b>
1.1 Overview.....	1
1.2 Objectives.....	2
1.3 Thesis organization .....	2
<b>2 Chapter 2 .....</b>	<b>4</b>
2.1 Direct dental restorative materials .....	4
2.2 Glass ionomer cements .....	6
2.2.1 Physicochemical nature of GICs.....	7
2.2.2 Setting reaction .....	9
2.2.3 Role of water.....	13
2.2.4 Fluoride release.....	14
2.2.5 Adhesion to the tooth surface .....	16
2.2.6 Reinforcement methods .....	19
2.2.6.1 Fibers.....	20
2.2.6.2 Metallic powder .....	20
2.2.6.3 Hydroxyapatite.....	21
2.2.6.4 Bioactive glass particles.....	21
2.2.7 Atraumatic Restorative Treatment (ART) .....	22
2.2.8 Aluminum-free glass ionomer cements .....	23
2.3 Bioactive materials.....	23
2.3.1 Bioactive glasses and glass-ceramics.....	25
2.3.2 45S5 Bioglass® .....	28
2.3.2.1 Structure.....	29



2.3.2.2	Thermal behavior .....	30
2.3.2.3	45S5 Bioglass <sup>®</sup> -ceramic .....	31
<b>3</b>	<b>Chapter 3 .....</b>	<b>34</b>
3.1	Introduction .....	35
3.2	Materials and Methods.....	37
3.2.1	Materials .....	37
3.2.2	Heat treatment processes.....	37
3.2.3	Characterization .....	39
3.3	Results and discussion .....	40
3.3.1	Thermal analysis .....	40
3.3.1.1	Heat treatment design.....	45
3.3.2	Degree of crystallinity.....	46
3.3.3	Microstructures .....	50
3.4	Conclusion .....	52
<b>4</b>	<b>Chapter 4 .....</b>	<b>54</b>
4.1	Introduction.....	55
4.2	Materials and Methods.....	57
4.2.1	Bioglass <sup>®</sup> synthesis and heat treatment.....	57
4.2.2	Cement preparation.....	58
4.2.3	Mechanical testing .....	58
4.2.3.1	Compressive strength.....	59
4.2.3.2	Diametral tensile strength (DTS) .....	60
4.2.3.3	Microhardness.....	61
4.2.4	In vitro studies in simulated body fluid (SBF).....	61
4.3	Results and Discussions .....	62
4.3.1	Optimum degree of crystallinity .....	62
4.3.2	Compressive strength.....	64
4.3.3	Diametral tensile strength (DTS).....	65
4.3.4	Microhardness.....	66

4.3.5	Fractography and strengthening mechanisms .....	67
4.3.6	In vitro studies in SBF .....	70
4.3.6.1	pH measurements .....	70
4.3.6.2	FTIR .....	71
4.3.6.3	XRD Characterization .....	73
4.3.6.4	SEM Analysis .....	74
4.4	Conclusions .....	76
<b>5</b>	<b>Chapter 5 .....</b>	<b>78</b>
5.1	Introduction .....	79
5.2	Materials and methods .....	81
5.2.1	Bioglass <sup>®</sup> synthesis, heat treatment and characterization .....	81
5.2.2	Cement preparation .....	82
5.2.3	Cement properties .....	83
5.3	Results and discussions .....	84
5.3.1	Bioglass <sup>®</sup> characterization .....	84
5.3.2	Cement properties .....	86
5.3.2.1	Mechanical properties .....	88
5.3.2.2	FTIR analysis .....	92
5.4	Conclusions .....	95
<b>6</b>	<b>Chapter 6 .....</b>	<b>96</b>
6.1	Summary of conclusions .....	96
6.2	Contributions to Knowledge .....	98
6.3	Future work .....	100
	REFERENCES .....	101
	Appendix A .....	124

## List of Figures

Fig. 2. 1. The data points representing the experimental fluoroaluminosilicate glass compositions from Wilson et al. . . . .	7
Fig. 2. 2. Chemical structure acrylic acid monomer . . . . .	8
Fig. 2. 3. The setting mechanism of glass ionomer cements . . . . .	10
Fig. 2. 4. The structure of the fully set cement . . . . .	10
Fig. 2. 5. A schematic of a polymer chain restricted in a tube of 3D entanglements . . . . .	13
Fig. 2. 6. Cumulative fluoride ion (F) release per specimen area ( $\mu\text{g}/\text{cm}^2$ ) from various commercial GICs: a) Vitremer, b) Fuji II LC, c) Ketak Nano and d) Dyract Flow . . . . .	15
Fig. 2. 7. Structure of a typical incisor tooth . . . . .	17
Fig. 2. 8. A proposed mechanism for adhesion of GICs to hydroxyapatite . . . . .	18
Fig. 2. 9. The interaction zone formed between tooth surface and GIC . . . . .	18
Fig. 2. 10. Compositional diagram of melt-derived glasses in $\text{SiO}_2 - \text{CaO} - \text{Na}_2\text{O}$ system containing 6 wt% $\text{P}_2\text{O}_5$ . . . . .	28
Fig. 2. 11. Network Structure of 45S5 Bioglass <sup>®</sup> . Note that Na and Ca ions are removed for clarity. NBO = non-bridging oxygen, BO = bridging oxygen . . . . .	30
Fig. 2. 12. 45S5 Bioglass <sup>®</sup> structural transformations . . . . .	31
Fig. 2. 13. Effect of percent crystallization of the 45S5 glass-ceramic on the onset time of CHA formation (stage 5) . . . . .	32
Fig. 3. 1. The results of DSC analyses on the Bioglass <sup>®</sup> powder (before heat treatment) at various heating rates of a) 5, b) 7, c) 10, d) 15, and e) 20 °C/min. . . . .	41
Fig. 3. 2. XRD patterns of the 45S5 Bioglass <sup>®</sup> heat treated up to various temperatures a) 600, b) 650, c) 700, d) 750, and e) 800°C. The corresponding DSC curve obtained at rate of 5°C/min. (Fig. 3.1a) is also presented. . . . .	42

Fig. 3. 3. Kissinger ● , Ozawa ▲ , and Yinnon ■ plots for determining the activation energy for crystallization of combeite.....	44
Fig. 3. 4. XRD patterns of the 45S5 Bioglass® heat treated via regime I (Table 3.1): Crystallization of combeite after a) 2 min., b) 1h, c) 3h, d) 6h, e) 12h, and f) 24h nucleation time at 550 °C followed by growth at 620 °C for 2 min. Note that patterns a to f correspond to the heat treatments a to f of regime I in Table 3.1. ....	47
Fig. 3. 5. XRD patterns of the 45S5 Bioglass® heat treated via regime II (Table 3.1): Crystallization of combeite after 6h nucleation time at 550 °C followed by 5 min. growth time at a) 620, b) 640, c) 660, and d) 680 °C. Note that patterns a to d correspond to the heat treatments a to d of regime II in Table 3.1.....	48
Fig. 3. 6. XRD patterns of the 45S5 Bioglass® heat treated via regime III and IV (Table 3.1): Crystallization of combeite after 6h nucleation time at 550 °C followed by a) 10, b) 30, c) 60, and d) 120 min. growth time at 680 °C. Note that patterns a to d correspond to the heat treatments a to d of regime III in Table 3.1. Pattern (e) which represents 100% crystallinity corresponds to the Bioglass® heat treated via regime IV.....	49
Fig. 3. 7. Crystallinity of the 45S5 glass-ceramics heat treated via regime I ■■ , II ■■, III ■■ and IV ■■. The letters a to f on the X-axis correspond to those letters in Table. 1 by which the heat treatments in each regime are denoted.....	50
Fig. 3. 8. Optical microscopy images of the heat-treated glass-ceramic with 74% crystallinity before (a) and after (b) etching showing the transparency of the particles in both states. SEM images of the glass-ceramic particles before (c) and after (d and e) the etching. These SEM images were captured from larger particles to better show the grains and boundaries. Note that, the results of EDS analysis on a similar glass-ceramic sample are presented in Fig. 3.9. ....	51
Fig. 3. 9. a) SEM image of the etched Bioglass® with 74% crystallinity, along with corresponding X-ray map analysis for various elements: b) Ca, c) O, d) Na, e) Si, and f) P. ....	52

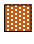


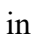



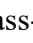

Fig. 4. 1. Measuring the compressive strength of a GIC specimen before (a) and after (b) failure (the crack formed within the sample is indicated by the arrow).....	59
Fig. 4. 2. Measuring the DTS of a GIC specimen before (a) and after (b) failure (the crack formed within the sample is indicated by the arrow) as well as the schematic of the diametral tensile test (c). .....	60
Fig. 4. 3. Effect of the 45S5 Bioglass <sup>®</sup> -ceramic crystallinity on the compressive strength (a), DTS (b) and microhardness (c) of hybrid GICs containing 5 wt% Bioglass <sup>®</sup> -ceramic (n = 6). .....	63
Fig. 4. 4. Compressive strength of hybrid GICs containing various amounts of Bioglass <sup>®</sup> -ceramic particles with 74% crystallinity after soaking for 1d  and 7d  in distilled water (n = 6). .....	64
Fig. 4. 5. DTS of hybrid GICs containing various amounts of Bioglass <sup>®</sup> -ceramic particles with 74% crystallinity after soaking for 1d  and 7d  in distilled water (n = 6).....	66
Fig. 4. 6. Microhardness of hybrid GICs containing various amounts of Bioglass <sup>®</sup> -ceramic particles with 74% crystallinity after soaking for 1d  and 7d  in distilled water (n = 6).....	67
Fig. 4. 7. SEM images captured from the fracture surfaces (after the compression test) of the commercial GIC (a) as well as hybrid GICs containing 2 wt% (b and c), 5 wt% (d), 10 wt% (e) and 15 wt% (f) of Bioglass <sup>®</sup> -ceramic with 74% crystallinity. “P” represents the 45S5 Bioglass <sup>®</sup> -ceramic particles .....	68
Fig. 4. 8. SEM images captured from the fracture surfaces of the hybrid GIC containing 5 wt% Bioglass <sup>®</sup> -ceramic with 74% crystallinity after the compression test. Various strengthening mechanisms induced by the incorporation of Bioglass <sup>®</sup> -ceramic particles are shown in these images (indicated by the arrows): crack deflection (a and b); particle pull-out (c), and crack branching (d). Note that, “P” represents the Bioglass <sup>®</sup> -ceramic particles.....	69
Fig. 4. 9. Change in pH of SBF as a function of immersion time for the commercial GIC  as well as hybrid GICs containing 5 wt%  and 10 wt%  bioglass-ceramic particles with 74% crystallinity (n = 3).....	71

Fig. 4. 10. FTIR spectra of the hybrid GIC containing 5 wt% Bioglass®-ceramic before (a) and after (b) 14 d in SBF and the hybrid GIC containing 10 wt% bioglass-ceramic before (c) and after (d) 14 d in SBF. ....	72
Fig. 4. 11. XRD results for the commercial GIC after 14 d in SBF (a) as well as the hybrid GIC containing 5 wt% Bioglass®-ceramic after 7 d (b) and 14 d (c) immersion in SBF.....	74
Fig. 4. 12. SEM images captured from the surfaces of the commercial GIC (left column) and hybrid GICs containing 5 wt% (middle column) and 10 wt% (right column) after 1 d (a-c), 3 d (d-f), 7 d (g-i) and 14 d (j-l) immersion in SBF.....	75
Fig. 5. 1. XRD patterns, particle size distributions and SEM micrographs of a) the as-received Bioglass® powder and b) heat treated Bioglass®-ceramic particles with 74% crystallinity. The XRD patterns are adapted with permission from [29]. Copyright 2014, Elsevier.....	85
Fig. 5. 2. SEM images captured from the surface of a) C0, b) C20, c) C50 and d) C100 cements after setting.....	88
Fig. 5. 3. Compressive strength and microhardness of cements containing various amounts of Bioglass®-ceramic particles (Table 5.1) after 7 d immersion in distilled water. (n = 6). ....	89
Fig. 5. 4. SEM images captured from the fracture surface of the C50 cement after the compression tests (a, b and c). The circles and arrows indicate crack-tip shielding (a and b) and crack deflection mechanisms (c), respectively. Fig. 5.4d and 4e show the fracture surface of the C50 cement and a commercial GIC (Chemfil Rock, Dentsply), respectively.....	90
Fig. 5. 5. The effect of immersion time in DW on compressive strength and microhardness of the C50 cement (n = 6).....	91
Fig. 5. 6. FTIR spectra of the C0, C50 and C100 cements after 7 d immersion in DW (a); and the C50 cement after 1, 10 and 20 days of immersion in DW (b). ....	93

Fig. 5. 7. Change in intensity of the absorbance peaks of  $\text{COO}^- \text{Ca}^{2+}$  ( $1550 \text{ cm}^{-1}$ ) and  $\text{COOH}$  ( $1650 \text{ cm}^{-1}$ ) during FTIR analysis of the C50 system as a function of time. The subplots in the upper left of spectra depicts the ratio of  $1550 \text{ cm}^{-1}$  to  $1650 \text{ cm}^{-1}$  ( $\blacklozenge$ ) and  $1410 \text{ cm}^{-1}$  to  $1650 \text{ cm}^{-1}$  ( $\blacksquare$ ) band intensities ( $n = 3$ ). Note that the peak assigned to symmetric vibration band of  $\text{COO}^- \text{Ca}^{2+}$  ( $1410 \text{ cm}^{-1}$ ) which was used in the subplot is not presented here. .... 94

## List of Tables

Table 2. 1. Composition of the first GIC glass G-200 .....	11
Table 2. 2. Composition of enamel and dentin .....	16
Table 2. 3. ISO requirements for physical properties of clinical grade GICs .....	19
Table 2. 4. Different types of calcium phosphates according to their Ca/P molar ratio .....	24
Table 2. 5. Mechanical properties of dense HA and 45S5 Bioglass <sup>®</sup> .....	25
Table 2. 6. Selected properties of melt-derived 45S5 Bioglass <sup>®</sup> .....	29
Table 3. 1. Heat treatment regimes designed in this study to induce various degrees of crystallinity in 45S5 Bioglass <sup>®</sup> .....	38
Table 3. 2. Characteristic temperatures obtained from the DSC graphs in Fig. 3.1. ....	41
Table 3. 3. Combeite crystallite size in the heat treated Bioglass <sup>®</sup> calculated based on the XRD results using Eq. (1). ....	43
Table 5. 1. Bioglass <sup>®</sup> and Bioglass <sup>®</sup> -ceramic contents; powder to liquid ratios; and setting times (n=3) of the cements. ....	86



## Abbreviations

<i>(A/W) glass-ceramic</i>	Apatite-wollastonite glass-ceramic
<i>ART</i>	Atraumatic Restorative Treatment
<i>ASPA</i>	Aluminosilicate polyacrylate
<i>BFS</i>	Biaxial flexural strength
<i>CHA</i>	Carbonated hydroxyapatite
<i>CS</i>	Compressive strength
<i>DMF</i>	Dimethylformamide
<i>DSC</i>	Differential scanning calorimetry
<i>DTS</i>	Diametral tensile strength
<i>DW</i>	Distilled water
<i>EDS</i>	Energy-dispersive X-ray spectroscopy
<i>FDA</i>	Food and Drug Administration
<i>FTIR</i>	Fourier transform infrared spectroscopy
<i>GIC</i>	Glass ionomer cement
<i>HA</i>	Hydroxyapatite
<i>HEMA</i>	2-hydroxyethyl methacrylate
<i>NSERC</i>	Natural Sciences and Engineering Research Council
<i>P:L</i>	Powder to liquid ratio
<i>PAA</i>	Polyacrylic acid
<i>PMMA</i>	Poly(methyl methacrylate)
<i>PSA</i>	Particle size distribution analysis

<i>RM-GIC</i>	Resin-modified glass ionomer cement
<i>SBF</i>	Simulated body fluid
<i>SD</i>	Standard deviation
<i>SEM</i>	Scanning electron microscope
$T_c$	crystallization onset temperature
<i>TCP</i>	Tricalcium phosphate
<i>TFS</i>	Three-point flexural strength
$T_g$	Glass transition temperature
<i>TGA</i>	Thermogravimetric analysis
$T_m$	Melting temperature
$T_p$	Crystallization peak temperature
<i>XRD</i>	X-ray diffractometry analysis

# Chapter 1

## 1.1 Overview

Two of the most fascinating fields in science today are materials science and biomedicine. Biomedicine is an area of science with extremely high rate of growth of knowledge that seeks improved medical solutions to the endless human need for curing the disease. On the other hand, materials science and engineering is one of the most thriving disciplines in modern applied science that has produced a massive deal of technology since its introduction after World War II. Over the past half century, materials science has constantly and progressively redeveloped itself into new territories.

Inevitably, the interface between these two fields of science is drawing enormous attention to research community as materials science can be applied to functionally address the existing problems in biomedicine. Resulting from this ever-growing attention, biomaterials science has been emerged as a substantial new branch of materials science.

Biomaterials can imperfectly yet functionally replace limited number of biological structures. Dental restoratives are among those functional replacements that are used as a treatment to resume hard tissue of teeth masticatory function as well as its aesthetic effects resulting from caries. Glass ionomer cements (GICs) are a major class of dental restorative materials that offer an outstanding combination of properties. However, similar to other functional replacement biomaterials, they are imperfect. They suffer mainly from poor mechanical properties as well as low remineralizing capacity which have restrained their high demanding potential. The aim of this study is to enhance not only the mechanical properties of GICs, but also to improve their biomineralizing capacity via a functional approach.

## 1.2 Objectives

The main objectives of each step of this study are presented according to the sequence of chapters in this thesis.

- To develop a set of controlled and comprehensive heat treatment profiles to tailor the crystallinity of 45S5 Bioglass<sup>®</sup> within a wide range of 5% to 100% via the formation of solely combeite which is a mechanically strong and bioactive crystalline phase. (*presented in Chapter 3*)
- To produce 45S5 Bioglass<sup>®</sup>-ceramic particles with optimum degree of crystallinity (containing only combeite) as reinforcing agent for GICs. (*presented in Chapter 4*)
- To develop hybrid GICs with improved mechanical and remineralizing properties via the incorporation of an optimum amount of 45S5 Bioglass<sup>®</sup>-ceramic with optimum degree of crystallinity as reinforcing agent. (*presented in Chapter 4*)
- To produce a novel aluminum-free GIC consisting of 45S5 Bioglass<sup>®</sup> and polyacrylic acid aqueous solution with appropriate mechanical performance and potentially enhanced remineralizing and adhesion properties comparable to commercially available GICs. (*presented in Chapter 5*)

## 1.3 Thesis organization

This thesis contains six chapters which are briefly described here. Chapter 1 provides the overview and objectives of the investigation. Chapter 2 presents the literature review on dental restorative materials; in particular glass ionomer cements (GICs). The chemical composition and setting reaction of these materials as well as their mechanical and physical properties are discussed in detail and various attempts to overcome their drawbacks are also reviewed. Furthermore, bioactive glasses, particularly 45S5 Bioglass<sup>®</sup>, and glass-ceramics are reviewed.

Chapter 3 provides an understanding about the crystallization behavior of 45S5 Bioglass<sup>®</sup> through controlled heat treatment. The steps involved in controlling the nucleation and growth temperatures and times of combeite phase resulting in the development of heat treatment regimes

to tailor the crystallinity of 45S5 glass-ceramics by the formation of combeite over a wide range of 5% to 100% to are discussed. Also, in this chapter the activation energy for crystallization of combeite and the Avrami exponent of the 45S5 Bioglass<sup>®</sup> powder are investigated and calculated using various classic thermal analysis approaches.

Chapter 4 focuses on the development of hybrid GICs with improved mechanical and remineralizing properties through incorporation of 45S5 Bioglass<sup>®</sup>-ceramic particles. 45S5 Bioglass<sup>®</sup> crystallization to various degrees of crystallinities using suitable heat treatments developed in the previous chapter is discussed. The approaches to finding the optimum degree of crystallinity which provides the highest mechanical performance are explored and the mechanical properties of the incorporated hybrid GICs are assessed. Furthermore, the active strengthening mechanisms involved are discussed using fractography. Also, an in vitro study in simulated body fluid (SBF) is conducted to investigate the biomineralizing properties of the hybrid GICs.

In Chapter 5, a novel aluminum-free 45S5 Bioglass<sup>®</sup>-based GIC with standard mechanical properties is introduced. In this chapter, 45S5 Bioglass<sup>®</sup> and its Bioglass<sup>®</sup>-ceramic as the only solid component of the experimental GIC is studied. The microstructure of fractured surfaces is also investigated to study the strengthening mechanisms involved. Also, the progression of the setting reaction at the early stages of setting is monitored.

Chapter 6 summarizes the conclusions and contributions of this research and proposes a list of recommendations for future studies.

## Chapter 2

### 2.1 Direct dental restorative materials

Direct dental restorative materials are a substantial yet complicated part of the modern restorative dentistry which are extensively used to restore the lost tooth functions caused by cavity formation [1]. Whilst the proper mechanical and chemical performance of these materials (i.e. strength and biocompatibility<sup>1</sup>) are the primary goals, aesthetics considerations are also of high demand as patients are concerned with cosmetic aspects of teeth restoration as much as performance [2]. Currently, the three main clinically available direct restorative materials are amalgams, resin composite and glass ionomer cement (GIC) [3].

Amalgam is a direct restorative that is held in place by mechanical retention which results in highly invasive tooth repair. It is prepared by mixing powders of Ag-Sn alloy with liquid mercury. For the past 150 years, amalgam has been widely used in dentistry due to its strength, durability, low cost and bacteriostatic effect [4]. However, they offer poor aesthetics and no adhesive properties. Therefore, today's dentistry is showing a strong tendency to move away from metal restorations towards tooth-colored non-metal ones [5].

Resin composite is prepared by mixing of an inorganic filler and an organic liquid to make a paste which is used to fill the tooth cavity [6]. The resulting paste can either be cured through self-initiation or light-initiation to polymerize the monomers and create a three-dimensional solid matrix containing dispersed filler particles. A variety of inorganic filler types can be used in resin composites including borosilicate glass, quartz, lithium/barium aluminum silicate glass, and borosilicate glass containing zinc/strontium/lithium [4].

Before discussing the properties and structure of GICs in section 2.2, a brief history of dental cements will be presented.

---

<sup>1</sup> Biocompatibility is defined as the ability of a material to perform with an appropriate host response in a system [1].

In majority of the restorative dental history, silver amalgam and gold foils were predominantly used for functional repair of the tooth. In 1855, the first dental cement, namely zinc oxychloride was introduced resulting from reaction of zinc oxide powder with aqueous solution of zinc chloride. Even though this cement had poor clinical performance (e.g. manipulation difficulty and high erosion rate), it was at least white and more matching to the appearance of the tooth compared to its metallic counterparts [7].

Zinc phosphate cement was invented next. When first formulated in 1878, it was not clinically popular due to excessively exothermic setting reaction between zinc oxide and aqueous phosphoric acid. Modifications were made to both components in 1902 to control the setting reaction and decrease the heat generated [1]. Due to its good handling properties, appealing aesthetics and appropriate dimensional stability, the modified zinc phosphate cement still provides great service in clinical dentistry, particularly for luting crowns [8].

The third developed dental cement is silicate cement which was the most clinically important one among the three. It also paved the road to development of glass ionomer cements (GICs). The first competent version of silicate cement appeared in 1908 consisting of a i.e. fluoride-containing calcium aluminosilicate glass and a liquid i.e. concentrated solution of phosphoric acid [9]. The resulting material was an off-white paste with proper workability which sets quickly to a strong translucent mass. Silicate cements offered three main advantages over zinc phosphate cements: 1) translucency which made them suitable for aesthetic tooth repair, 2) therapeutic benefit of sustained fluoride release, and 3) higher compressive strength [10]. Despite all these advantages that made them the only tooth-colored dental restorative available until the mid-1950's [11]. They had a number of drawbacks including vulnerability against acids (e.g. citric acid) in oral environment, a porous structure, tendency to stain, poor dimensional stability and insufficient adhesion to the tooth [10].

In early 1960's when the Laboratory of the Government Chemist in the UK was investigating silicate cements searching for potential improvements [12], it was realized that the range of optimum performance for silicate cements was relatively narrow and they had hardly any potential scope for chemical variation. However, these findings led to a series of innovative steps which eventually led to development of other dental cements [13]. In 1968, zinc polycarboxylate cement was invented from the reaction of zinc oxide with aqueous solution of polyacrylic acid. It was the

first time that a weak organic acid was used in making a dental cement. Zinc polycarboxylate cement represent a big step forward in restorative dentistry as it was the first cement to show inherent adhesion to the tooth surface. It remains a functional material in clinical dentistry and is used as a liner/base, luting cement and periodontal dressing<sup>1</sup> [10].

Glass ionomer cements will be reviewed in the following section (2.2).

## **2.2 Glass ionomer cements**

Wilson and Kent invented glass ionomer cements in 1969 in Laboratory of the Government Chemist in the UK by combining the benefits of two existing dental restoratives namely zinc polycarboxylate cement and silicate cement [14]. For the past 50 years GICs have remained a key class of dental restorative materials [9] due to their unique combination of properties. They can form direct chemical bonding to untreated dentin and enamel allowing a desirable seal of the cavity. They also offer anticariogenic properties due to sustained release of fluoride. GICs have coefficient of thermal expansion similar to that of the tooth structure which results in proper thermal compatibility with tooth enamel and dentin expansion [9]. Other advantages of GICs include low cytotoxicity and proper biocompatibility with the oral environment, minimized shrinkage after setting reaction, and reasonable aesthetics [15].

Disadvantages of the GICs, on the other hand, include relatively prolonged setting reactions, low wear resistance, sensitivity to water uptake, and more importantly, low compressive and tensile strength particularly at the early stages of placement (first 24 h). They cannot be subjected to excessive masticatory load unless they are sufficiently supported by surrounding tooth structure. Their weak mechanical strengths compared to dental composite resins and amalgam have excluded the GICs as the first choice of restorative material for multi surface restorations (e.g. Class I and II cavities), especially posterior restoration [9].

---

<sup>1</sup> Surgical dressing used to protect the wound created by periodontal therapy.



### 2.2.1 Physicochemical nature of GICs

GICs, in essence, are composite materials composed of a cross-linked polyacid matrix in which the glass particles are dispersed [16]. The generic name of glass ionomers is rooted in the original components being the fluoroaluminosilicate glass and the polyacrylic acid. The GIC is the outcome of an acid-base reaction between the ion leachable fluoroaluminosilicate glass and the polyacrylic acid homo and copolymers. The GIC glass component is a finely ground powder with ability to react with acid which serves as a source of ions for the cement forming reaction. Conventionally, the main components of GIC glass powder are  $\text{SiO}_2$ ,  $\text{Al}_2\text{O}_3$ ,  $\text{CaF}_2$  (as the flux) and commonly  $\text{NaF}$ ,  $\text{Na}_3\text{AlF}_6$  and  $\text{AlPO}_4$ . The data points indicated in the ternary diagram of  $\text{SiO}_2 - \text{Al}_2\text{O}_3 - \text{CaF}_2$  (Fig. 2.1) represent the experimental glass compositions investigated by Wilson et al. [17].

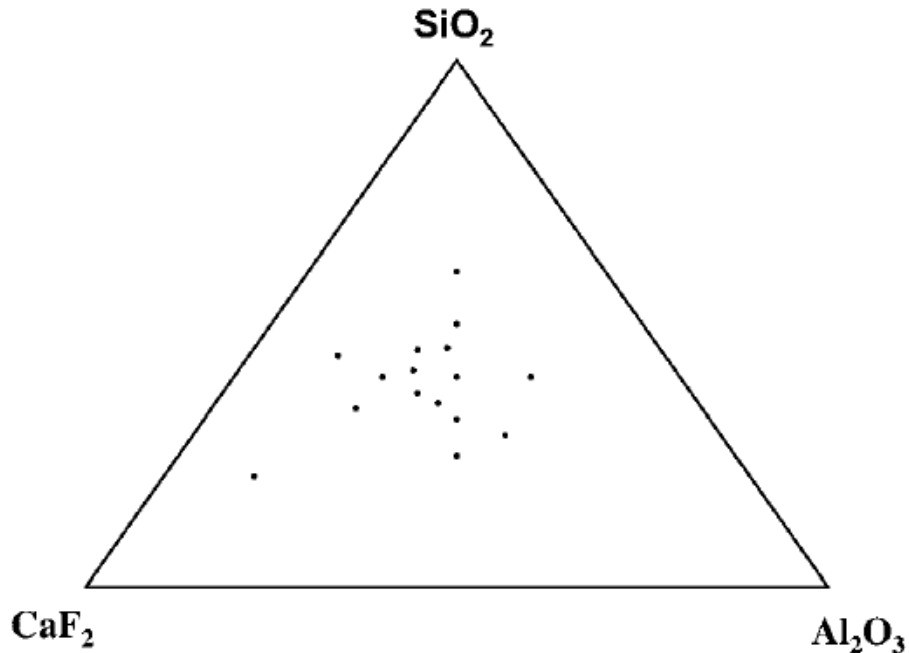


Fig. 2. 1. The data points representing the experimental fluoroaluminosilicate glass compositions from Wilson et al. [17].

Originally, the reason behind including the fluorine in the glass structure was it to serve as a network disrupter (i.e. network modifier) facilitating the ion release required for setting reaction.

However, the anticariogenic effect imparted by fluoride release from the glass particles was clinically proven at the early stages of development of GICs [1, 9, 10].

To synthesize the GIC glass powder, components are well mixed then melted at elevated temperatures (1100-1500 °C depending upon the glass chemical composition). The molten mixture then is quenched down to room temperature and ground into fine powder. Silica and alumina form the backbone of glass structure while phosphate and fluoride ions modify the setting characteristics of the GIC [14].

The other major component of the glass ionomer cements is the liquid (i.e. polyacid) which is a polymeric acid with carboxylic groups. In order to avoid gelation, the molecular weight of the acid should be low [1]. In the formulation of the earliest experimental GICs, an acrylic acid homopolymer solution (50 wt%) was used as liquid element [18]. The chemical structure of acrylic acid is shown in Fig. 2.2 The liquid component of the GIC will be discussed in further details later in this chapter.

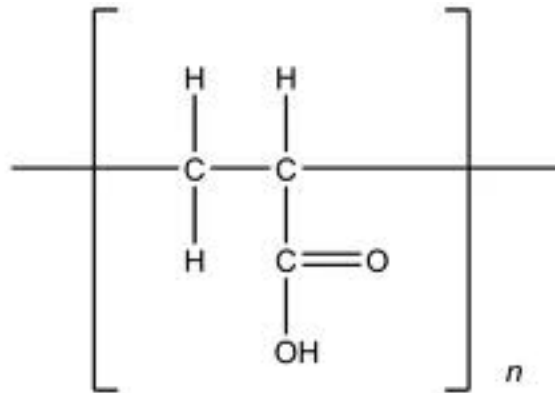


Fig. 2. 2. Chemical structure acrylic acid monomer [14].

GICs are divided to two major categories: conventional, and resin-modified. Both conventional and resin-modified GICs (RG-GICs) are considered conservative materials as they require relatively minimal cavity preparations allowing more natural tooth material to be retained [19]. The main difference is that the RG-GICs contain a polymerizable monomer, 2-hydroxyethyl methacrylate (HEMA), as an additional component along with the polyacid. They also contain suitable initiators to cause the HEMA to polymerize. Typically, these polymerization initiators are light-activated thereby the commercially available RM-GICs are mostly light curable. Originally

introduced as a liner/base material, RM-GICs are known to have similar mechanical properties to those of conventional GICs [19]. They have typically been the material of choice where aesthetics is important. However, RM-GICs have inferior biocompatibility compared to conventional GICs mainly for two reasons: Firstly, due to HEMA content, free monomers can be released from the set cement [20]. HEMA has been shown to exhibit cytotoxicity when in contact with the dental pulp tissue and osteoblasts by inhibiting cell proliferation [21]. Secondly, RM-GIC undergo an excessively high setting exotherm which can be harmful to the surrounding soft tissues [22].

Due to their extensive variations, nowadays GICs are regarded as a ‘group’ of materials [1]. They are classified in three different types depending on their applications: Luting and bonding materials, restorative materials, and liner or base cements [1]. Luting and bonding GICs are used to hold indirect restorations such as bridges, crowns and orthodontic brackets in place [9]. Restoratives GICs are radiopaque materials with higher compressive strength and wear resistance compared to those of other types owing to their higher powder/liquid ratio (P:L) [9, 19]. Liner/base cements are typically used as a thin layer underneath the restoration to act as either a thermal insulator or dentin replacement [9, 19]. All three types of GICs are delivered as either conventional or resin-modified materials [19].

### **2.2.2 Setting reaction**

The setting reaction in GICs is greatly dependent on the composition of the glass powder and the liquid. In principle the hardening process of all GICs is rooted in the acid-base reaction characteristic of dental cements. Upon mixing, the polyacid liquid attacks the surface of the ion-leachable glass particles. As a result of glass surface dissolution, metal ions such as aluminum, calcium and strontium are released. The released ions cross-link with polyacid to form a hydrogel matrix in which the glass particles are embedded [23]. A schematic illustration of setting reaction of GICs is shown in Fig. 2.3.

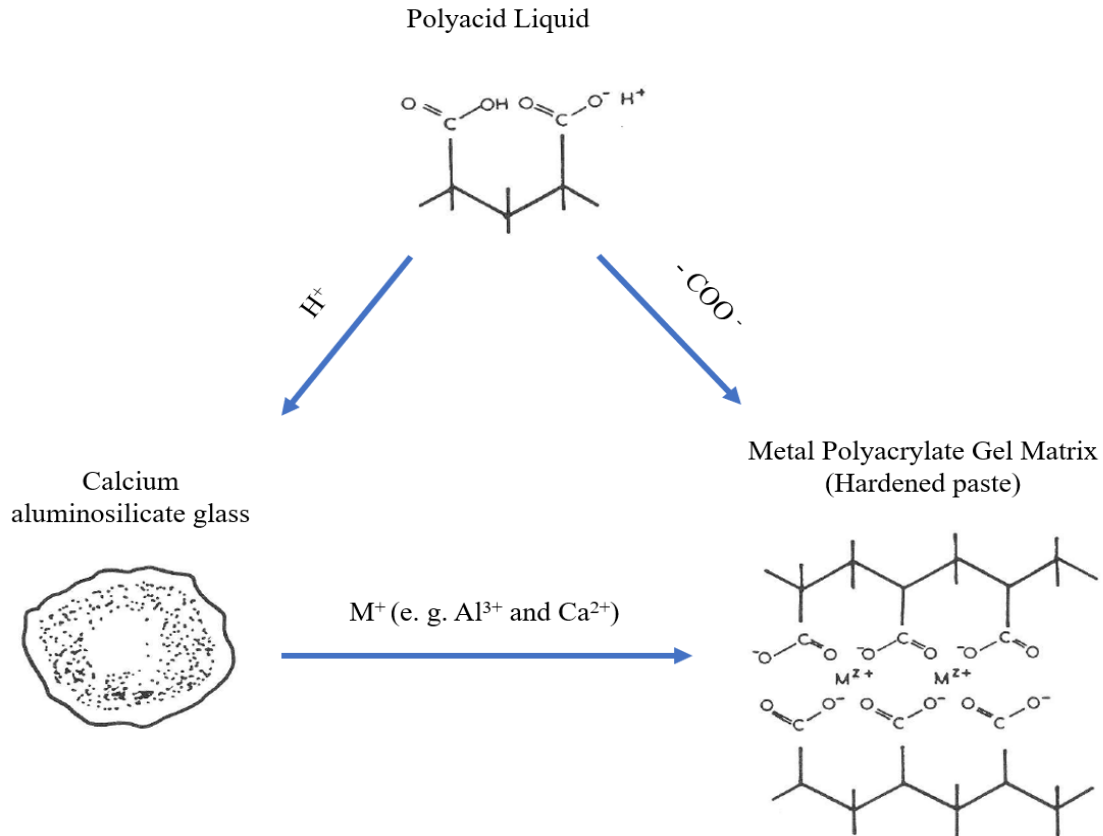


Fig. 2. 3. The setting mechanism of glass ionomer cements [24].

A completely set GIC can be described as a composite in which silica-gel-surrounded glass particles are uniformly dispersed in a matrix of polyanions cross-linked by ionic bonds [23, 24]. Fig. 2.4. presents a scheme of the structure of a fully set GIC.

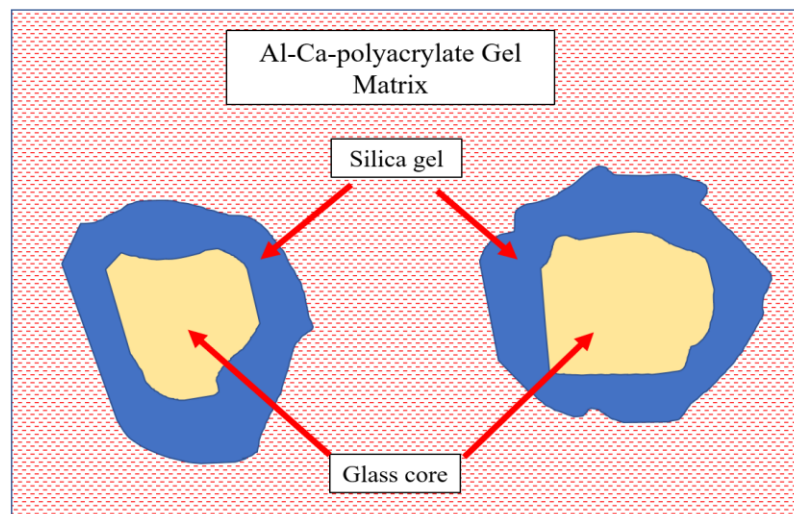


Fig. 2. 4. The structure of the fully set cement [24].

G-200 was the first glass composition ( $\text{SiO}_2\text{-Al}_2\text{O}_3\text{-AlF}_3\text{-CaF}_2\text{-NaF-AlPO}_4$ ) capable of forming a clinically useable dental cement when mixed with a 50 % polyacrylic acid solution [3]. The composition of G-200 is presented in Table 2.1.

Table 2. 1. Composition of the first GIC glass G-200 [1].

Component	Wt %
$\text{SiO}_2$	30.1
$\text{Al}_2\text{O}_3$	19.9
$\text{AlF}_3$	2.6
$\text{CaF}_2$	34.5
$\text{NaF}$	3.7
$\text{AlPO}_4$	10.0

The G-200 -derived cement which was the first practical GIC was reported to be an aluminosilicate polyacrylate (ASPA) cement [14]. It was named ASPA-I. Despite being clinically usable, there were concerns regarding the ASPA-I such as sluggish set and limited working time. It had also poor aesthetics which was attributed to the high fluoride content of G-200 resulting in the glass becoming densely opaque rather than translucent. To overcome these limitations, the role of a third component, a chelating agent, in the setting reaction was investigated. It was found that the addition of tartaric acid, as a reaction controlling additive, prolonged the working time [9]. The tartaric acid prevented the formation of calcium polyacrylate resulting in restriction of the initial set allowing the GIC to retain fluidity for a longer duration. It was also reported that tartaric acid accelerated the final setting by promoting the formation rate of aluminum polyacrylate. Shortening the setting time favorably reduced the cement exposure to the damaging effects of moisture during clinical placement [25]. Tartaric acid also enhanced the compressive strength and improved the resistance to acid dissolution of cement [26].

ASPA-II was the updated version of ASPA-I containing tartaric acid, polyacrylic acid and G-200 glass. It presented improved handling characteristics. The discovery of the effect of tartaric acid in GIC formulation opened the door for further investigations including the use of more

translucent glasses replacing the opal G-200 which resulted in subsequent versions of ASPA-II with favorable clinical characteristics [18].

As mentioned earlier, tartaric acid was added to the liquid formulation in order to improve the handling properties. Despite positive effects, tartaric-acid-modified-GICs showed inadequate shelf time (limited to 10-30 weeks) restricting their potential for commercialization. Inadequate shelf time was attributed to the gelation caused by intermolecular hydrogen bond formation [3]. It was suggested that copolymers of acrylic acid with other unsaturated carboxylic acids such as itaconic acid and maleic acid, would increase the shelf life. This was due to the presence of two carboxyl groups in the copolymer structures which resulted in higher degree of crosslinking. Consequently, the intermolecular hydrogen bond formation was reduced providing adequate shelf time [27]. The development of copolymers of acrylic acid with itaconic acid or maleic acid has also been reported to enhance mechanical performance of GICs [3].

The molecular weight and the concentration of polyacrylic acid have been reported to affect GIC properties [28]. At low concentrations of polyacrylic acid, due to further distance between polymer chains, crosslinking between the molecules during setting is inhibited which leads to reduced compressive strength and modulus of elasticity in GICs [29]. Higher polyacid concentration and molecular weight leads to increased crosslinking between polymer chains resulting in a progressive improvement in diametral tensile strength, compressive strength, modulus of elasticity, and three-point flexural strength [30]. It should be mentioned that there is limit to the concentration and molecular weight of the polyacrylic acid solution above which the viscosity of the liquid is excessively increased making the solution clinically unemployable [29].

Dynamic mechanical thermal analysis of GICs identifies these materials as thermoplastic polymer composites in which the ionic crosslinks are repeatedly breaking and reforming [31]. The fracture of GICs may be explained by the entanglement theory [32] where a polymer chain under stress is viewed as being contained within a tube which is formed by the neighboring chains (Fig. 2.5). It has been reported that the longitudinal movement of the chain is confined by the interlinkages of polar side groups between neighboring chains whereas the chain lateral movement is restricted by the proximity of the neighboring chain entanglements. Since the movement of such polymer chain confined in a tube of entanglements is similar to that of a snake, the entanglement theory is also known as the reptation model [3].

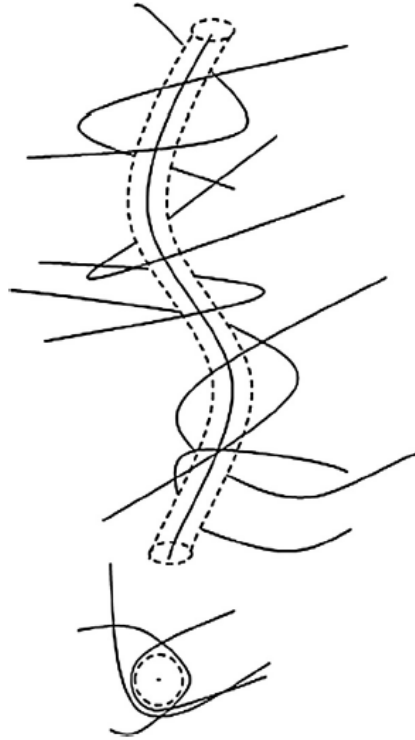


Fig. 2. 5. A schematic of a polymer chain restricted in a tube of 3D entanglements [33].

### 2.2.3 Role of water

Water is an essential element in GIC structure. It acts as reaction agent during the hardening process. When the carboxylate groups are active and ready for ion transfer, the water provides the proper medium for ion movement [10]. When the cement is set, water hydrates the GIC which leads to stabilization of the cement and prevents desiccation. It also allows for ions such as fluoride to diffuse and inhibit secondary caries [34].

After setting, there are gradual changes in GICs that slowly continue for a significant time, at least a year [25]. These changes are generally described as maturation. For instance, a freshly set GIC shows a degree of plastic character. However, it becomes less plastic and progressively rigid over time as ionic crosslinking increases resulting in increase in compressive and diametral tensile strength [35]. These changes in mechanical properties is known to be attributed to increase of proportion of bound water within the GIC. Since GICs are based on water soluble polymers with no phase separation on hardening, their structure and setting characteristics are heavily

affected by the role of water within the set cement [16]. GICs contain water in two distinguishable states of “loosely bound” and “tightly bound”. This division is based on whether or not the water can be eliminated through either storage in a desiccator or by heating at 105 °C for an hour [18, 24, 35]. It is known that the ratio of bound water increases as GIC matures which coincides with aforementioned increase in compressive and diametral tensile strength and decrease in plasticity [36]. It also has been shown that, translucency improves upon maturation [19].

Newly placed GICs are capable of exchanging water with the surroundings. They gain water in humid conditions and lose water at low humidity. In a condition of 80 % relative humidity, GICs are found to be stable in terms of water gain or loss. Freshly prepared GICs are vulnerable to early contact with moisture as it causes swelling and dissolutions of ions into the saliva leading to destroyed aesthetics and roughened surface. Typically, a layer of varnish or petroleum jelly is applied immediately after GIC placement to protect it from water exchange. As the cement ages, GIC water sensitivity tends to decrease due to increase in proportion of bound water [37].

#### **2.2.4 Fluoride release**

GICs ability to release fluoride is one of their main clinically advantageous characteristics. This feature allows them to potentially preclude and heal early carries attack [38]. Fluoride release is known to be an independent phenomenon in GICs which takes place in a sustainable fashion over at least five years after cement initial placement [39]. As a result of a study on long-term fluoride release of the GICs [40], the following equation was proposed to describe the releasing process:

$$\text{Total release} = Bt + At^{1/2}$$

where A and B are experimental constants and t is time. The study showed that despite the long duration of the experiment (two and a half years), the GICs did not reach equilibrium which made it impossible to determine the diffusion coefficient. Nevertheless, it was confirmed that fluoride release consists of two stages. The first stage involved a quick short-term process called “early wash-out” which has a direct correlation with time. This high initial burst of fluoride occurred in the first 24 h of GIC placement. The amount of fluoride release was reported to be material



dependent. The second stage, on the other hand, involved a gradual and long diffusion-based process where fluoride release was proportional to the square root of time [41].

It has been shown that the amount of fluoride release increases in an acidic environment [19, 9]. Lower pH promotes the erosion of the GIC matrix resulting in higher dissolution rates which maximizes the fluoride release into the surrounding environment. Interestingly, GICs are able to assist with controlling the demineralization around adjacent teeth and cavity margins through their own dissolution when exposed to acid attack [42, 43]. In a study [44], the effect of pH of the environment on fluoride release from various commercially available GICs including Vitremer (3M-ESPE), Fuji II LC (GC Corp), Ketac Nano (3M-ESPE) and Dyract Flow (Dentsply) up to 84 days after setting was investigated. It was shown that not only fluoride release increased in lower pH but also the fluoride release rate is material dependent (Fig. 2.6).

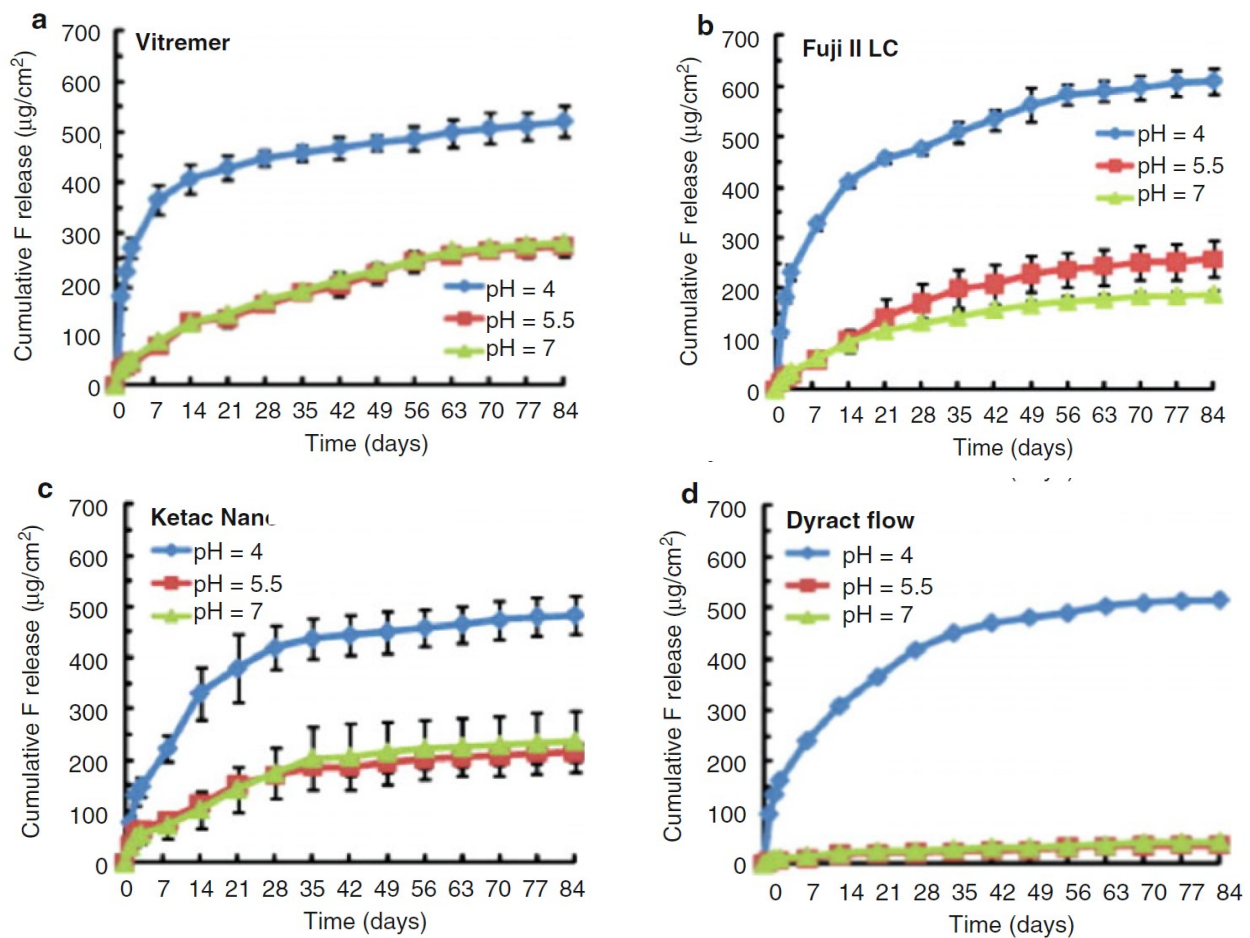


Fig. 2. 6. Cumulative fluoride ion (F) release per specimen area ( $\mu\text{g}/\text{cm}^2$ ) from various commercial GICs: a) Vitremer, b) Fuji II LC, c) Ketac Nano and d) Dyract Flow [44].

GICs not only can release fluoride, but also can be “recharged” and act as a fluoride reservoir [45]. Their ability for refluoridation can be attributed to the presence of loosely bound water and the solutes in the porosities in GIC structure which enables the cement to exchange ions with an external medium (i.e. fluoridated agents) via passive diffusion [46]. Typically, refluoridation becomes more effective when the concentration of the fluoridated agent and frequency of fluoride application are increased [45]. Also, when refluoridated, GICs have been reported to have much better potential for fluoride re-release compared to that of other dental restoratives e.g. compomers and composites [47].

### 2.2.5 Adhesion to the tooth surface

The tooth structure (Fig. 2.7) consists of two types of tissue, enamel and dentin. Their compositions are presented in Table 2.2. As shown in Table 2.2, dentin consists of more water and less mineral phase compared to enamel making it more challenging to bond for dental adhesives [19]. There are fluid-filled tubules in dentin structure which may discharge moisture and compromise the bonding. Owing to their hydrophilic nature, both conventional and resin modified GICs can properly wet the surface of freshly cut dentin and form a reliable adhesive bond [9].

Table 2. 2. Composition of enamel and dentin [48].

	Enamel	Dentin
Mineral phase (hydroxyapatite)	97%	69%
Organic phase (mainly collagen)	1%	20%
Water	2%	11%

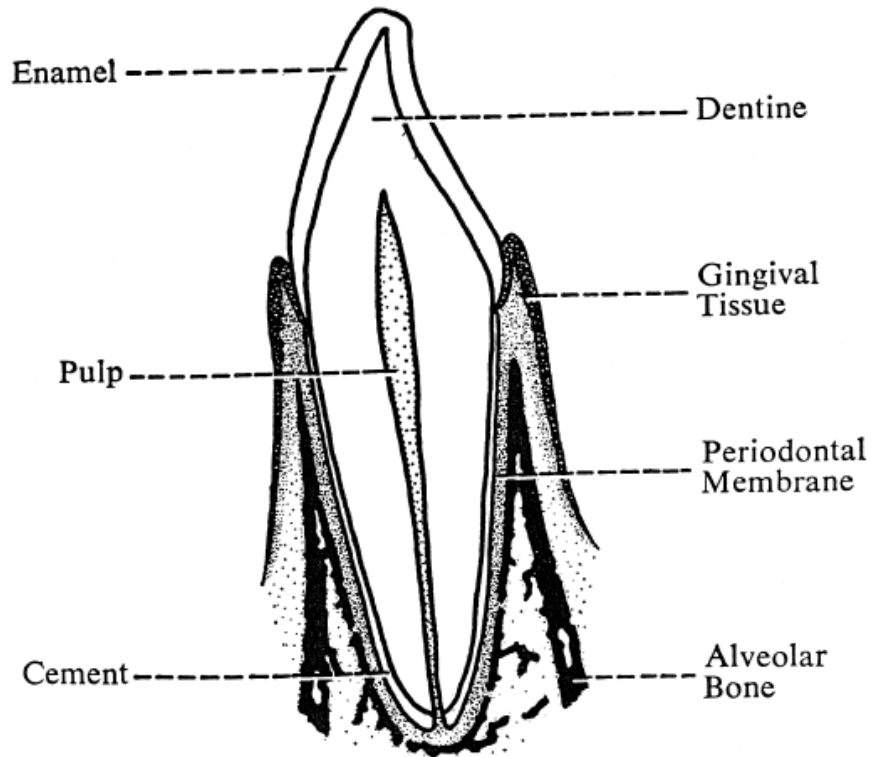


Fig. 2. 7. Structure of a typical incisor tooth [48].

The adhesion develops quickly where about 80% of the final bond strength is achieved in the first 15 min of placement followed by a gradual increase for several days [49]. The adhesion mechanism starts when newly mixed GIC paste wets the tooth surface. The free carboxyl groups in the GIC form hydrogen bonds to the layer of tightly bound water on the surface of the mineral phase of the tooth (i.e. hydroxyapatite). These hydrogen bonds which are the main cause of rapid development of adhesion in GICs, are gradually replaced by genuine ionic bonds formed from the released cations from the carboxylate functional groups of the GIC and the hydroxyapatite surface [1]. A schematic illustration of this mechanism is shown in Fig. 2.8. Subsequently, this process leads to slow formation of an interfacial ion-exchange layer between the carboxylate groups of the polyacrylic acid and the tooth surface [19, 50]. This interfacial ion-exchange layer has been called the interaction zone and is shown in Fig. 2.9.

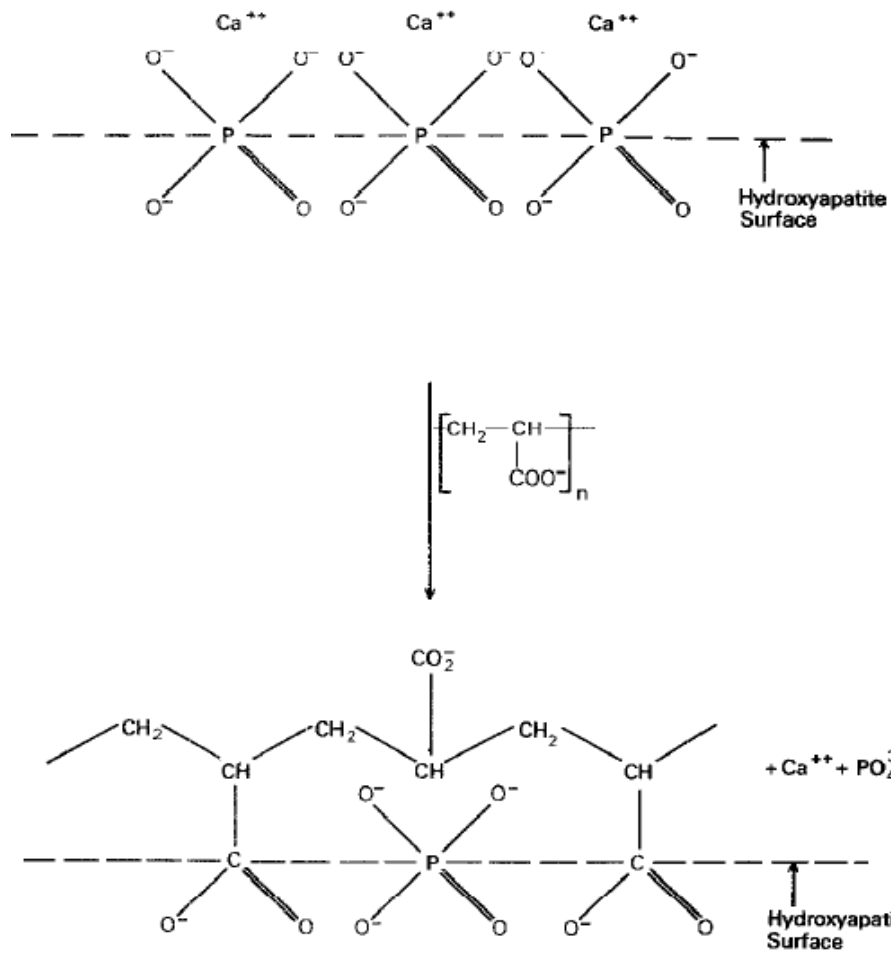


Fig. 2. 8. A proposed mechanism for adhesion of GICs to hydroxyapatite [50].



Fig. 2. 9. The interaction zone formed between tooth surface and GIC [50].

In addition to formation of true chemical bonds which was described earlier, mechanical interlocking also has been shown to contribute to the adhesion of GICs to the tooth [19]. Mechanical interlocking is caused by two phenomena: (1) the formation of short cement tags within the surface of the dentin and (2) the development of a thin hybrid layer between collagen fibrils which are coated in hydroxyapatite, at the interface of freshly cut tooth surface and the newly placed GIC [19].

### 2.2.6 Reinforcement methods

Before discussing the reinforcement methods, it is worth mentioning that the clinical grade GIC must meet the minimum requirements described in the corresponding ISO standard (ISO9917-1: dental water-based cements; 2003) [51] which is selectively presented in Table 2.3.

Table 2. 3. ISO requirements for physical properties of clinical grade GICs [51].

Property	Luting cement	Restorative cement
Setting time (min)	2.5-8	2-6
Compressive strength (MPa)	70 (minimum)	100 (minimum)
Opacity, $C_{0.70}$	-	0.35-0.90

Since ASPA was introduced to the dental market in early 1970s, GICs have been constantly subjected to modification in order to overcome their limitations. To enhance the mechanical properties of GICs and enable their clinical use in posterior regions, various attempts have been made including the reinforcement of the GIC matrix by the incorporation of different types of additives to the GIC glass component. In this section, a selection of these attempts will be reviewed.

### 2.2.6.1 *Fibers*

Sced et al. [3] studied the effect of incorporation of carbon and alumina fibers to a commercial GIC (Chembond, Dentsply DeTrey) on flexural strength of the cement. The fibers were >1000 mm in length and ranged from 10 to 20 mm in diameter. They reported that incorporation of 25 vol% of carbon and alumina fibers into the GIC powder component resulted in an increase in flexural strength from 10 MPa to 53 MPa and 44 MPa, respectively. In another study, Kobayashi et al. [52] investigated the addition of short glass fibers of CaO–P<sub>2</sub>O<sub>5</sub>–SiO<sub>2</sub>–Al<sub>2</sub>O<sub>3</sub> (with varying lengths of 33.5–100.4 mm and diameters of 9.7–21.5 mm) to a commercially available hand-mixed GIC (HY Bond Glasionomer CX; Shofu Inc.). Glass fibers were added to the GIC powder component from 0 to 100 wt% and the resulting mixture was hand-mixed with the associated GIC liquid. Following 24 h water storage, the diametral tensile strength (DTS) of the prepared cements (60 wt% short glass fiber incorporation) increased from 11 MPa to 18 MPa. The three-point flexural strength (TFS) value was also enhanced from 8 MPa to 35 MPa (60 wt% short glass fiber incorporation). Addition of > 60 wt% short glass fiber led to major deteriorations of DTS and TFS values compared to those of the commercial GIC [3].

### 2.2.6.2 *Metallic powder*

Simmons et al. [53, 54] studied the incorporation of amalgam alloy powder (Lumi Alloy, GC Corporation) to the glass component of commercially available GIC of Fuji II (GC Corporation). The GIC that resulted from this study (spherical amalgam alloy powder ratios from 5:1 to 8:1 g:g) was later marketed by GC Corporation as Miracle Mix [54]. The compressive strength of the Miracle Mix ( $104 \pm 7$  MPa) were reported to be significantly higher than that of Fuji II ( $65 \pm 4$  MPa) after 1 h of storage in water [55]. However, due to the poor interfacial bonding between amalgam powder and GIC matrix, the reinforcing effect of the amalgam alloy to GIC was reported to be limited [56].

In another study [57], Fuji II was reinforced with acid-etched stainless-steel powder (mean = 9  $\mu$ m) and the resulting cements were compared to Miracle Mix. Compressive strength ( $268 \pm 15$  MPa) and DTS ( $23 \pm 2$  MPa) values of experimental stainless-steel reinforced cements (17 vol% addition) was reported to be higher than those obtained from Miracle Mix ( $169 \pm 10$  MPa

and  $11 \pm 2$  MPa, respectively). Despite improving the mechanical performance, metal reinforced GICs were not tooth-colored and showed poor biocompatibility [56].

#### 2.2.6.3 *Hydroxyapatite*

As shown in Table 2.2, hydroxyapatite (HA) is the main constituent of tooth structure [3]. The incorporation of HA into two experimental GIC glasses G-200D (16.6 wt%  $\text{Al}_2\text{O}_3$ , 29.0 wt%  $\text{SiO}_2$ , 5.0 wt%  $\text{NaAlF}_6$ , 34.3 wt%  $\text{CaF}_2$ , 5.3 wt%  $\text{AlF}_3$ , 9.9 wt%  $\text{AlPO}_4$ ) and MP-4 (35.0 wt%  $\text{Al}_2\text{O}_3$ , 28.0 wt%  $\text{SiO}_2$ , 26.0 wt%  $\text{CaO}$ , 11.0 wt%  $\text{Na}_2\text{O}$ ) was studied [58]. In both cases, it was reported that increasing the HA content in GIC powder component, negatively affected the compressive strength of the resulting cements following 24 h water storage. Compressive strength of G-200D derived GIC was reduced from  $20 \pm 1$  MPa to  $8 \pm 1$  MPa when the HA content was increased to 50 wt% while MP-4 derived GIC showed a decrease in compressive strength from  $55 \pm 8$  MPa to  $26 \pm 2$  MPa after incorporation of 25 wt% HA [58].

The effects of addition of HA (5 wt%) nano powder with particle size ranged from 100 to 200 nm to Fuji II on compressive strength, DTS, and biaxial flexural strength (BFS) was studied [59]. As a result, an extensive improvement in mechanical properties was reported where the compressive strength increased from 160 MPa to 177 MPa, the DTS increased from 12 MPa to 16 MPa and the BFS increased from 14 MPa to 26 MPa in comparison to those of Fuji II control specimens [59].

#### 2.2.6.4 *Bioactive glass particles*

There has been a growing interest in improving the mechanical performance of GICs through incorporation of bioactive materials (e.g. bioactive glasses and bioactive glass-ceramics) [21, 58, 60, 61, 62, 63, 64] where GICs remineralizing capacity can also be benefited. Ca and  $\text{PO}_4$  ions released from GICs containing bioactive particles can promote the HA formation leading to enhanced interfacial adhesion between the GIC and the tooth surface [61]. GICs with enhanced mechanical and remineralizing properties are of special interest since they can notably broaden

GICs potential applications [64]. Bioactive glasses and glass-ceramics will be further discussed in section 2.3.1.

The effects of incorporation of S53P4 bioglass particles (Vivoxid Ltd.) in Fuji II was studied by Yli-Urpo et al. [65]. They reported that the compressive strength of the cements after 1 d of storage dropped from  $120 \pm 20$  MPa to  $105 \pm 30$  MPa when 10 wt% bioactive glass was substituted in GIC powder component.

Kim et al. [63] reported that incorporation of bioglass nanoparticles (85 mol% SiO<sub>2</sub>, 15 mol% CaO) into conventional GICs increased their mechanical properties including compressive strength, DTS and flexural strength. Surface bioactivity (i.e. in vitro biomineralization) was also reported as a result of bioglass incorporation. In another study, Valanezhad et al. [21] reported that the incorporation of 3 wt% nanoparticles of a sol-gel derived bioactive glass (70 mol% SiO<sub>2</sub>, 30 mol% CaO) resulted in increasing the flexural strength of the tested RM-GIC by up to 30%.

### **2.2.7 Atraumatic Restorative Treatment (ART)**

It is known that dental caries are the most common noncommunicable disease in the globe [66]. In response to the unavailability of dental restorative care for underserved communities, a minimally invasive operative approach namely Atraumatic Restorative Treatment (ART) was developed in the 1980s. Utilizing only hand instruments and a high viscosity GIC, ART provides an affordable alternative to manage decayed teeth and prevent it from being extracted where essential resources for modern dental treatment (e.g. plumbed water and electricity) are in short supply [66, 67]. In ART procedure, firstly, markedly softened carious enamel and dentin are removed using hand instruments. Then, the resulting cavity as well as the associated pits and fissures are restored using a hand-mixed high viscosity GIC [68]. Lastly, the material is pushed into the cavity for a few seconds using an index finger. Owing to their instant durable adhesion as well as their remineralizing effect when in contact with the hard tissues, GICs are the main, if not only, material of choice for ART [9].



### **2.2.8 Aluminum-free glass ionomer cements**

Although Al serves as a key element in GIC setting reaction, there are concerns regarding the release of Al ions from the GIC matrix. Al ion has been recognized as a neurotoxin which acts in favor of cellular oxidation [69] and breaks cellular homeostasis apart [70]. It has been reported that up to 77 days following implantation of an aluminum-containing bone cement, Al can be traced in the brain, cerebral spinal fluid, urine and blood [71]. Also, the pathological process of many neurological disorders such as Parkinson's disease are thought to be related to Al presence [72]. Due to the aforementioned concerns, there has been a growing tendency for development of Al-free glass ionomers in the field of orthopedics and dentistry [71]. Since Al plays a key role in physicochemical properties, removing it from the structure poses challenges in achieving a GIC that meets standard requirements. These challenges as well as a novel straight forward approach to tackle them are discussed in chapter 5.

## **2.3 Bioactive materials**

In general, a bioactive material is a material that has been engineered to induce certain biological activity [73]. In a more particular sense, a bioactive material goes through specific surface reactions when implanted into the body or exposed to biological fluid which leads to formation of a hydroxyapatite-like layer through which it forms a firm bond with the host tissue [74]. To assess if a material is bioactive, typically, it is immersed in simulated body fluid (SBF) and formation of a hydroxyapatite-like layer on the surface can be an indication of material bioactivity [73].

Depending on the rate of bone regeneration induced by the bioactive materials, they are classified into Class A and Class B. Class A bioactive materials can bond with both hard and soft tissues. They are both osteoconductive and osteoproducer which leads to the rapid formation of hydroxyapatite followed by the mineralization process resulting in the formation of a mature hard tissue structure [75, 76]. On the other hand, Class B bioactive materials are only osteoconductive so they are unable to provide a proper environment to stimulate the few osteoprogenitor cells to start the cell-division cycle [77].

The invention of the first bioactive glass (i.e. 45S5 Bioglass<sup>®</sup>) by Hench in 1969 launched the field of bioceramics<sup>1</sup> resulting in development of many new materials and products [77]. Various types of ceramic materials have been reported to be bioactive. They can be categorized in three groups [78]: 1) calcium phosphates, 2) bioactive glasses and glass-ceramics 3) other bioactive ceramics. Calcium phosphates are briefly discussed in the following while bioactive glasses and glass ceramics will be reviewed in section 2.3.1.

Synthetic hydroxyapatite (HA;  $\text{Ca}_5(\text{PO}_4)_3(\text{OH})$ ) and tricalcium phosphate (TCP;  $\text{Ca}_3(\text{PO}_4)_2$ ) are the most important bioactive calcium phosphates. Depending on the condition, TCP is stable in various polymorphs where the  $\alpha$ - and  $\beta$ -TCP are the two main forms [79]. The type of calcium phosphates can be determined by the molar ratio of Ca/P in their structure using Table 2.4.

Table 2. 4. Different types of calcium phosphates according to their Ca/P molar ratio [79].

Ca/P molar ratio	Calcium phosphate type
< 1.67	$\alpha$ - or $\beta$ -TCP
> 1.67	CaO + HA phase
= 1.67 (2.15 in weight ratio)	HA

A great deal of research has been carried out on synthetic HA due to its similar chemical structure to the hard tissue. However, its Class B bioactivity along with its poor fracture toughness and low in vivo degradation rate, have restricted its applications [79, 78]. The  $\beta$ -TCP has better mechanical performance and higher dissolution rate in comparison to synthetic HA [78]. Here are the dissolution rates of calcium phosphates: Amorphous HA >  $\alpha$ -TCP >  $\beta$ -TCP > Crystalline HA [80].

One of the notable modifications of bioactive glasses is apatite-wollastonite (A/W) glass-ceramic [79]. This glass-ceramic which was first invented in Japan in 1982, consists of a glassy

---

<sup>1</sup> “Bioceramic” is a general term that covers glasses, ceramics and glass-ceramics which are used as implant materials [82].

matrix (17 wt% MgO, 24 wt% CaO, 59 wt% SiO<sub>2</sub>) that contains 34 wt% of oxyfluorapatite (Ca<sub>10</sub>(PO<sub>4</sub>)<sub>6</sub>(O,F)<sub>2</sub>) (50–100 nm) and 28 wt% wollastonite (CaO.SiO<sub>2</sub>). A/W glass-ceramics are used in load bearing implants owing to their good mechanical properties and proper bioactivity [79]. Table 2.5 summarizes various mechanical properties of dense HA, 45S5 Bioglass<sup>®</sup> and A/W glass-ceramic.

Table 2. 5. Mechanical properties of dense HA and 45S5 Bioglass<sup>®</sup> [80].

Material	Compressive strength (MPa)	Tensile strength (MPa)	Elastic modulus (GPa)	Fracture toughness (MPa m <sup>1/2</sup> )
HA	>400	~40	~100	~1.0
45S5 Bioglass <sup>®</sup>	~500	42	35	0.5-1
(A/W) glass-ceramic	1080	215	118	2.0

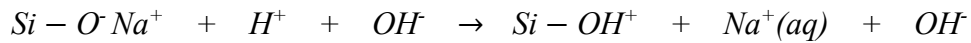
### 2.3.1 Bioactive glasses and glass-ceramics

Bioactive glasses and glass-ceramics are the only materials that are capable of forming a bond with both soft and hard tissues *in vivo* [77]. These materials can be made in a variety of compositions and forms including powders, fibers, bulk and porous monoliths which lead to their extensive range of applications [80, 81]. There are several types of bioactive glasses such as silicate glass (e.g. Bioglass<sup>®</sup>), phosphate-based glass and borate-based glass [82]. Phosphate and borate glasses have higher dissolution rates compared to that of silicate glass. Particularly, borate glass has delivered promising clinical results in healing of chronic wounds (e.g. diabetic ulcers) which would not heal via conventional treatment [83]. The ability of borate glasses to response to soft tissues is thought to be associated with their fast dissolution rate. In fact, both borate and phosphate glasses benefit from their very rapid solubility rather than bioactivity which is an area dominated by silicate glasses [83]. The focus of this section will be on silicate glasses made by conventional melt and quench technique.

The mechanism that leads to bonding between a bioactive glass (or glass-ceramic) and the host tissue is associated with initial glass dissolution followed by formation of a carbonated hydroxyapatite (CHA) layer on the glass surface. CHA is a biologically active phase which has a similar structure to hard tissues and is believed to interact with collagen fibrils and form a bond with the host tissue [80, 84].

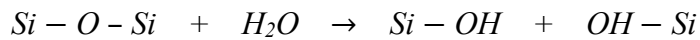
Formation of the CHA layer after dissolution of the bioactive glass or glass-ceramic takes place through a mechanism similar to conventional glass corrosion. Dissolution byproducts alter the chemical composition as well as the pH of the environment leading to formation of surface sites suitable for CHA nucleation [85]. Although a full understanding of the mechanism is yet to be achieved, it has been proposed that the following five stages are involved in forming the CHA layer (i.e. bone bond) in bioactive glasses and glass-ceramics *in vivo* or *in vitro* [86]:

- I. Rapid exchange of modifier cations ( $\text{Na}^+$  and/or  $\text{Ca}^{2+}$ ) with  $\text{H}^+$  from the solution which results in formation of silanol bonds ( $\text{Si}-\text{OH}$ ) on the bioglass surface:



As a result, the pH of the environment increases leading to formation of a silica-rich region close to the bioglass surface. If there is any phosphate present in the composition, it is dissolved from the glass at this stage.

- II.  $\text{OH}^-$  groups attack the silica glass network and break  $\text{Si}-\text{O}-\text{Si}$  bonds due to high local pH. Soluble silica is released to the solution in the form of  $\text{Si}(\text{OH})_4$  which leaves more silanol groups ( $\text{Si}-\text{OH}$ ) at the interface of the bioglass and the solution:



- III. Condensation of silanol groups near the bioglass surface and formation of  $\text{Si}-\text{O}-\text{Si}$  bonds resulting in repolymerization of the silica-rich layer.
- IV. Diffusion of  $\text{Ca}^{2+}$  and  $\text{PO}_4^{3-}$  groups to the surface via silica-rich layer leading to formation of an incipient amorphous  $\text{CaO}-\text{P}_2\text{O}_5$ -rich film.
- V. Crystallization of the  $\text{CaO}-\text{P}_2\text{O}_5$ -rich film to CHA on the surface of the bioglass following incorporation of hydroxyls and carbonate groups from solution.

Similar to other properties of glass, the dissolution rate and thereby formation rate of CHA can only be understood in light of understanding the atomic structure of glass. The glass network consists of silica tetrahedra which are joined together by  $-\text{Si}-\text{O}-\text{Si}-$  bridging oxygens. Silicon acts as a network former and develops the glass structure by covalent bonding [77]. On the other hand, network modifiers such as sodium and calcium disrupt the structure by forming non-bridging oxygens (e.g.  $\text{Si} - \text{O}^- \text{Na}^+$ ). Glass modifiers bond ionically to the network [77, 87]. According to, NMR analysis, there are no  $\text{P}-\text{O}-\text{Si}$  bonds in glass structure and phosphorous is present in the glass network in an orthophosphate form with charge balanced with Na and/or Ca [88]. As a result, the P is somehow isolated from the glass network and diverts network modifiers such as Na and Ca from their role. That is the reason behind rapid dissolution of P from the glass when exposed to aqueous medium [89]. Also, it has been known that the presence of orthophosphate in a bioactive glass promotes glass-in-glass phase separation which is why melt-derived bioglasses having  $\geq 6$  mol% phosphate mostly exhibit two glass transition temperatures ( $T_g$ ) [90].

Network connectivity,  $N_c$ , is defined as the mean number of bridging oxygens per Si atom [90]. High silica content leads to high  $N_c$  meaning more chemical and physical stability which reduces the dissolution rate of the glass and therefore its bioactivity. Increasing the network modifiers content results in lower connectivity through disrupting the silica network. Since network modifying cations such as Na and Ca charge-balance the orthophosphate, higher phosphate content is shown to increase network connectivity. It has been reported that glasses with  $N_c$  values higher than 2.6 are most probably not bioactive because their structure resists dissolution [82].

Fig. 2.10 illustrates the compositional diagram of all melt-derived silicate glasses in  $\text{SiO}_2 - \text{CaO} - \text{Na}_2\text{O}$  system with 6 wt%  $\text{P}_2\text{O}_5$ . In region D, which is the silica-poor side of the diagram, there is no glass formation because of insufficient amount of network formers. Region B, on the other hand, is rich in silica ( $> 60$  wt%) yet the resulted glass is bio-inert due to high network connectivity and minimal dissolution rate [91]. Region A represents the compositional area of glasses (52 – 60 wt%  $\text{SiO}_2$ ), which are able to bond to the hard tissue in 2 – 4 weeks. The glasses with compositions in region S, where silica content is 42 – 52 wt%, demonstrate Class A

bioactivity which means they can bond to both soft and hard tissues. The highest bioactivity index<sup>1</sup> belongs to the glass compositions in the small region of E which includes 45S5 Bioglass<sup>®</sup> [77].

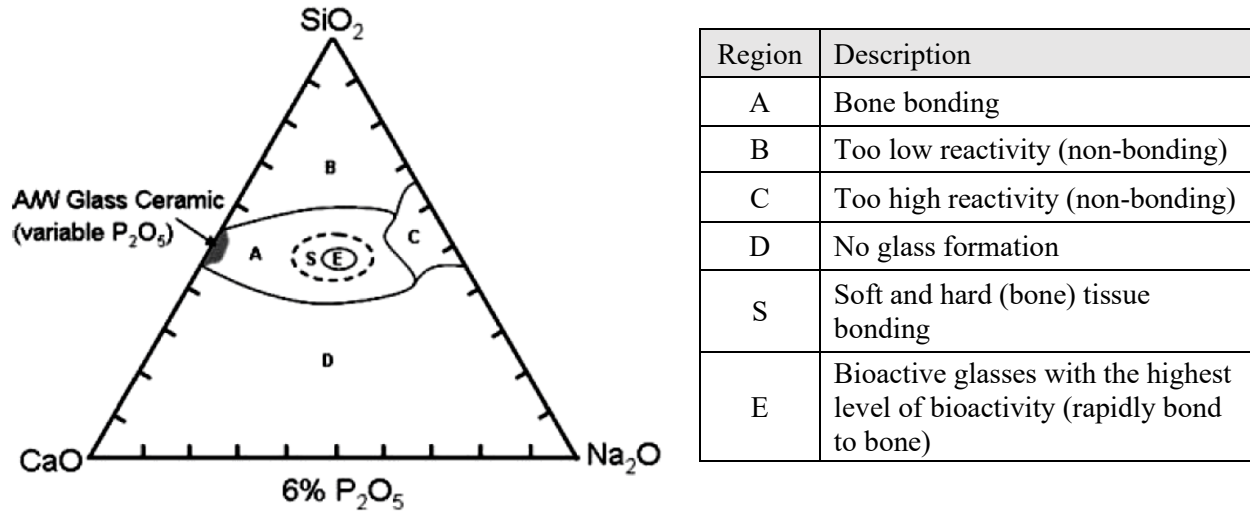


Fig. 2. 10. Compositional diagram of melt-derived glasses in  $\text{SiO}_2 - \text{CaO} - \text{Na}_2\text{O}$  system containing 6 wt%  $\text{P}_2\text{O}_5$  [77].

### 2.3.2 45S5 Bioglass<sup>®</sup>

45S5 Bioglass<sup>®</sup> was discovered by Hench at the University of Florida in 1969 [79]. The idea of finding a material which could form a bond to human bone was implanted in his mind after a bus ride conversation with a colonel from US Army who just returned from the Vietnam war. The colonel asked him about the possibility of developing a material that could withstand the harsh environment of the human body. Back at the time, all available implants reportedly resulted in fibrous encapsulation when implanted. Hench focused on making a degradable glass in  $\text{Na}_2\text{O}-\text{CaO}-\text{SiO}_2-\text{P}_2\text{O}_5$  system, high in Ca content, and close to an eutectic in  $\text{Na}_2\text{O}-\text{CaO}-\text{SiO}_2$  equilibrium phase diagram. The resulting composition was 45 wt%  $\text{SiO}_2$ , 24.5 wt%  $\text{CaO}$ , 24.5

<sup>1</sup> Proposed by Hench, bioactivity index ( $I_B$ ) is used to assess and compare the bioactivity of the materials.  $I_B$  is defined as a 100 divided by the time required for more than 50% of the material's surface bonds to the surrounding tissues ( $t_{50bb}$ ) [77].

wt% Na<sub>2</sub>O, and 6.0 wt% P<sub>2</sub>O<sub>5</sub> which was later termed 45S5 Bioglass<sup>®</sup>. “45S” represents 45 wt% SiO<sub>2</sub>, the main glass former in this composition, and 5 is the key Ca:P molar ratio. As mentioned before, 45S5 Bioglass<sup>®</sup> has the highest bioactivity index (I<sub>B</sub>=12.5) among the bioactive glass compositions (see Fig. 2.10) [77]. A selection of properties of melt-derived 45S5 Bioglass<sup>®</sup> are presented in Tables 2.5 and 2.6.

Table 2. 6. Selected properties of melt-derived 45S5 Bioglass<sup>®</sup> [82].

Property	Value
Density	2.7 g/cm <sup>3</sup>
Network connectivity	2.12
Thermal expansion coefficient	15.1 × 10 <sup>-6</sup> °C <sup>-1</sup>
Elastic modulus	35 MPa

45S5 Bioglass<sup>®</sup> particles with high specific surface area have been reported to have antibacterial effect. This effect is key in areas such as tissue repairing in dentistry where infected root canals are involved [92]. Rapid solubility of 45S5 Bioglass<sup>®</sup> nanoparticles results in sharp increase in pH of the surrounding aqueous environment, a condition cannot be tolerated by microbiota [93].

### 2.3.2.1 Structure

The network structure of the 45S5 Bioglass<sup>®</sup> is shown in Fig. 2.11. Si, as the main network former, covalently bonds to bridging oxygen atoms while the network modifiers, Na and Ca, are ionically bonded to the glass structure through broken oxygen bonds. The formation of ionic bonds between non-bridging oxygen atoms and modifiers is due to maintaining the electroneutrality [82, 86]. The presence of network modifiers has various effects on the Bioglass<sup>®</sup> properties. They decrease chemical, physical and mechanical stability through disrupting the silica network. They also play a key role in the first step of formation of the CHA layer *in vivo* and *in vitro* as they are rapidly exchanged with H<sup>+</sup> from the solution that results in formation of silanol bonds (Si–OH) on the Bioglass<sup>®</sup> surface. In fact, the high content of network modifiers in the composition (total

of 49 wt%) is one of the main reasons for outstanding bioactivity of the 45S5 Bioglass<sup>®</sup> because it makes the network easier to break down resulting in more rapid solubility rate [94].

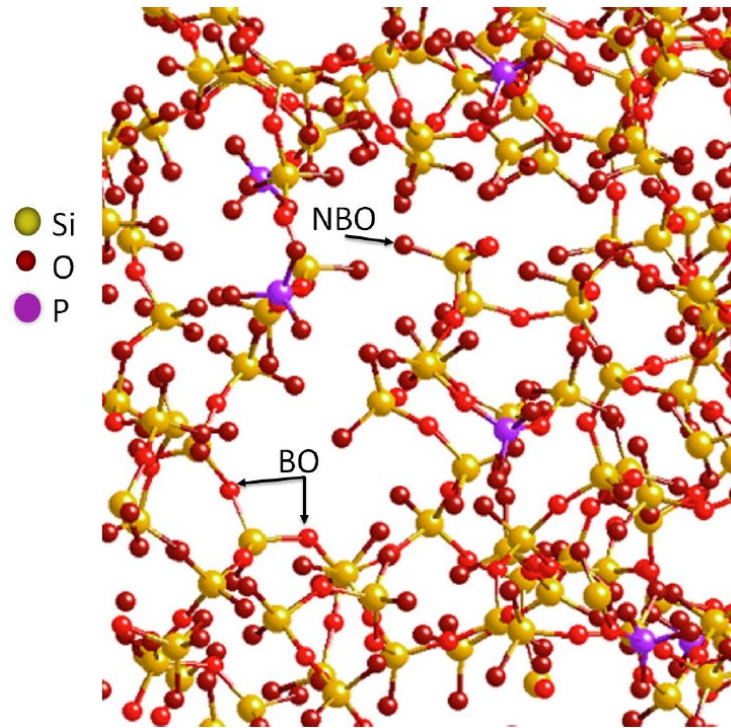


Fig. 2. 11. Network Structure of 45S5 Bioglass<sup>®</sup>. Note that Na and Ca ions are removed for clarity. NBO = non-bridging oxygen, BO = bridging oxygen [82].

Surprisingly, despite the great deal of research carried out on bioactive glasses over the past almost 50 years, no other bioglass composition has been known to have better biological characteristics than 45S5 Bioglass<sup>®</sup> composition [82].

#### 2.3.2.2 Thermal behavior

Thermal behavior of 45S5 Bioglass<sup>®</sup> has been thoroughly researched in the literature [95, 96, 97] and it will be discussed in detail in chapter 3. In brief, following the glass transition at  $T_{g1} = 550$  °C, 45S5 Bioglass<sup>®</sup> undergoes a glass-in-glass phase separation at 580 °C resulting in formation of two glassy phases: a silicate-rich phase and a phosphate-rich phase. Higher silica content results in high viscosity in the silica-rich phase thereby the flow behavior is dominated by this phase [96]. The formation of the phosphate-rich domains is known to have a catalytic effect



on crystallization of the silica-rich phase. They act as nucleation sites and reduce the required energy for nucleation of the silicate-rich nuclei. Combeite ( $\text{Na}_2\text{Ca}_2\text{Si}_3\text{O}_9$ ), which is known to be a mechanically strong phase due to high silica content, crystallizes from the silica-rich glassy phase between 610 to 700 °C whereas silico-rhenanite ( $\text{Na}_2\text{Ca}_4(\text{PO}_4)_2\text{SiO}_4$ ) evolved from the phosphate-rich phase at 800 °C. It should be noted that the phosphate-rich phase is still present after combeite crystallization [95]. A second glass transition occurs at  $T_{g2} = 850$  °C and eventually, melting occurs in the range of 1070–1278 °C [96]. Fig. 2.12 demonstrates the 45S5 Bioglass<sup>®</sup> thermal phase transformations.

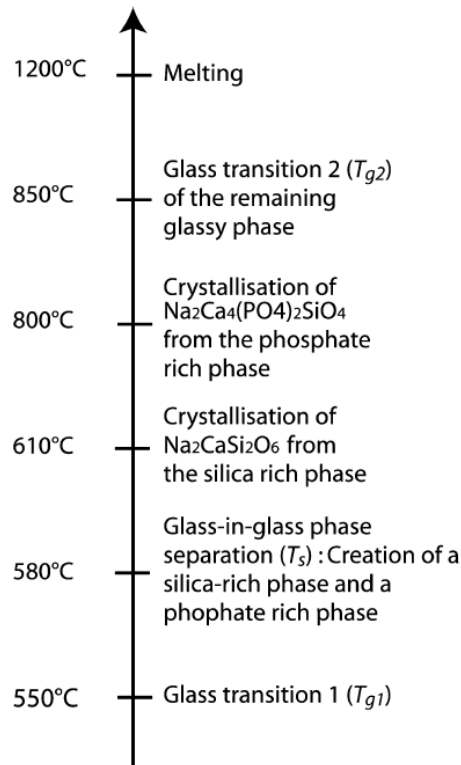


Fig. 2. 12. 45S5 Bioglass<sup>®</sup> structural transformations [96].

### 2.3.2.3 45S5 Bioglass<sup>®</sup>-ceramic

A major shortcoming that restricts the application of bioactive glasses as implants in load-bearing areas is their low mechanical properties [96]. Transformation of bioactive glasses to glass-ceramics through heat treatment is one of the practical techniques to improve their mechanical

properties. Although crystallization of bioactive glasses leads to diminishing or sometimes neutralizing their bioactivity [98], it has been reported that the bioactivity is maintained in crystalline 45S5 [99]. Filho et al. [100] studied the effect of crystallization of 45S5 Bioglass<sup>®</sup> on CHA layer formation *in vitro*. It was shown that after 20 h exposure to SBF, the glass-ceramics with < 60% crystallinity were able to form a crystalline CHA layer whereas the glass-ceramics with more than 60% crystallinity developed only an amorphous calcium phosphate within the same time period. Interestingly, increasing the SBF exposure time to 40 h resulted in fully development of a crystalline CHA layer on the surface of glass-ceramics containing > 60%. It was concluded that crystallization of 45S5 Bioglass<sup>®</sup> did not compromise its bioactivity and 45S5 glass-ceramics with crystallinity ranged from 8 to 100% remain bioactive *in vitro*, however, the onset time of CHA layer formation was reported to increase from 10 h for amorphous Bioglass<sup>®</sup> up to 22-25 h for the material with 60-100% crystallinity (Fig. 2.13). Also, the rate of CHA layer formation of 45S5 glass-ceramics was found to be up to seven times higher than that reported of A/W glass-ceramics [99, 100]

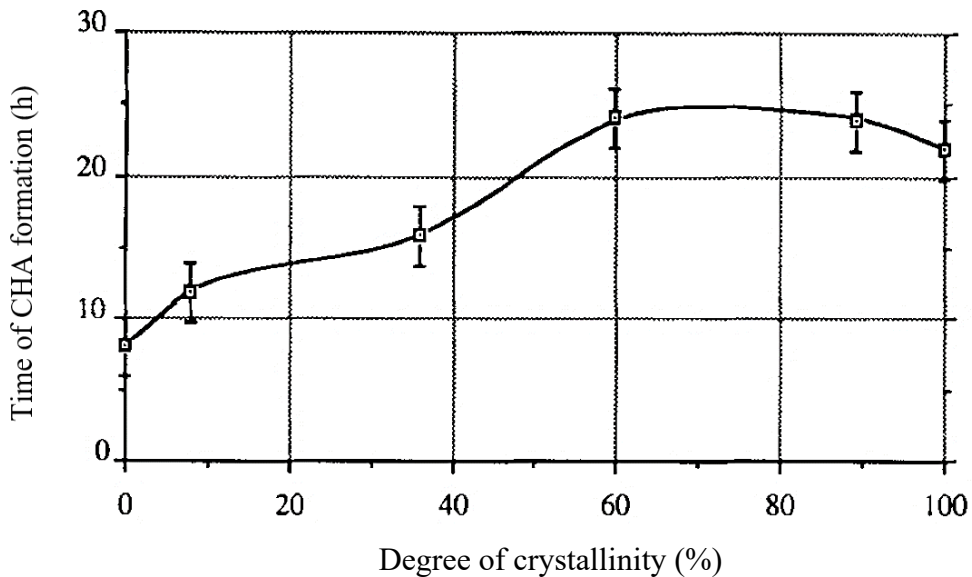


Fig. 2. 13. Effect of percent crystallization of the 45S5 glass-ceramic on the onset time of CHA formation (stage 5) [100].

The mechanical properties of an amorphous material are known to increase as it crystallizes thereby, transforming the 45S5 Bioglass<sup>®</sup> to Bioglass<sup>®</sup>-ceramic through controlled heat treatment is a practical approach to enhance their performance [80]. Consequently, along with outstanding remineralizing properties (i.e. bioactivity), improved mechanical performance can also be exploited from 45S5 Bioglass<sup>®</sup>-ceramics. This in fact was the underlying idea behind the approach chosen in this research work in developing glass ionomer cements with improved mechanical and remineralizing properties by incorporation of 45S5 glass-ceramic.

## Chapter 3

# Crystallization behavior of combeite in 45S5 Bioglass<sup>®</sup> via controlled heat treatment <sup>1</sup>

Alireza Zandi Karimi <sup>a</sup>, Ehsan Rezabeigi <sup>b</sup>, and Robin A.L. Drew <sup>a</sup>

<sup>a</sup> *Department of Mechanical, Industrial & Aerospace Engineering, Concordia University, Montréal, Quebec H3G 1M8, Canada.*

<sup>b</sup> *Department of Mining and Materials Engineering, McGill University, Wong Building, 3610 Rue University, Montréal, Quebec H3A 0C5, Canada.*

**Abstract.** Combeite ( $\text{Na}_2\text{Ca}_2\text{Si}_3\text{O}_9$ ) is a mechanically strong phase that crystallizes from 45S5 Bioglass<sup>®</sup> during heat treatments. 45S5 glass-ceramics are expected to not only retain desirable levels of bioactivity but also exhibit improved mechanical properties compared to those of the amorphous 45S5 Bioglass<sup>®</sup>. However, producing crystalline 45S5 glass-ceramics containing solely combeite is challenging since other phase(s) may also form during the heat treatment process. In this study, we developed a comprehensive set of heat treatment regimes that can be used to control the formation of combeite in order to tailor the crystallinity of 45S5 glass-ceramics over a wide range of 5% to 95%. These heat treatments were designed based on controlling the nucleation and growth temperatures and times of the combeite phase, also preventing other potential phases from forming. Correspondingly, the activation energy for crystallization of combeite was calculated based on three different analytical methods and then used to obtain the Avrami exponent of the Bioglass<sup>®</sup> powder ( $n = 0.71$ ). The results indicated that the crystallization of combeite occurred mainly on the surface of the particles.

Depending on the target application, different levels of mechanical properties and bioactivity in bioglasses may be required. The crystallinity of 45S5 Bioglass<sup>®</sup> can be adjusted by applying the appropriate heat treatment regime selected from the profiles developed in this study.

Keywords: Combeite; 45S5 Bioglass<sup>®</sup>; Heat treatment; Crystallinity

---

<sup>1</sup> This Chapter is published as: A. Zandi Karimi, E. Rezabeigi, and R. A. L. Drew, “Crystallization behavior of combeite in 45S5 Bioglass<sup>®</sup> via controlled heat treatment,” *J. Non. Cryst. Solids*, vol. 502, pp. 176–183, 2018.

### 3.1 Introduction

45S5 Bioglass<sup>®</sup>, 45% SiO<sub>2</sub>, 24.5% CaO, 24.5% Na<sub>2</sub>O and 6% P<sub>2</sub>O<sub>5</sub> (wt.%), is the first bioactive material reported in 1969 by Hench [84]. This bioglass which is approved by the US Food and Drug Administration (FDA) has been extensively studied due to its Class A bioactivity and successful clinical history [86, 101-103]. Class A bioactive glasses are osteoconductive and osteopductive and exhibit the highest rate of hydroxyapatite (HA) formation (i.e. mineralization) *in vitro* and *in vivo* which are essential for tissue engineering applications [104]. However, there is still a great deal of ongoing research carried out on this bioglass as an additive to other biomaterials such as bioactive composite scaffolds [105] and dental restoratives (i.e. glass ionomer cements (GICs) [61]. The 45S5 bioactive glass is one of the main compositions that is currently being investigated for the next generation of biomaterials designed to prevent tissue loss which shows the importance and tremendous potential of this bioglass [106, 107].

In general, increasing crystallinity of a glass structure enhances its mechanical properties [96]. For example, apatite/wollastonite (A/W) glass ceramics are widely used not only for their bioactivity, but also their relatively high mechanical properties including compressive strength, tensile strength and fracture toughness [108]. The application of 45S5 as an additive or a load-bearing implant is limited due to its overall low mechanical properties, in particular fracture toughness [108]. Alternatively, mechanical properties of this bioglass can be improved via controlled heat treatments allowing for the formation of crystalline phases with higher strength such as the silica-rich combeite phase which will be further discussed below [98, 99]. An appropriate heat treatment can also cause reduction in thermal stresses produced during shock cooling of the glass [109]. Although the bioactivity level of most bioactive glasses is drastically diminished upon crystallization, it has been shown that 45S5 glass-ceramic containing combeite (Na<sub>2</sub>Ca<sub>2</sub>Si<sub>3</sub>O<sub>9</sub>) crystals with a high degree of crystallinity, even up to 100%, can maintain its bioactivity [100]. The high bioactivity of 45S5 composition is mainly attributed to the relatively large amount of specific glass modifiers, sodium and calcium, in its structure, making it easier to dissolve *in vitro* and *in vivo* [111-113].

During heating scans, the first glass transition of 45S5 composition occurs at 550°C, followed by a spinodal transformation of the glassy phase into two immiscible phases at 580°C [96]. This glass-in-glass phase separation is due to the coexistence of Si<sup>4+</sup> and P<sup>5+</sup> in glass structure as both of these ions have high valence numbers and each ion type prefers to concentrate separately [115, 116]. As a result, one of the phases is rich in phosphorus (P-rich) and the other phase is rich in silicon (Si-rich) of which the latter forms an important crystalline phase known as combeite (Na<sub>2</sub>Ca<sub>2</sub>Si<sub>3</sub>O<sub>9</sub>). Most studies [106, 117–120] have reported the formation of combeite as the dominant crystalline phase as a result of heat treatment of the Bioglass<sup>®</sup> above 600°C. Further increase in the temperature, up to 800°C, may also result in the formation of a P-rich crystalline phase known as silicorhenanite (Na<sub>2</sub>Ca<sub>4</sub>(PO<sub>4</sub>)<sub>2</sub>SiO<sub>4</sub>) [96].

There has been always a dilemma associated with synthetic biomaterials: biomaterials which are mechanically stiff tend to be bioinert, whereas degradable biomaterials are normally relatively fragile. Chen et al. [98, 99] showed that combeite is a mechanically strong phase which can improve the overall stiffness of the bioactive 45S5 composition. Depending on the amount of combeite formed (i.e. the degree of crystallinity), bioactivity and stiffness of the Bioglass<sup>®</sup> can be tailored to suitable levels according to the requirements of target applications such as bone scaffolds and GICs [105, 121]. However, obtaining 45S5 glass-ceramic containing only combeite is challenging due to the possibility of the formation of a secondary crystalline phase during the heat treatment of 45S5 Bioglass<sup>®</sup> [96, 97].

The main focus of this study is to develop four controlled heat treatment profiles which can be used to tailor the crystallinity of 45S5 Bioglass<sup>®</sup> within a wide range of 5% to 100% via the formation of combeite as the only crystalline phase in the resulting glass-ceramic structures. We designed three of these heat treatment regimes (crystallinity from 5% to 95%) based on controlling the nucleation and growth temperatures and times of the combeite phase. The result of thermal analysis under various conditions are used to design these three heat treatment processes which are then verified by characterizing their resulting glass-ceramic products using various methods. The fourth regime adopted from the literature to achieve 100% crystallinity in the 45S5 Bioglass<sup>®</sup> [100].

## **3.2 Materials and Methods**

### **3.2.1 Materials**

The 45S5 Bioglass<sup>®</sup> used in this study was kindly donated by Dr. Robert Hill from Queen Mary University of London. The Bioglass<sup>®</sup> was produced via a melting-quenching process described elsewhere [119]. Briefly, all reactants were mixed and melted in a platinum/rhodium crucible at 1380 °C for 1 hour in an electric furnace followed by quenching in deionized water. After drying and re-melting the frit for 30 min., the resulting glass was ground using a vibratory mill (Gy-Ro mill, Glen Creston) for 7 min [119]. The as-received Bioglass<sup>®</sup> powder was analyzed by X-ray diffractometry (XRD) confirming its amorphous nature. Next, the glass powder was annealed at 460 °C for 8 h in order to remove any internal stresses that may be introduced during the grinding process [100]. Note that this temperature is below all phase transformation temperatures of 45S5 Bioglass<sup>®</sup> [97]. Hydrofluoric acid (Fisher Scientific) was used to prepare the etching solution.

### **3.2.2 Heat treatment processes**

Four heat treatment profiles were carried out on the Bioglass<sup>®</sup> to obtain a wide range of combeite crystallization from 5% to 100% crystallinity. The heat treatment processes were performed under ambient atmosphere using a quartz tube furnace (model: GSL-1100X) and alumina crucibles. After the heat treatment cycles were finished, the furnace was shut down and the samples were allowed to cool inside the furnace down to room temperature. As presented in Table 3.1, three heat treatment profiles were designed and used to obtain crystallinity range from 5% to 95% crystallinity which will be discussed further in section 3.1.1.

Table 3. 1. Heat treatment regimes designed in this study to induce various degrees of crystallinity in 45S5 Bioglass®.

Heat treatment regimes		Nucleation process		Growth process	
		Temperature	Dwell time	Temperature	Dwell time
Regime I	a	550 °C	2 min.	620 °C	2 min.
	b		1 h		
	c		3 h		
	d		6 h		
	e		12 h		
	f		24 h		
Regime II	a	550 °C	6 h	620 °C	5 min.
	b			640 °C	
	c			660 °C	
	d			680 °C	
Regime III	a	550 °C	6 h	680 °C	10 min.
	b				30 min.
	c				60 min.
	d				120 min.
Regime IV [100]		550 °C	150 h	680 °C	113 min.



In order to achieve 100% crystallinity, the Bioglass<sup>®</sup> was nucleated at 550 °C for 150 h followed by another heating cycle up to 680 °C for 113 min to induce crystallization [100]. A heating rate of 10 °C/min was used in both cases. The resulting materials was then lightly ground in a pestle and mortar to eliminate the agglomerated particles produced during the heat treatment process. The as-received and heat-treated powders were stored in a desiccator for subsequent characterization. Each heat treatment profile was performed on five different Bioglass<sup>®</sup> samples.

### 3.2.3 Characterization

The as-received Bioglass<sup>®</sup> powder, after annealing at 460 °C for 8 h, was examined by XRD, to confirm that the resulting powder was fully amorphous. Laser scattering particle size distribution analysis (PSA; Horiba LA-920) was used to measure the mean particle size and the particle size distribution of this powder. Isopropyl alcohol was used as the dispersant.

The heat treated Bioglass<sup>®</sup> powders were characterized by XRD (X'Pert Pro, PANalytical) using Cu K $\alpha$  radiation to identify the amorphous structures as well as the degree of crystallinity. The  $2\theta$  values were collected in the range of 20 to 120°, however only those parts of the pattern containing useful information are reported here ( $15^\circ < 2\theta < 65^\circ$ ). X'Pert HighScore Plus Rietveld analysis software [124] was used to analyze the XRD patterns. The crystal size is also estimated based on the XRD results using the Scherrer equation.

The thermal behavior of the Bioglass<sup>®</sup> and the glass-ceramics was also examined by differential scanning calorimetry (DSC; Setaram, Setsys 12) using 30 mg of powder and alumina crucibles. The DSC tests were conducted under nitrogen atmosphere at heating rates of 5, 7, 10, 15, and 20 °C/min. Also, the enthalpy of crystallization ( $\Delta H$ ) was computed using SETSOFT 2000.

The grain structure of the heat-treated particles was observed using a 3D optical microscope (VHX-5000). Samples were examined further by scanning electron microscopy (SEM; HITACHI, S-3400N) equipped with energy-dispersive X-ray spectroscopy (EDS; Oxford Instruments; Wave Model). Prior to the SEM/EDS examination, the powder samples were lightly ground, cold mounted, polished, and etched with 0.02% HF solution for 20 s. Variable pressure

mode was used for imaging with probe current, accelerating voltage and emission current set to 60  $\mu\text{A}$ , 15 kV and 78  $\mu\text{A}$ , respectively.

### 3.3 Results and discussion

Note that, based on the results of the particle size analysis, the mean particle size of the Bioglass<sup>®</sup> powder before the heat treatments was 4.6  $\mu\text{m}$  wherein 60% of the particles were in the range of 0.5 to 15  $\mu\text{m}$ .

#### 3.3.1 Thermal analysis

The DSC results for the Bioglass<sup>®</sup> powder obtained at five heating rates are shown in Fig. 3.1. Each DSC curve shows an endothermic peak corresponding to the glass transition temperature ( $T_g$ ), followed by an exothermic peak corresponding to the crystallization process with the onset temperature of  $T_c$  and crystallization peak temperature of  $T_p$  [106]. Note that increasing the heating rate shifts the glass transition and crystallization peaks to higher temperatures and also makes them more pronounced [109]; whereas it does not affect the  $T_c$  [120]. Higher heating rates provide atoms with less time to diffuse and rearrange, thus obtaining thermal equilibrium is delayed causing all phase transformations including glass transition and crystallization to occur at higher temperatures [121, 125]. All the characteristics temperatures as well as the enthalpy of crystallization ( $\Delta H$ ) obtained from these curves are presented in Table 3.2. The enthalpy of crystallization ( $\Delta H$ ) is the area under the crystallization peak on the curve of heat flow versus time [126]. The  $\Delta H$  values calculated for our systems are very close (mean =  $153 \pm 4$  J/g) and independent of heating rate which is consistent with literature [125, 126].

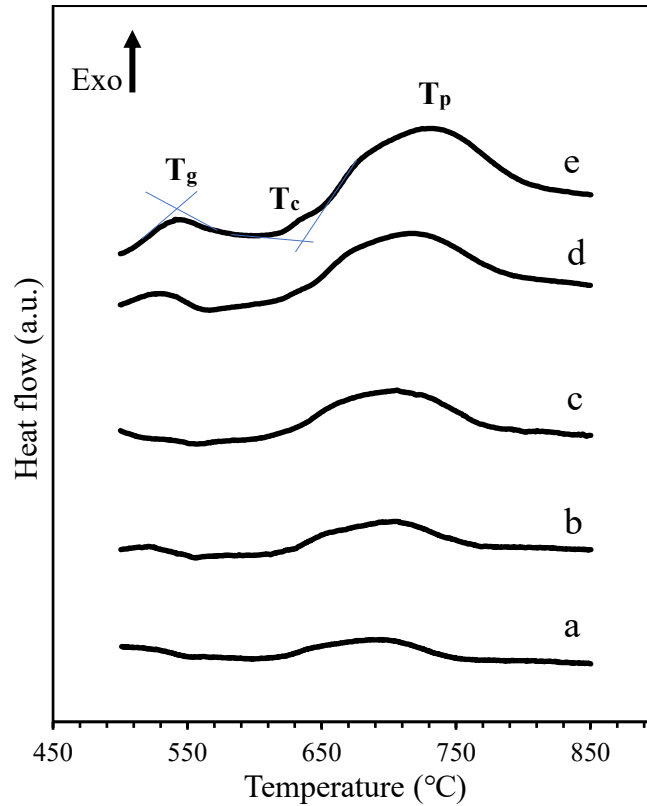


Fig. 3. 1. The results of DSC analyses on the Bioglass<sup>®</sup> powder (before heat treatment) at various heating rates of a) 5, b) 7, c) 10, d) 15, and e) 20 °C/min.

Table 3. 2. Characteristic temperatures obtained from the DSC graphs in Fig. 3.1.

Rate (°C/min.)	T <sub>g</sub> (°C)	T <sub>c</sub> (°C)	T <sub>p</sub> (°C)	ΔH (J/g)
5	539	620	694	149
7	545	621	704	156
10	549	622	706	153
15	553	625	714	159
20	556	626	725	150

Fig. 3.2 shows the results of the XRD analysis on the Bioglass<sup>®</sup> after heat treatment at various temperatures. No peak is observed in the pattern of the Bioglass<sup>®</sup> heat treated at 600 °C, whereas crystallization occurred by increasing the heat treatment temperature to 650 °C, which is consistent with the results obtained from the DSC analyses (Fig. 3.1). The crystallized phase formed in the Bioglass<sup>®</sup> heated at 650 °C and above is combeite. Also, according to Fig. 3.1a and Table 3.2, the onset of crystallization in our bioglass is around 620 °C which is consistent with the crystallization temperature of combeite reported in other works [96, 106, 107].

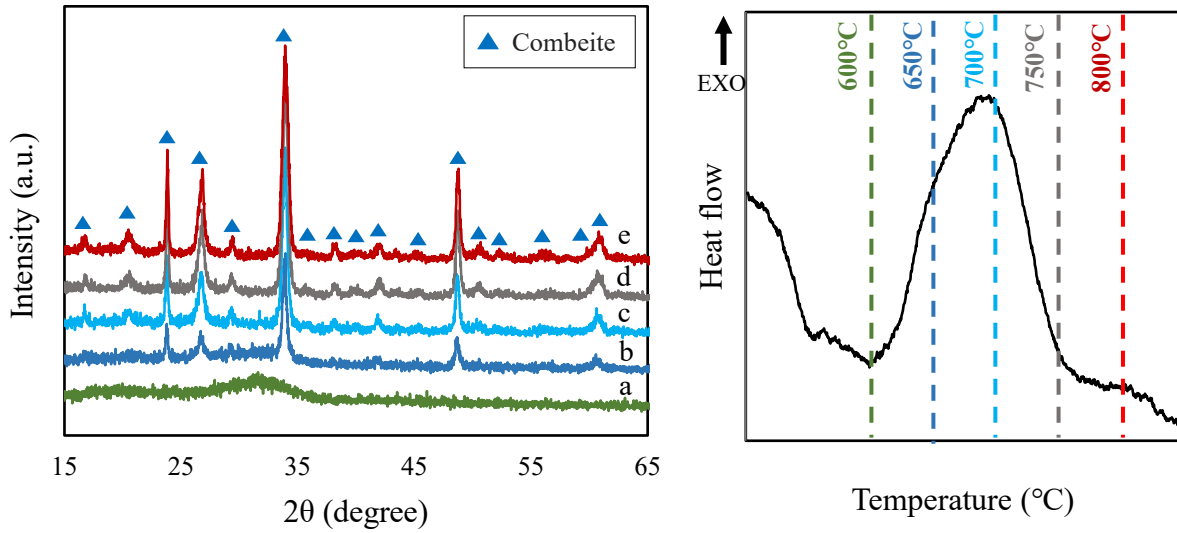


Fig. 3. 2. XRD patterns of the 45S5 Bioglass<sup>®</sup> heat treated up to various temperatures a) 600, b) 650, c) 700, d) 750, and e) 800°C. The corresponding DSC curve obtained at rate of 5°C/min.

(Fig. 3.1a) is also presented.

The XRD patterns containing crystalline peaks (Fig. 3.2 b, c, d and e) were used to obtain the crystallite size of combeite at various heat treatment temperatures using the Scherrer equation [122] applied to peaks with the highest intensity ( $2\theta \approx 34^\circ$ )

$$\beta = \frac{k \cdot \lambda}{\zeta \cdot \cos \theta} \quad \text{equation (1)}$$

where  $\beta$  is the width of the peak at half maximum (in radian),  $\zeta$  is the size of the crystallite (in meters),  $k$  is the Scherrer constant (0.89) and  $\lambda$  is the wavelength of the incident X-ray ( $1.5406 \times 10^{-10}$  m).

The crystal size of combeite calculated using Eq. (1) and the XRD patterns of Fig. 3.2 are summarized in Table 3.3. The results show that the size of the combeite crystals increases up to 27 nm by increasing the heat treatment temperature from 650 °C and 800 °C [96].

Table 3. 3. Combeite crystallite size in the heat treated Bioglass<sup>®</sup> calculated based on the XRD results using Eq. (1).

Heat treatment Temperature (°C)	650	700	750	800
Crystal size (nm)	21	17	15	27

The results obtained from the DSC curves, including the characteristic temperatures of the Bioglass<sup>®</sup> (Table 3.2), were used to design the heat treatments in section 3.1.1. The DSC results can be also used to calculate the activation energy for crystallization which is an important kinetic parameter indicating the thermal stability of the amorphous phases. In other words, it can quantitatively anticipate the phase transformation behavior during the heat treatment of the Bioglass<sup>®</sup> [126].

Here, we calculate the activation energy for crystallization (E) of our bioglass based on three methods using the information obtained from the DSC curve of 5 °C/min. (Fig. 3.2a). The Kissinger's method [123] is one of the most common approaches to calculate E via a linear correlation between  $1/T_p$  and  $(T_p^2/V)$ :

$$\ln\left(\frac{T_p^2}{V}\right) = \frac{E}{RT_p} + C \quad \text{equation (2)}$$

where V is the heating rate, C is a constant and R is the Boltzmann constant.

Another approach to calculate the activation energy for crystallization is the Ozawa's [124] which suggests E/R is the slope of  $\ln(V)$  as a function of  $1/T_p$  (Eq. 3).

$$\ln V = \frac{E}{RT_p} + C \quad \text{equation (3)}$$

Yinnon and Uhlmann [125] showed that E can be also determined by plotting  $\ln(T_p/V)$  as a function of  $1/T_p$  according to the following equation:

$$\ln\left(\frac{T_p}{V}\right) = \frac{E}{RT_p} + C \quad \text{equation (4)}$$

Using the information from Table 3.1 and 2, Eqs. 2 to 4 were plotted as linear regression for the Bioglass<sup>®</sup> and the activation energy for crystallization (E) of combeite is calculated. In all three numerical approaches the slope of the resulting line was used to calculate the activation energy for crystallization. Thus, the linearity of the outcome shows the precision of the calculation. The R<sup>2</sup> value for all three approaches is larger than 0.95. The three E values, 186, 198 and 192 kJ/mol obtained from the Kissinger, Ozawa and Yinnon methods, respectively are in a good agreement. The average of these three values is considered as the activation energy for crystallization of combeite for our bioglass which is then used to calculate the Avrami exponent as explain in the following paragraphs.

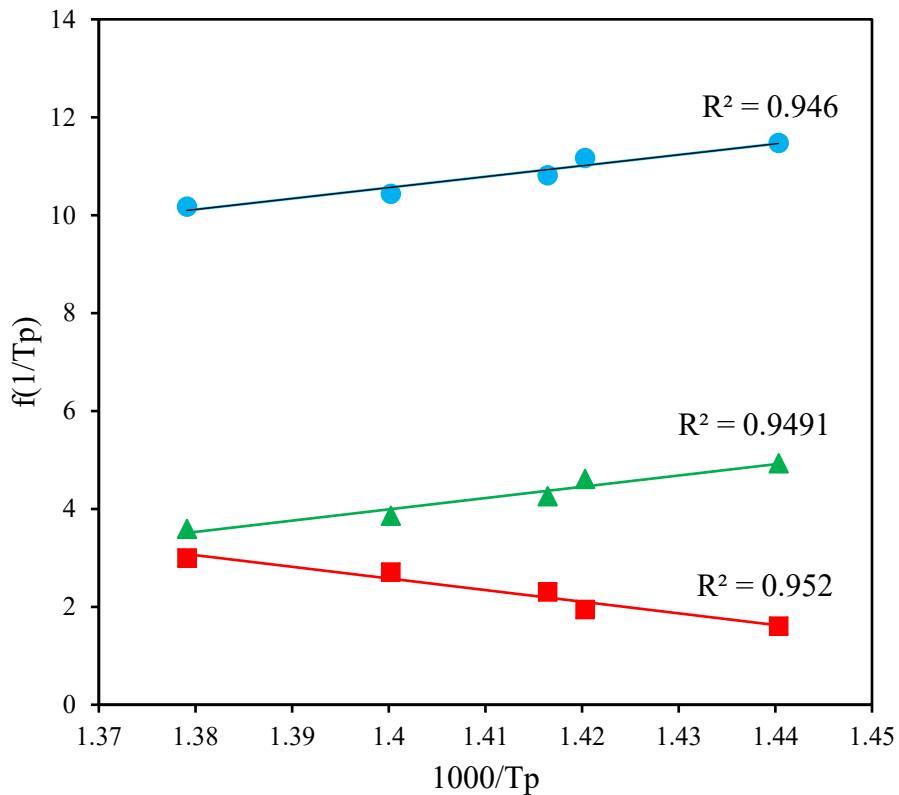


Fig. 3. 3. Kissinger ● , Ozawa ▲ , and Yinnon ■ plots for determining the activation energy for crystallization of combeite.

The mechanism of nucleation and growth of crystals can be defined by the Avrami exponent (n) which reveals whether the crystallization occurs mainly on the surface or within the bulk of the material [132, 133]. The Avrami exponent (n) is calculated using the following equation [123]:

$$n = \left( \frac{2.5}{\Delta T} \right) \frac{RT_p^2}{E} \quad \text{equation (5)}$$

where  $\Delta T$  is the width of the crystallization peak at half maximum and E value is considered as 192 kJ/mol as explained earlier. Thus, the Avrami exponent for our system is 0.71 which indicates that the crystallization of the combeite mainly occurs on the surface of the Bioglass<sup>®</sup> particles.

### 3.3.1.1 Heat treatment design

The process for designing our heat treatment regimes (Table 3.1) are explained as follows. A combination of three parameters, nucleation time, growth time and growth temperature, was used to obtain a wide range of crystallinity of combeite in the 45S5 Bioglass<sup>®</sup>. As explained before, the objective of this study was to have only combeite as a mechanically strong yet bioactive phase in the 45S5 glass-ceramics; thus, the nucleation temperature in all the heat treatment regimes was set at 550 °C which is the nucleation temperature of combeite [100]. In all heat treatment regimes, growth temperature ranged from 620 °C, which is the onset crystallization temperature of combeite (Table 3.2 and Fig. 3.2), to 680 °C above which the P-rich crystalline phase formed. Note that, the Avrami exponent calculated for our system is less than one which indicates that combeite nucleation occurred by a surface crystallization mechanism. Dominant surface nucleation and growth may be caused by relatively large surface area of the Bioglass<sup>®</sup> particles [106].

In order to obtain lower crystallinity values (up to 36%) in the Bioglass<sup>®</sup>, a short growth time of 2 min. was employed in heat treatment regime I (Table 3.2). Note that, various dwell times from 30 s to 5 min. were tested for the growth process of regime I, and 2 min. was selected as the

minimum time that delivered the results expected. Moreover, the lowest growth temperature for combeite, 620 °C [96], was used. The slow kinetic of combeite nucleation allows for maintaining the crystallinity within the low range of 5% to 36% using a wide range of nucleation times from 2 min. to 24 h (Table 3.1) combined with 2 min. of growth time.

The heat treatment regimes II and III were designed to achieve higher crystallinities (up to 95%) which for the role of crystal growth can be more significant than that of the nucleation process. Thus, the growth temperature of these two regimes varied between 620 and 680 °C [96] whereas their nucleation temperature and time were kept constant at 550 °C and 6 h, respectively. In order to achieve higher amounts of combeite, the growth time of regime III (10 min. to 120 min.) was increased in comparison with that of regime II (5 min.). The heat treatment regime IV was used to obtain a fully crystalline (100%) 45S5 containing only the combeite phase [100].

In the next section these heat treatment regimes are assessed and validated through calculating the crystallinity of their resulting heat treated 45S5 Bioglass<sup>®</sup> using their XRD patterns.

### 3.3.2 Degree of crystallinity

In this section, XRD patterns of the Bioglass<sup>®</sup> powder which was heat treated according to various regimes (Table 3.1) are presented. These patterns were then used to calculate the degree of crystallinity of the heat treated material using Eq. 6 [128]:

$$\text{Percent crystallinity} = \frac{I_g - I_x}{I_g - I_B} \times 100 \quad \text{equation (6)}$$

where  $I_g$  is the noncrystalline scattering intensities measured at a single value of  $2\theta$  for the parent glass (zero crystallinity);  $I_x$  is the intensity for the partly crystallized glass; and  $I_B$  is the intensity the crystalline compounds chemically equivalent to the parent glass. The angle ( $2\theta$ ) selected for this analysis must exhibit high noncrystalline scattering for the parent glass and is also free of crystalline scattering for both partly and fully crystallized glasses.



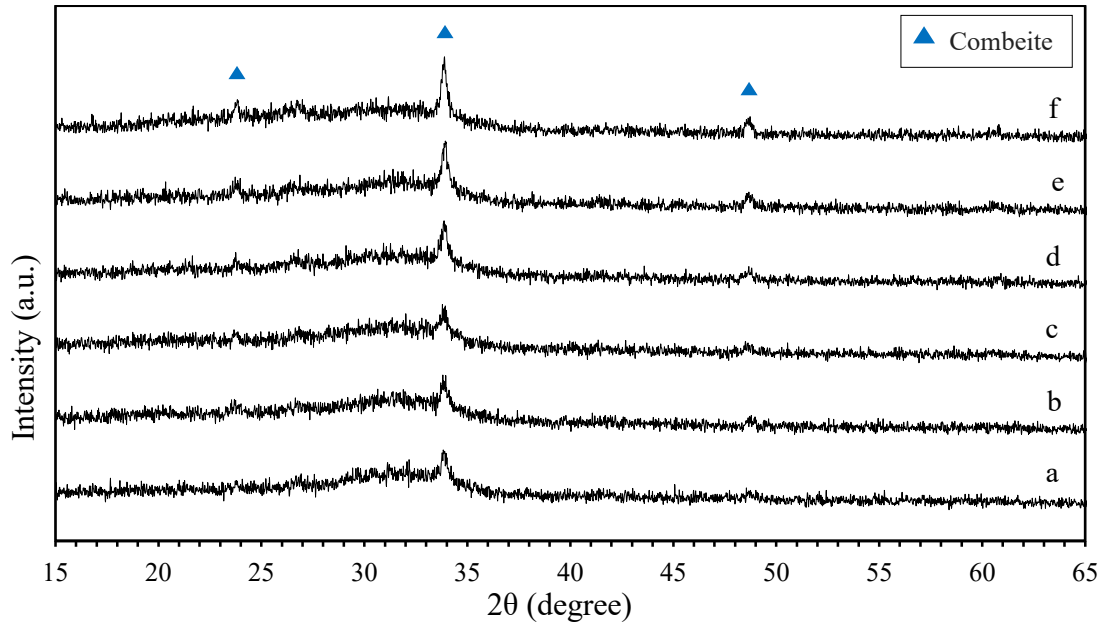


Fig. 3. 4. XRD patterns of the 45S5 Bioglass<sup>®</sup> heat treated via regime I (Table 3.1): Crystallization of combeite after a) 2 min., b) 1h, c) 3h, d) 6h, e) 12h, and f) 24h nucleation time at 550 °C followed by growth at 620 °C for 2 min. Note that patterns a to f correspond to the heat treatments a to f of regime I in Table 3.1.

The XRD patterns of the Bioglass<sup>®</sup> powder heat treated via regime I are presented in Fig. 3.4. Note that all peaks in these patterns correspond to combeite. By increasing the nucleation time, the intensity of the main peak at  $2\theta \approx 34^\circ$  increased and a second peak gradually appeared. Using Eq. (6) the degree of crystallinity corresponding to these patterns (a to f) is 5, 10, 16, 21, 29 and 36%, respectively.

The XRD patterns of the Bioglass<sup>®</sup> heat treated via regime II are presented in Fig. 3.5 showing more of the characteristic peaks of combeite with higher intensities compared to those of Fig. 3.4. As expected, the powders resulted from the heat treatment regime II have higher crystallinities (40, 57, 67 and 74%) than those produced via regime I.

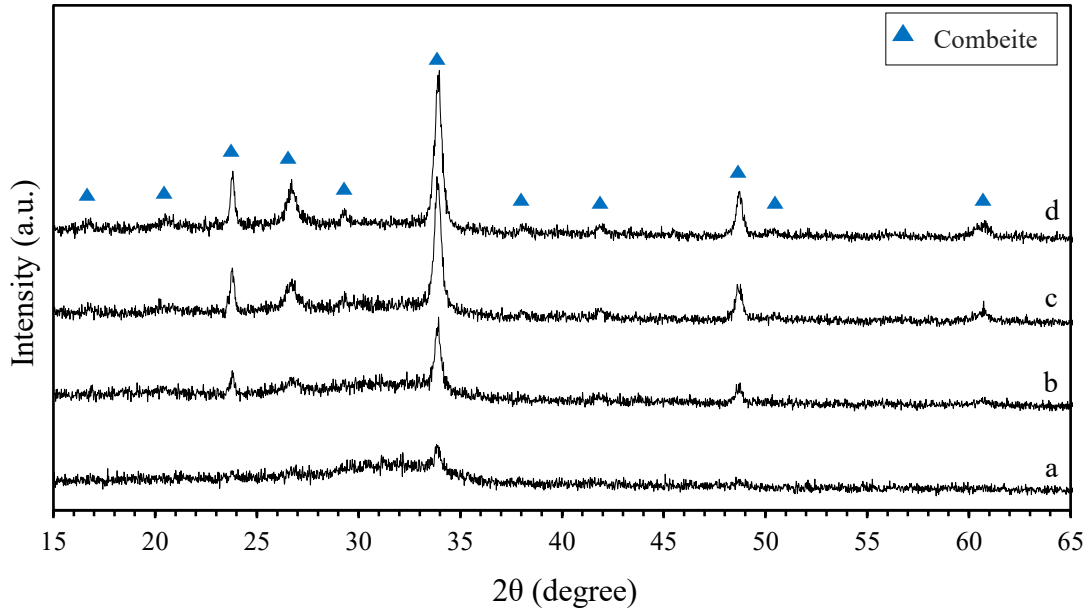


Fig. 3. 5. XRD patterns of the 45S5 Bioglass<sup>®</sup> heat treated via regime II (Table 3.1): Crystallization of combeite after 6h nucleation time at 550 °C followed by 5 min. growth time at a) 620, b) 640, c) 660, and d) 680 °C. Note that patterns a to d correspond to the heat treatments a to d of regime II in Table 3.1.

The XRD patterns of the Bioglass<sup>®</sup> powders heat treated regime III (Fig. 3.6 a to d) show that the crystallinity of these powders is respectively 84, 88, 91 and 95% which is higher than that of obtained from regime II (Fig. 3.5).

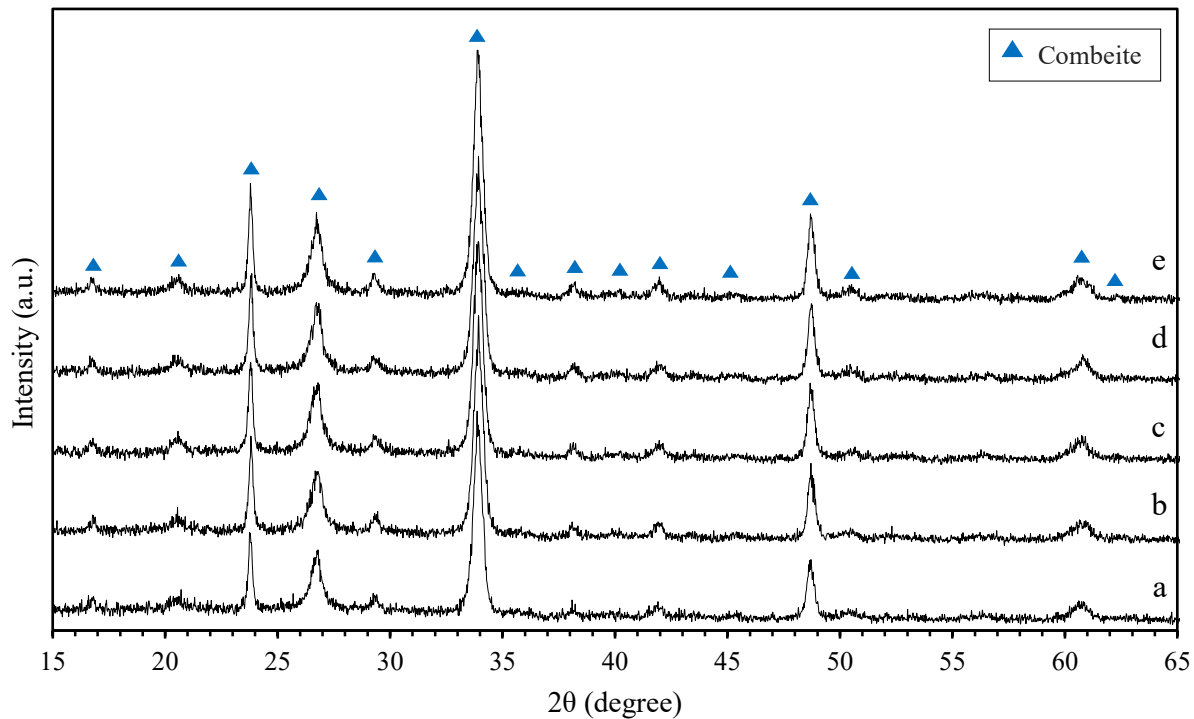


Fig. 3. 6. XRD patterns of the 45S5 Bioglass<sup>®</sup> heat treated via regime III and IV (Table 3.1): Crystallization of combeite after 6h nucleation time at 550 °C followed by a) 10, b) 30, c) 60, and d) 120 min. growth time at 680 °C. Note that patterns a to d correspond to the heat treatments a to d of regime III in Table 3.1. Pattern (e) which represents 100% crystallinity corresponds to the Bioglass<sup>®</sup> heat treated via regime IV.

The 100% crystallinity is achieved using the heat treatment route proposed by Hench [100] which involves a nucleation at 550 °C for 150 h followed by crystallization and growth at 680 °C for 113 min.

Fig. 3.7 summarizes the crystallinity of the 45S5 glass-ceramics heat treated via regime I, II, III and IV. As shown in this figure, a wide range of crystallinity can be developed using the heat treatment processes designed in this study which provides the opportunity of selecting the 45S5 glass-ceramic with appropriate crystallinities for a particular target application.

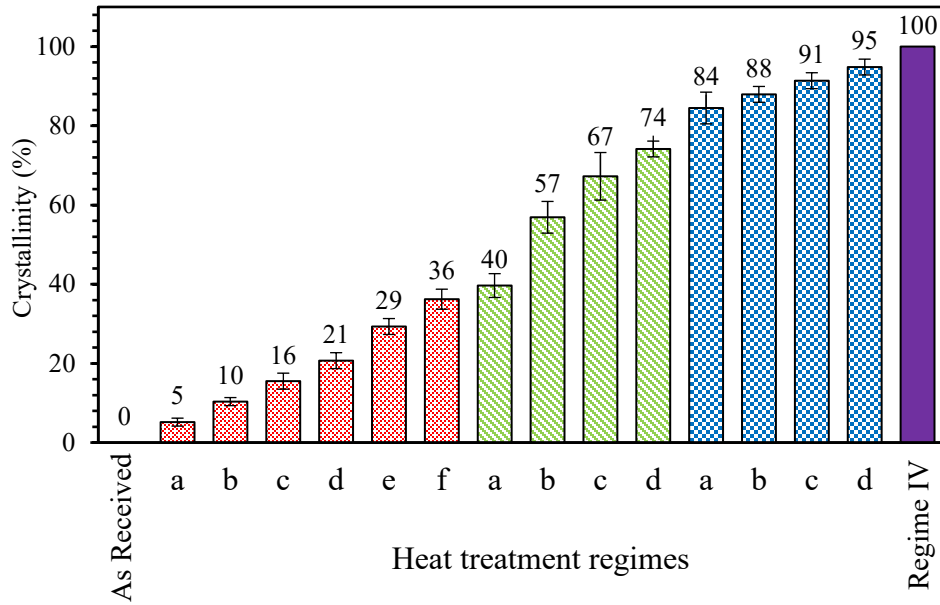



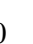


Fig. 3. 7. Crystallinity of the 45S5 glass-ceramics heat treated via regime I , II , III  and IV . The letters a to f on the X-axis correspond to those letters in Table 3.1 by which the heat treatments in each regime are denoted.

### 3.3.3 Microstructures

As an example, the microstructure of one of the heat-treated glass-ceramics with 74% crystallinity, obtained from regime II (Fig. 3.7), was examined and is discussed in this section. The micrographs of these glass-ceramic particles are presented in Fig. 3.8. The grain microstructure of the particles after etching was observed by optical microscopy and examined further by SEM.

After nucleation of combeite phase, grains start to grow which eventually leads to Oswald ripening wherein larger grains grow in expense of the smaller grains [96]. As a result of surface crystallization predicted by the Avrami exponent ( $n=0.71$ ), the etched combeite grains observed on the surface of the particles (Fig. 3.8 b, d and e) were the result of partial dissolution of the amorphous phase trapped between the grains, which is less chemically stable than combeite [113].

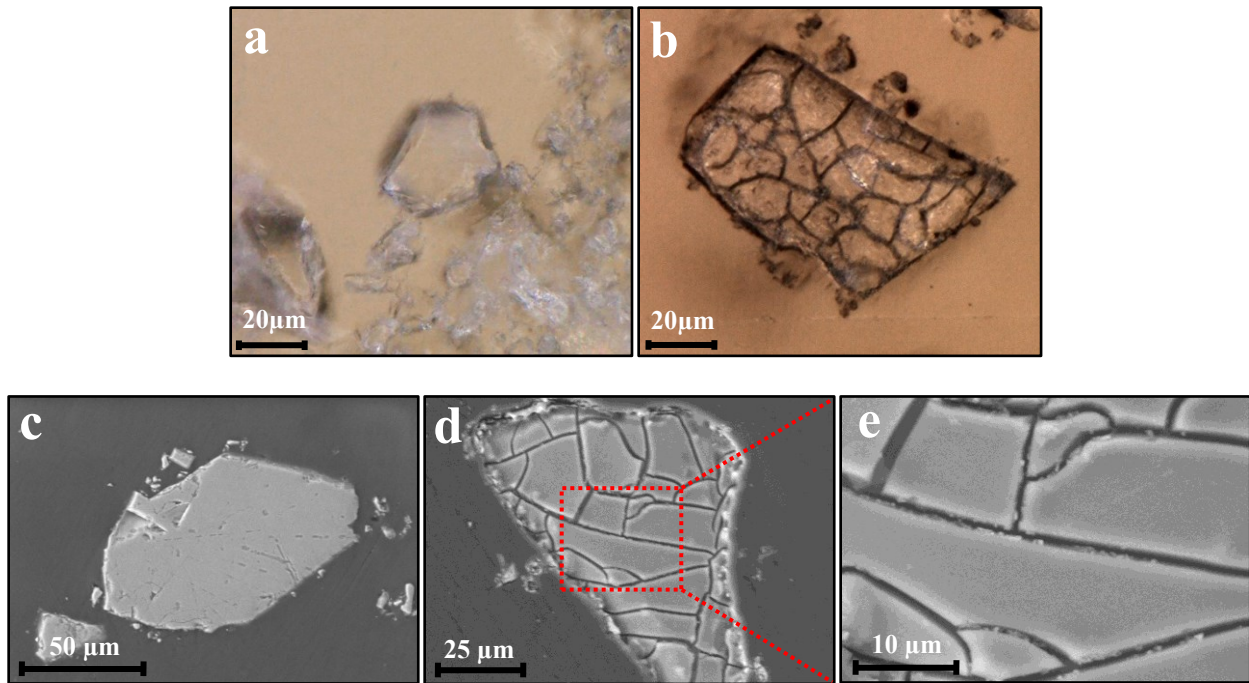


Fig. 3. 8. Optical microscopy images of the heat-treated glass-ceramic with 74% crystallinity before (a) and after (b) etching showing the transparency of the particles in both states. SEM images of the glass-ceramic particles before (c) and after (d and e) the etching. These SEM images were captured from larger particles to better show the grains and boundaries. Note that, the results of EDS analysis on a similar glass-ceramic sample are presented in Fig. 3.9.

The two glass formers, Si and P [129], in 45S5 Bioglass<sup>®</sup> separate into two glassy phases, a Si-rich and a P-rich, at around 580 °C [96]. The higher viscosity of the Si-rich phase governs the flow behavior of the resulting phase separated system. As the temperature increases to 620 °C, combeite crystallizes from the Si-rich phase at its interface with the P-rich phase. The high energy interface between these two glasses creates suitable nucleation sites for combeite crystallization [97]. The P-rich phase remained amorphous since silicorhenanite ( $\text{Na}_2\text{Ca}_4(\text{PO}_4)_2\text{SiO}_4$ ) only crystallizes at 800 °C [96, 97]. At these low temperatures, the combeite crystals continue to grow, while rejecting P and enriching the P-rich amorphous phase. This ultimately results in combeite crystallites surrounded by a P-rich glassy phase. This discussion is also confirmed by the compositional analysis performed on the etched samples (Fig. 3.9) as explained in the following.

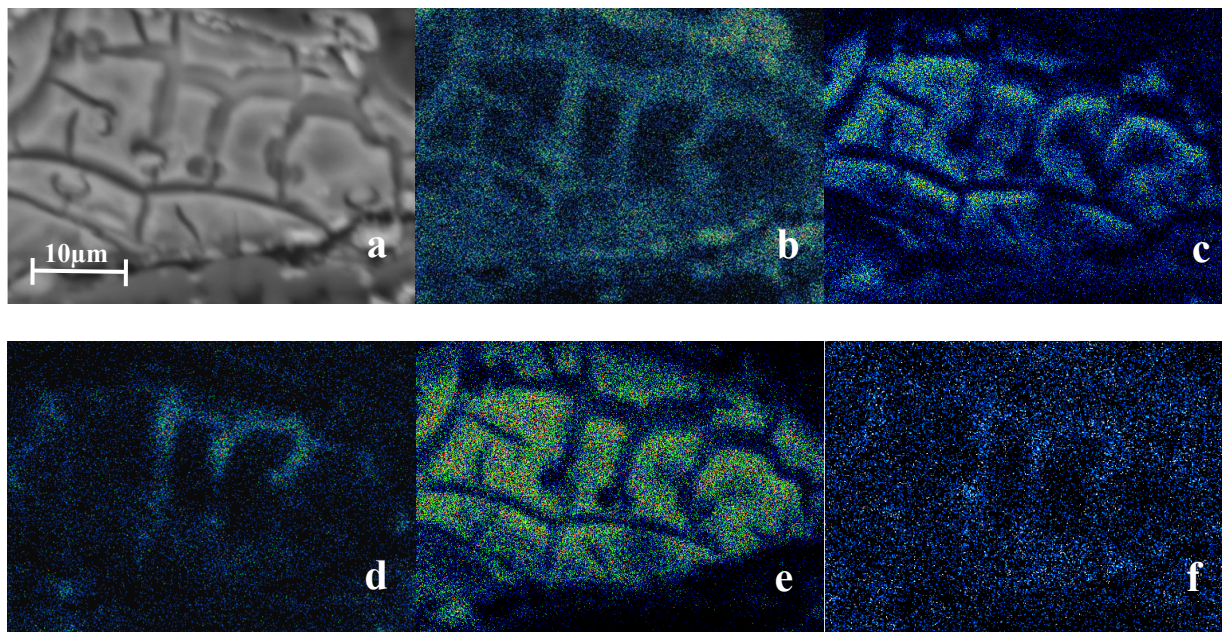


Fig. 3. 9. a) SEM image of the etched Bioglass<sup>®</sup> with 74% crystallinity, along with corresponding X-ray map analysis for various elements: b) Ca, c) O, d) Na, e) Si, and f) P.

The results of X-ray mapping analysis revealed two distinct elemental distribution patterns within and between the grains. Fig. 3.9 e and c, respectively, show high concentrations of Si and O within the grains indicating that these grains correspond to combeite ( $\text{Na}_2\text{CaSi}_3\text{O}_9$ ). On the other hand, considerable concentrations of Ca and P are observed between the grains (Fig. 3.9 b and f). Thus, the intergranular region between the combeite crystals is the P-rich amorphous phase which was preferentially dissolved during etching due to its lower chemical stability compare to combeite. This confirms that the combeite grains on the surface (Fig. 3.8) were surrounded by the P-rich phase prior to the etching as discussed above [113].

### 3.4 Conclusion

In this study, we introduced a comprehensive set of heat treatment regimes providing the possibility of tailoring the crystallinity of 45S5 Bioglass<sup>®</sup> between 5% and 95% by controlling the nucleation and growth of combeite as the only crystalline phase formed in this system. The heat treatment profiles were developed based on the results of DSC and XRD analyses on a melt-

derived 45S5 Bioglass<sup>®</sup> powder. These results were also used to calculate the crystallization energy for and obtain the Avrami exponent of combeite which were then used to discuss its crystallization mechanism. It was shown that the combeite crystallization mostly occurred on the surface of the particles which was also confirmed by the SEM/EDS results.

45S5 glass-ceramics containing combeite as the sole crystalline phase are known to have improved mechanical properties while maintaining desirable levels of bioactivity. Such glass-ceramics with appropriate degree of crystallinity for specific applications such as bone regeneration and additives for dental restoratives can be produced using the results presented in this study.

## **Acknowledgment**

Funding provided by NSERC under the Discovery Grants program and Concordia University. The authors gratefully thank Prof. Robert Hill (Barts and The London School of Medicine and Dentistry) for providing the melt derived 45S5 Bioglass<sup>®</sup> for this work.

## Chapter 4

# Glass ionomer cements with enhanced mechanical and remineralizing properties containing 45S5 Bioglass<sup>®</sup>-ceramic particles<sup>1</sup>

Alireza Zandi Karim <sup>a</sup>, Ehsan Rezabeigi <sup>b</sup>, and Robin A.L. Drew <sup>a</sup>

<sup>a</sup> Department of Mechanical, Industrial and Aerospace Engineering (MIAE), Concordia University, Montréal, Quebec H3G 1M8, Canada.

<sup>b</sup> Department of Mining and Materials Engineering, McGill University, Wong Building, 3610 Rue University, Montréal, Quebec H3A 0C5, Canada.

**Abstract.** The clinical applications of glass ionomer cements (GICs) are limited by their relatively poor mechanical properties and insufficient remineralizing capacity. In this study, we produced hybrid GICs with improved mechanical and remineralizing properties via incorporation of an optimum amount (5 wt%) of 45S5 Bioglass<sup>®</sup>-ceramic particles. Also, we found that Bioglass<sup>®</sup>-ceramic particles with 74% crystallinity best act as both remineralizing and reinforcing agents. The degree of crystallinity of the additives, is completely overlooked in this context in other research. At around 74% crystallinity, there is sufficient amounts of combeite and an amorphous phosphorous-rich phase in the 45S5 Bioglass<sup>®</sup>-ceramic particles to respectively promote their reinforcing role and simultaneously allow them to effectively partake in the setting process creating an excellent interfacial bond with the GIC matrix. As a result, several strengthening mechanisms such as crack deflection and crack-tip shielding are activated within the hybrid GIC containing 5 wt% Bioglass<sup>®</sup>-ceramic with 74% crystallinity, contributing to its improved mechanical properties. The enhanced remineralizing and mechanical properties of such hybrid GICs can potentially improve their *in vivo* performance and broaden their clinical applications.

**Keywords:** Glass ionomer cements, Mechanical properties; 45S5 Bioglass<sup>®</sup>-ceramic; Remineralization; Crystallinity

---

<sup>1</sup> This chapter is published as: A. Zandi Karimi, E. Rezabeigi, and R. A. L. Drew, “Glass ionomer cements with enhanced mechanical and remineralizing properties containing 45S5 bioglass-ceramic particles,” *J. Mech. Behav. Biomed. Mater.*, vol. 97, pp. 396–405, 2019.



## 4.1 Introduction

Glass ionomer cements (GICs), first invented in 1972 by Wilson and Kent [130], are the family of biomaterials which are extensively used in clinical dentistry and bone replacement [19, 131]. GICs are the result of an acid-base reaction between an aqueous solution of polyalkenoic acid (either polyacrylic acid or acrylic/maleic acid copolymer) and an aluminosilicate glass powder [132]. The acid component attacks the glass particles resulting in the release of  $\text{Ca}^{2+}$  and  $\text{Al}^{3+}$  which then leads to the crosslinking of polymeric acid chains generating insoluble polysalts causing the cement to harden [133]. This hardening process gradually continues even after setting while the material becomes more translucent [19]. This post maturation process eventually leads to the formation of a silica gel layer around the glass particles during setting which detains further degradation [134].

GICs are known for their good biocompatibility, lack of exothermic polymerization, ability to make direct chemical bonds to teeth or bones, negligible shrinkage upon setting and chemical and mechanical stability in aqueous environment [135, 136]. GICs release  $\text{Ca}^{2+}$  and  $\text{PO}_4^{3-}$  *in vivo* which are the main constituents of hydroxyapatite (HA) that predominantly forms the inorganic portion of teeth and bones [19]. GICs also release  $\text{F}^-$  *in vivo* which not only promotes the growth of dental hard tissues when applied in appropriate dosage, but also is a well-documented anticariogenic agent for teeth [137, 136]. This is due to the fact that  $\text{F}^-$  forms fluorapatite ( $\text{Ca}_5(\text{PO}_4)_3\text{F}$ ) via reacting with the hydroxyl group of HA. Fluoroapatite is thermodynamically more stable than HA and has higher resistance against plaque acid attack [133].

Despite all these advantages, GICs suffer from insufficient mechanical properties (e.g. strength and toughness) [138] limiting their permanent clinical use in load-bearing locations [138, 139]. Efforts have been made to overcome this limitation by modifying the chemical composition of the aluminosilicate glass [134, 140] or the polyalkenoic acid [141, 142] as well as other approaches including the incorporation of reinforcing agents into GICs such as glass fibers [139] or metallic oxide particles [140]. The incorporation of reinforcing particles can trigger various strengthening mechanisms in GICs such as crack deflection, crack branching, crack-tip shielding and particle pull-out [145, 146]. There is a growing interest to improve the long-term mechanical properties of GICs through incorporation of bioactive materials (e.g. bioactive glasses) [58, 60, 61] which can

also promote their remineralization capacity in atraumatic restorative treatment (ART) [141]. By promoting the formation of HA (mineralization) within GICs containing bioactive particles due to the release of Ca and PO<sub>4</sub> ions, the interfacial adhesion between the cement and the native tissue(s) is improved via stronger chemical bonding. The development of GICs with enhanced mechanical and remineralizing properties can significantly improve their performance and broaden their potential applications.

In the context of dental materials, it has been recently suggested to limit the term “bioactive” only to those materials that can lead to certain biomineralization within their clinical environment via the release of substantial amounts of ions [142]. According to this statement, GICs can be considered as bioactive, because they are able to leach ions through dissolution of calcium aluminosilicate glass particles which can potentially promote the interaction of GICs with the HA of dentin. However, their bioactivity can be improved and exploited by the incorporation of bioactive glasses. If the added bioactive glass converts to HA in a controlled fashion and time, the dental hard tissues underneath the restoration can benefit from the resulting interfacial biomineralization and adhesion [142]. The addition of various bioactive glasses with different particle sizes into GICs has resulted in different outcomes [21, 63, 65, 150]. Yli-Urpo et al. [143] reported that, the incorporation of commercially available bioactive glass S53P4 into a conventional GIC reduced the compressive strength of the cements on average by 54%, while they showed its antimicrobial effects on both *S. mutans* and *C. albicans* [144]. However, Kim et al. [63] showed that incorporation of bioglass nanoparticles (85 mol% SiO<sub>2</sub>, 15 mol% CaO) into GICs increased their mechanical properties including compressive, diametral tensile and flexural strength as well as in vitro biomineralization. Also, Valanezhad et al. [21] exhibited that the addition of 3 and 5 wt% nanoparticles of a sol-gel derived bioactive glass (70 mol% SiO<sub>2</sub>, 30 mol% CaO) enhanced flexural strength of their resin modified glass ionomer cements (RM-GIC) up to 70% and 5%, respectively.

45S5 Bioglass<sup>®</sup> (45 wt.% SiO<sub>2</sub>, 24.5 wt.% Na<sub>2</sub>O, 24.5 wt.% CaO, 6 wt.% P<sub>2</sub>O<sub>5</sub>), which was first invented by Hench in late 1960's [95, 151], is known for its high bioactivity index [107] as well as its desirable antimicrobial properties [145]. However, Bioglass<sup>®</sup> that belongs to the most bioactive category of materials [146], normally exhibit inferior mechanical properties; thus, as an additive, it may diminish the compressive strength and microhardness of GICs [61]. Transformation of Bioglass<sup>®</sup> into a glass-ceramic through controlled thermal treatments, can

enhance its mechanical properties promoting its dual role as a remineralizing and reinforcing agent [95, 98, 100]. Heat treatments of 45S5 Bioglass<sup>®</sup> above 600 °C can result in formation of a mechanically strong phase named combeite ( $\text{Na}_2\text{Ca}_2\text{Si}_3\text{O}_9$ ) [98]. Such glass-ceramics containing combeite maintain their bioactivity and potentially convert to HA in a controlled manner and time while exhibiting improved mechanical properties [148, 149].

In this study, hybrid GICs containing various amounts of 45S5 Bioglass<sup>®</sup>-ceramic with crystallinities between 5% to 100% are developed; and the hybrid GICs leading to the best mechanical properties are identified. We show that, the incorporation of 5 wt% Bioglass<sup>®</sup>-ceramic particles with 74% crystallinity improves the mechanical properties of GICs by acting as reinforcing agent and simultaneously inducing mineralization within the cements.

## **4.2 Materials and Methods**

### **4.2.1 Bioglass<sup>®</sup> synthesis and heat treatment**

The 45S5 Bioglass<sup>®</sup> used in this work was kindly donated by Dr. Robert Hill from Queen Mary University of London. The synthesis process of this Bioglass<sup>®</sup> was explained elsewhere [119]. In brief, high purity precursors in the form of powder were weighed and mixed according to the 45S5 Bioglass<sup>®</sup> formula. This powder mixture was melted in a platinum/rhodium crucible at 1380°C for 1 h using an electric furnace followed by quenching in deionized water. The frit was then dried and re-melted for 30 min. followed by grinding for 7 min. using a vibratory mill [119].

The as-received Bioglass<sup>®</sup> powder was annealed for 8 h at 460 °C (mean particle size = 4.6  $\mu\text{m}$ ) to remove any internal stress created during the grinding process [100]. Although, 460 °C is below all the phase transformation temperatures of 45S5 Bioglass<sup>®</sup> [95, 96], the amorphous nature of the powder was verified by X-ray diffraction (XRD).

In this study, partially crystallized 45S5 Bioglass<sup>®</sup> (Bioglass<sup>®</sup>-ceramic) containing combeite was used. Four heat treatment profiles were used to obtain a wide range of crystallinities in the Bioglass<sup>®</sup> from 5% to 100% [95]. All the heat treatments were performed under atmosphere using a quartz tube furnace (GSL-1100X) and alumina crucibles. Note that these heat treatment profiles

are explained in detail in our previous study [95]. To eliminate the potential agglomerates produced during these heat treatments, the resulting powders were lightly ground in a pestle and mortar.

#### **4.2.2 Cement preparation**

The GIC capsules used in this study were obtained from ChemFil™ Rock Dentsply, Germany [147]. Each capsule contained a certain ratio of a calcium-aluminum-zinc-fluoro-phosphor-silicate glass powder to a liquid ionomer (polycarboxylic acid and tartaric acid) [147]. In order to incorporate our bioglass-ceramic into the GICs (i.e. to produce the hybrid GICs), the plunger was removed from the capsule and various portions of its original glass content were replaced (2, 5, 10, 15 and 20 wt%) with our 45S5 Bioglass®-ceramic with 74% crystallinity. Note that, Bioglass®-ceramic particles with 74% crystallinity can result in GICs with the highest mechanical properties, based on the results presented in section 3.1. Next, the two powders were mixed well using a Coulter mixer for 30 min. to reach homogeneity. The GIC capsule was then refilled with the resulting mixed powder and the plunger was reinserted. After activating the capsule, which initiated the reaction between the mixed powder and the ionomer liquid, it was immediately placed in a capsule mixer (HL-AH G5 Amalgamator) at 4000 rpm for 20 sec. The resulting material was then injected into cylindrical shaped silicone molds. Note that, all the samples were prepared at room temperature ( $21 \pm 2$  °C) throughout the whole process. Next, the cements were gently removed from the silicon molds and stored in an incubator at  $37 \pm 1$  °C for 1 h. Subsequently, each cement was individually immersed in distilled water and stored again in the incubator at  $37 \pm 1$  °C for 1 d or 7 d prior to the compression, diametral tensile and microhardness tests ( $n = 6$ ). Note that, the samples were randomly allocated to test groups [148, 149].

#### **4.2.3 Mechanical testing**

A series of preliminary compression, diametral tensile and microhardness tests ( $n = 6$ ) were carried out on the hybrid GIC specimens containing 5 wt% Bioglass®-ceramic with various crystallinities (5% to 100%) to determine the optimum degree of crystallinity that leads to the highest mechanical performance. Then, five groups of hybrid GICs containing 2, 5, 10, 15 and

20 wt% Bioglass<sup>®</sup>-ceramic with this optimum crystallinity (74%) as well as commercial GIC samples were analyzed for each mechanical test as described in the following sections.

#### 4.2.3.1 Compressive strength

Compression tests were carried out according to ISO 9917-1 for powder/liquid acid based cements [51]. Cylindrical GIC specimens ( $D = 4 \text{ mm}$  and  $h = 6 \text{ mm}$ ) were made by casting the final mixture into silicone molds. The tests were performed using an Instron 3382 Universal Testing Machine with a 5 kN load cell at a crosshead speed of 0.5 mm/min until failure occurred. The samples were placed with their flat sides in contact with the plates as shown in Fig. 4.1. The compressive strength was then calculated using the following equation:

$$CS = \frac{4P}{\pi D^2} \quad \text{eq (1)}$$

where CS is the compressive strength (MPa), P is the maximum applied load (N) and D is the diameter of the specimen (mm).

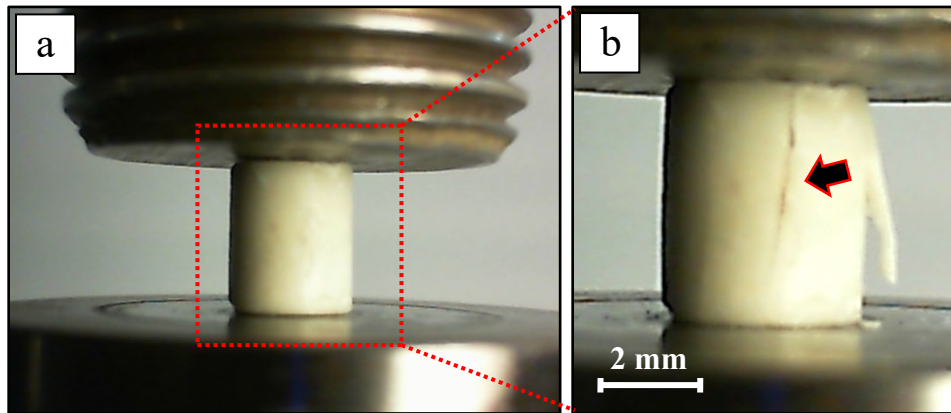


Fig. 4. 1. Measuring the compressive strength of a GIC specimen before (a) and after (b) failure (the crack formed within the sample is indicated by the arrow).

The fracture surface of the GICs after the compression test was examined using a scanning electron microscope (SEM; HITACHI, S-3400N) under high vacuum mode with the probe current, accelerating voltage and emission current set to 60  $\mu\text{A}$ , 15 kV and 78  $\mu\text{A}$ , respectively. Prior to

SEM, all specimens were coated with Au/Pd (70/30 wt %) using a rotary-pumped sputter coater (Quorum, Q150R ES).

#### 4.2.3.2 Diametral tensile strength (DTS)

This is an alternative approach for testing brittle materials under tension without using grips. The diametral tensile samples were prepared (Fig. 4.2 a and b) in compliance with ISO 9917-1 for powder/liquid acid based cements [51] with the exception of sample dimensions. Cylindrical specimens ( $D = 2 \text{ mm}$  and  $h = 4 \text{ mm}$ ) were again made by casting the final mixture into silicone molds. As schematically shown in Fig. 4.2c, the specimens were placed diametrically between the plates of the Universal Testing Machine. DTS (in MPa) were then calculated using the following equation:

$$DTS = \frac{2P}{\pi DL} \quad \text{eq (2)}$$

where P, D and L are the maximum applied load (N), the diameter of the specimen (mm) and the height of the specimen (mm), respectively. In spite of the compressive stress at the surface, cements fail in tension along the highly stressed diameter (Fig. 4.2c).

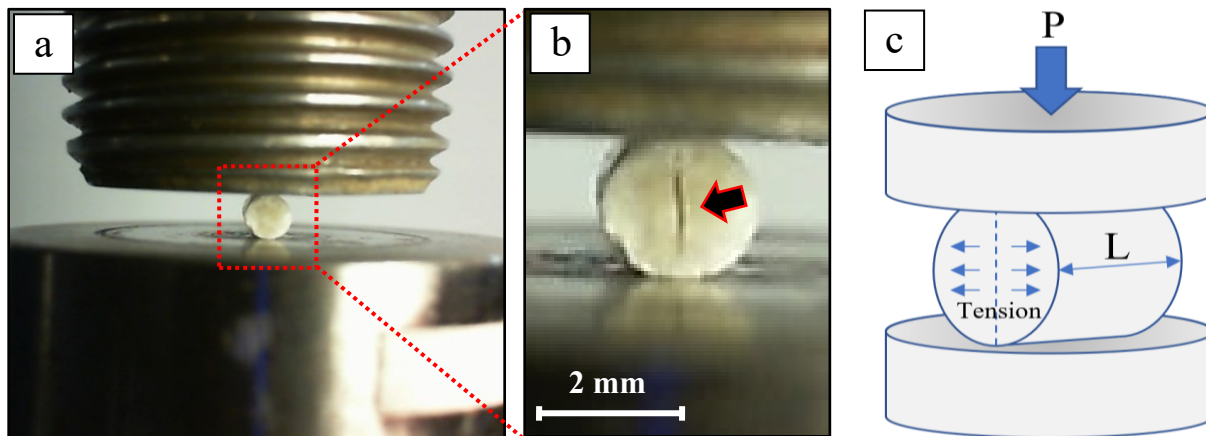


Fig. 4. 2. Measuring the DTS of a GIC specimen before (a) and after (b) failure (the crack formed within the sample is indicated by the arrow) as well as the schematic of the diametral tensile test (c).

#### 4.2.3.3 *Microhardness*

The Vickers microhardness of the GIC samples were measured using a microhardness tester (Mitutoyo MVK-H1). For each measurement, a 50 gf load was applied on the samples for 30 s. The microhardness value reported here for each GIC is the average of six measurements.

#### 4.2.4 **In vitro studies in simulated body fluid (SBF)**

SBF (pH = 7.4) was prepared according to the protocol outlined by Kokubo et al. [148] and stored in a fridge at 4 °C up to one month. Based on the results of the compression, diametral tensile and microhardness tests, two sets of GICs exhibiting the best mechanical properties (5 wt% Bioglass<sup>®</sup>-ceramic content) and where the mechanical properties drop (10 wt% Bioglass<sup>®</sup>-ceramic content), were selected for the SBF studies. For this purpose, cylindrical specimens (D = 4 mm and h = 6 mm) were prepared as explained in section 2.3.1 and stored at  $37 \pm 1$  °C for 1 h. Each GIC specimen was then immersed into 25 ml of SBF at  $37 \pm 1$  °C for various time periods of 1 d, 3 d, 7 d and 14 d. The SBF was refreshed every 2 days for all systems except for those used to monitor the change in pH of the SBF media (n = 3) using a digital pH meter (Hanna; HI 9126). At the end of each period of time, the GIC specimens were gently rinsed with distilled water and dried in a desiccator at room temperature for up to 2 d.

The hybrid GICs containing 5 wt% and 10 wt% Bioglass<sup>®</sup>-ceramic (74% crystallinity) before and after 14 d immersion in SBF were further characterized using a Fourier-Transform Infrared Spectrometer (FTIR; NEXUS 670 FT-IR) between 650 and 4000 cm<sup>-1</sup>. Also, the commercial GIC after 14 d immersion in SBF as well as the hybrid GICs containing 5 wt% Bioglass<sup>®</sup>-ceramic (74% crystallinity) after 7 d and 14 d immersion in SBF were analyzed by XRD (PANalytical X'Pert Pro) using Cu K $\alpha$  radiation ( $15^\circ < 2\theta < 90^\circ$ ). Note that, only the portions of the XRD patterns and FTIR spectra containing useful information are presented here. Also, the morphology of the cements after immersion in SBF was examined by SEM.

## 4.3 Results and Discussions

### 4.3.1 Optimum degree of crystallinity

As explained in section 2.3, in order to determine the degree of crystallinity of 45S5 Bioglass<sup>®</sup>-ceramic leading to the highest mechanical properties in GICs, a series of preliminary experiments were carried out. Fig. 4.3 presents the results of the compression, diametral tensile and microhardness tests on the GICs containing 5 wt% Bioglass<sup>®</sup>-ceramic particles with various degrees of crystallinity. As indicated in this figure, GICs containing Bioglass<sup>®</sup>-ceramic particles with 74% crystallinity exhibit a peak in their mechanical properties. Thus, the 45S5 Bioglass<sup>®</sup>-ceramic with 74% crystallinity was selected to be incorporated into GICs in this study.

The mechanical properties of these hybrid GICs depend on the mechanical properties of the Bioglass<sup>®</sup>-ceramic particles as well as their interfacial adhesion with the matrix both of which combined appear to simultaneously reach an optimum at ~74% crystallinity. There is an amorphous phosphorous-rich (P-rich) phase in this Bioglass<sup>®</sup>-ceramic [95], which has less chemical stability than that of the combeite phase, that may react more readily with the polymeric acid of the GIC; similar to that of the original glass of the GIC. As a result of this reaction, Ca<sup>2+</sup> ions can also leach out of this P-rich phase and partake in the formation of polysalts and the hardening process (i.e. setting), improving the interfacial adhesion and integration between the Bioglass<sup>®</sup>-ceramic particles and the GIC matrix. It was previously shown that bioactive materials containing Ca and a high amount of non-bridging oxygens (e.g. Bioglass<sup>®</sup>) are able to react with the polymeric acid of GICs [62, 157]. In general, the addition of 45S5 Bioglass<sup>®</sup> into a conventional GIC interferes with the setting reaction and competes with the ionomer glass. The high sodium content of Bioglass<sup>®</sup> results in the release of sodium in the polysalt matrix and premature hydrolytic stability and poor cement mechanical properties. Heat treating the 45S5 Bioglass<sup>®</sup> to increase its crystallinity, as conducted in this study, reduces its solubility and reactivity overcoming the aforementioned problems [62, 157]. Thus, it can be concluded that, 45S5 Bioglass<sup>®</sup>-ceramic with 74% crystallinity may contain an optimum balance of combeite and P-rich phase contributing to the improved mechanical properties of the particles and their interfacial adhesion with the GIC matrix, respectively.



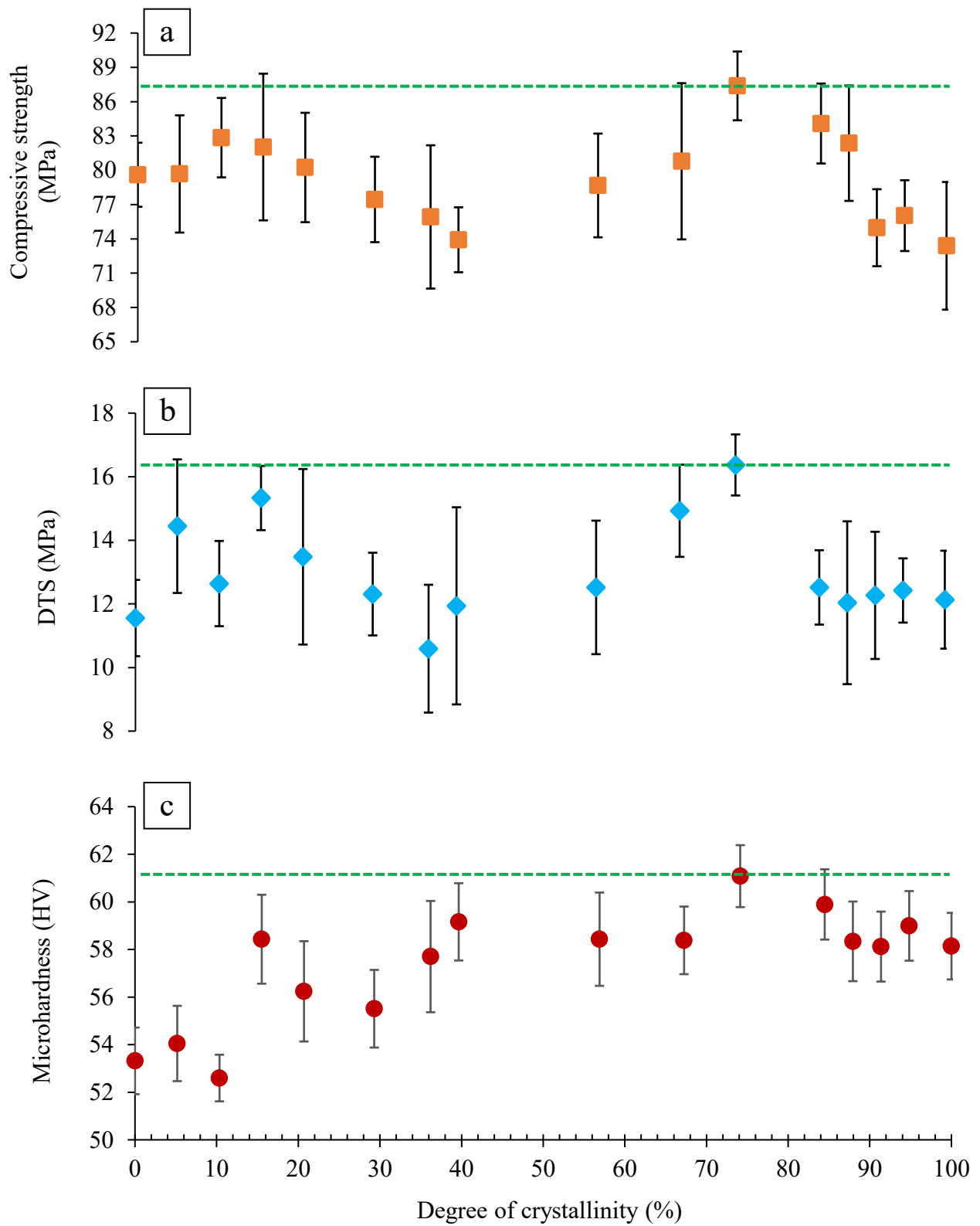


Fig. 4. 3. Effect of the 45S5 Bioglass<sup>®</sup>-ceramic crystallinity on the compressive strength (a), DTS (b) and microhardness (c) of hybrid GICs containing 5 wt% Bioglass<sup>®</sup>-ceramic (n = 6).

### 4.3.2 Compressive strength

The compressive strength of hybrid GICs containing various amounts of Bioglass<sup>®</sup>-ceramic particles with 74% crystallinity after 1 d and 7 d soaking in distilled water are presented in Fig. 4.4. It has been reported in previous studies [61, 149] that the addition of various types of bioactive glass particles into conventional GICs can lower their compressive strength. However, our GICs containing 2 wt% and 5 wt% Bioglass<sup>®</sup>-ceramic exhibit slightly higher compressive strength on average compared to that of the commercial GIC which can be attributed to the high crystallinity (74%) of the Bioglass<sup>®</sup>-ceramic particles, as explained in section 3.1. By increasing the Bioglass<sup>®</sup>-ceramic content to 10 wt% and higher, the compressive strength drops which is further explained in the following paragraph. The GICs containing 15 wt% and 20 wt% did not show sufficient strength even during handling prior to the test.

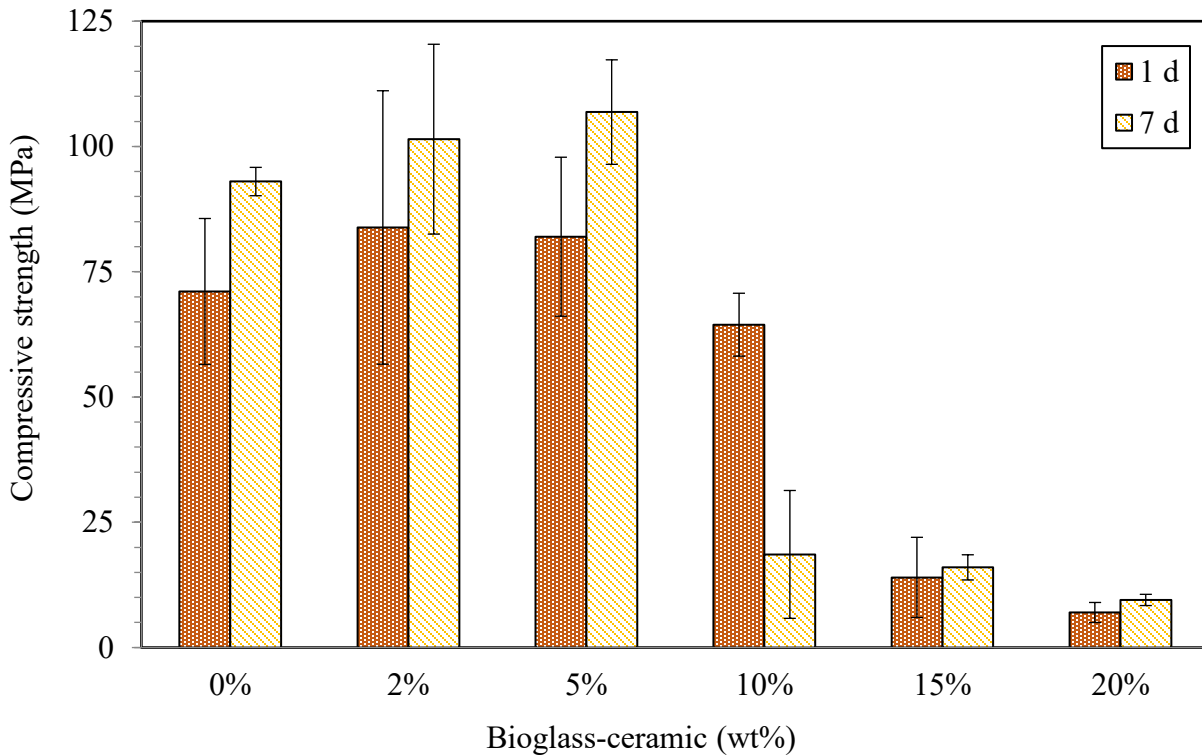
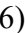



Fig. 4. 4. Compressive strength of hybrid GICs containing various amounts of Bioglass<sup>®</sup>-ceramic particles with 74% crystallinity after soaking for 1d  and 7d  in distilled water (n = 6).

It has been reported that the compressive strength of GICs increases with longer immersion in distilled water [149] due to the fact that the strength, stiffness and insolubility of GICs are gradually enhanced through crosslinking of the polymer matrix in a diffusion-controlled process [150]. During this process, a hard phase starts to form due to the continuous formation of aluminum salt bridges as the  $Al^{3+}$  ions create 3D crosslinks within the GIC [134]. This is consistent with our results for GICs containing up to 5 wt% Bioglass<sup>®</sup>-ceramic where longer soaking in distilled water (7 d) increases their compressive strength. However, this trend changes for the GICs containing 10 wt% Bioglass<sup>®</sup>-ceramic because their compressive strength decreases after 7 d soaking in water (Fig. 4.4). This can be attributed to the fact that the incorporation of excess Bioglass<sup>®</sup>-ceramic (10 wt%  $\leq$ ) can result in a higher number of particles remaining unreacted during the setting process and so are loosely attached to the GIC matrix (also observed in the SEM images in section 3.5). These loosely attached particles are also responsible for the drop in the compressive strength of the hybrid GICs containing excessive amounts of Bioglass<sup>®</sup>-ceramic particles (10 wt%  $\leq$ ). Such loosely attached particles may detach easily, especially after longer soaking times in distilled water (i.e. 7 d), lowering the compressive strength by creating potential crack initiation sites.

### 4.3.3 Diametral tensile strength (DTS)

The DTS of hybrid GICs containing various amounts of Bioglass<sup>®</sup>-ceramic particles with 74% crystallinity after 1 d and 7 d soaking in distilled water are presented in Fig. 4.5. Similar to compressive strength, it has been previously reported that the incorporation of bioactive glass particles into conventional GICs can decrease their DTS [61, 149]. For our hybrid GICs, the incorporation of 2 wt% Bioglass<sup>®</sup>-ceramic slightly decreases the DTS after 1 d soaking in distilled water. However, the DTS of the hybrid GIC containing 5 wt% Bioglass<sup>®</sup>-ceramic after 1 d and 7 d soaking in distilled water is higher on average than that of the commercial GIC. Similar to the compressive strength results (Fig. 4.4), the DTS drops for GICs containing 10 wt%  $\leq$  Bioglass<sup>®</sup>-ceramic (Fig. 4.5), which can be also due to the higher number of loosely attached unreacted particles within the GICs, as explained above in section 3.2. Under tension (e.g. DTS configuration), cracks can propagate more easily within GICs causing failure due to their inherent brittle nature [138].

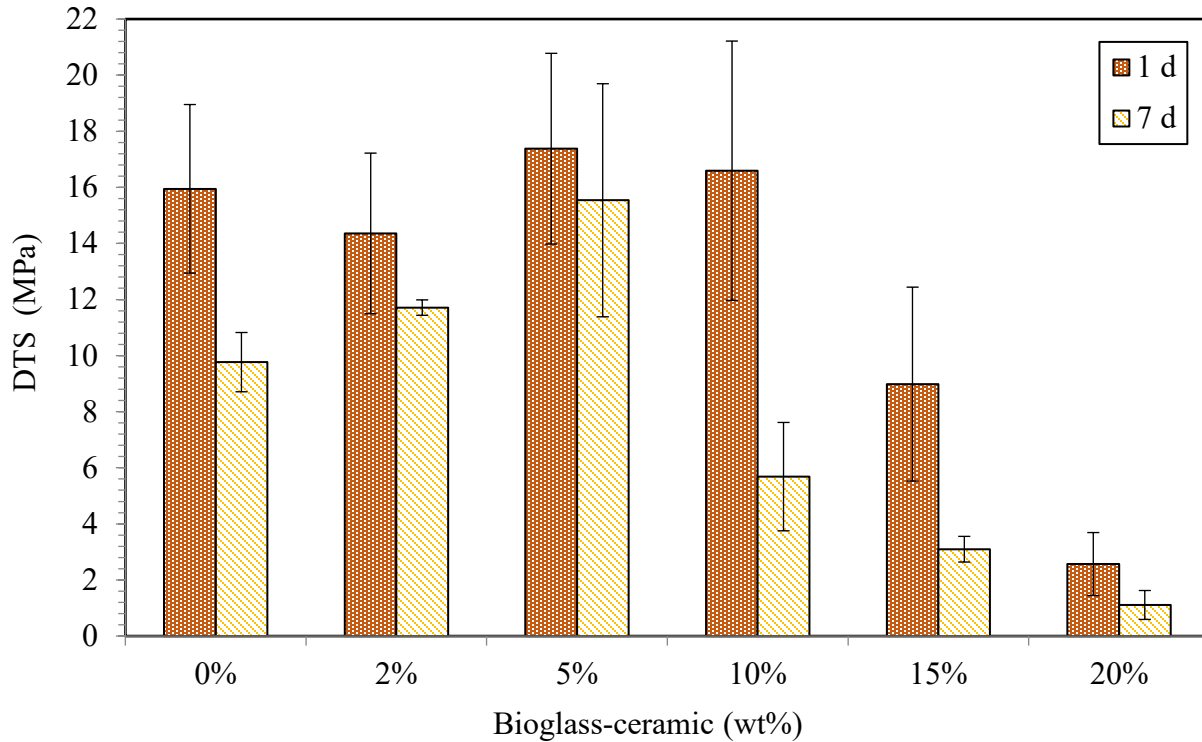


Fig. 4. 5. DTS of hybrid GICs containing various amounts of Bioglass<sup>®</sup>-ceramic particles with 74% crystallinity after soaking for 1d and 7d in distilled water (n = 6).

#### 4.3.4 Microhardness

The microhardness of hybrid GICs containing various amounts of Bioglass<sup>®</sup>-ceramic particles with 74% crystallinity after 1 d and 7 d soaking in distilled water are presented in Fig. 4.6. The results show that for both 1 d and 7 d soaking times, the incorporation of Bioglass<sup>®</sup>-ceramic particles decreases the microhardness of GIC with a drastic drop at 10 wt%  $\leq$  content which is similar to the drop observed for the compressive strength and DTS results. Fig. 4.6 also reveals that longer soaking time is in favor of the microhardness of GICs due to the continuous formation of the hardening phase over time which improves bonding within the GIC matrix. However, at 10 wt%  $\leq$  incorporation, this reaction is interrupted by the excess Bioglass<sup>®</sup>-ceramic particles in the system resulting in the drop in microhardness.

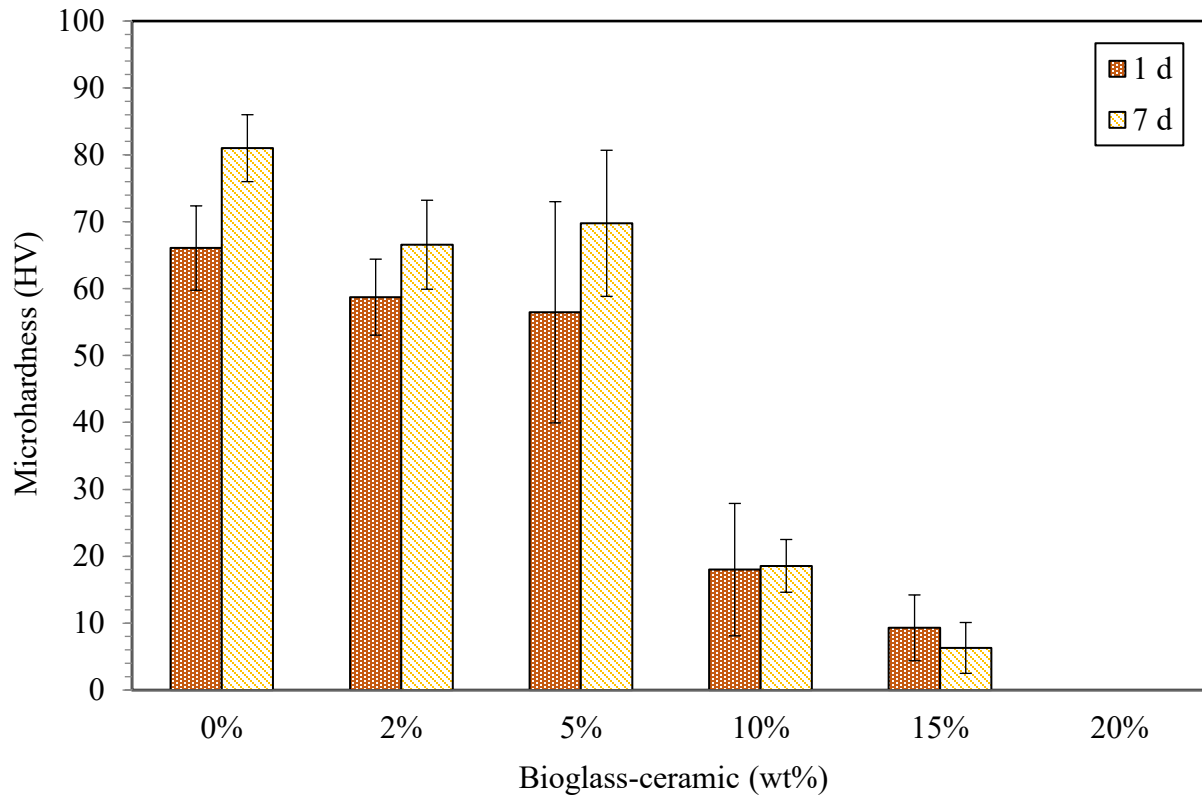
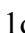



Fig. 4. 6. Microhardness of hybrid GICs containing various amounts of Bioglass<sup>®</sup>-ceramic particles with 74% crystallinity after soaking for 1d  and 7d  in distilled water (n = 6).

Based on all the mechanical properties results (Figs. 4.4-4.6), GICs containing 5 wt% Bioglass<sup>®</sup>-ceramic show the best combination of compressive strength, DTS and microhardness.

#### 4.3.5 Fractography and strengthening mechanisms

The SEM images of the fracture surface of GICs after the compression test are presented in Fig. 4.7. The dehydration cracks, which are common in commercial GICs, are observed in Fig. 4.7a [151]. In Fig. 4.7 b-f, examples of Bioglass<sup>®</sup>-ceramic particles embedded within the matrix of hybrid GICs are presented. For example, in the hybrid GIC containing 2 wt% Bioglass<sup>®</sup>-ceramic, a Bioglass<sup>®</sup>-ceramic particle bridging the crack surfaces [152] is evident (Fig. 4.7 b and c). This particle absorbs the energy of the crack by pinning its surfaces together contributing to the

crack extension resistance of the GIC. Fig. 4.7d shows a Bioglass<sup>®</sup>-ceramic particle that has formed a cohesive interface with the GIC matrix. Such excellent interfacial adhesion, allowing the mechanical stress to effectively transmit [146, 153] from the brittle matrix of the GIC to the reinforcing particles, may explain the higher compressive strength and DTS of this hybrid GIC containing 5 wt% Bioglass<sup>®</sup>-ceramic. According to Figs. 4.4-4.6, there was a drop in all mechanical properties of GICs containing 10 wt%  $\leq$  Bioglass<sup>®</sup>-ceramic which was attributed to the loosely attached and poorly bonded Bioglass<sup>®</sup>-ceramic particles to the GIC matrix which can be observed in Fig. 4.7 e and f.

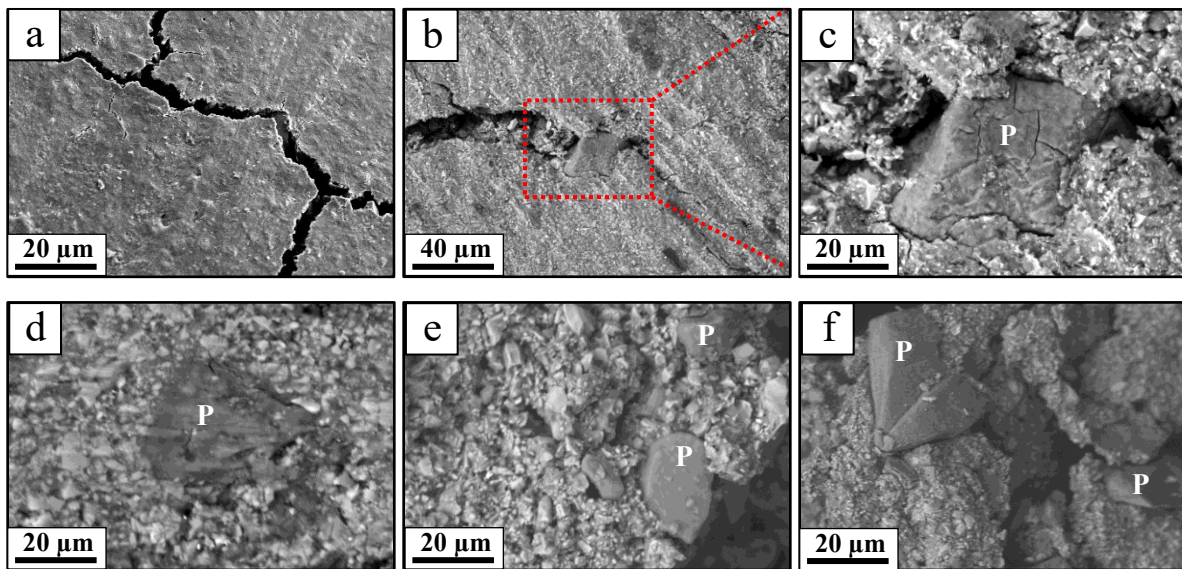


Fig. 4. 7. SEM images captured from the fracture surfaces (after the compression test) of the commercial GIC (a) as well as hybrid GICs containing 2 wt% (b and c), 5 wt% (d), 10 wt% (e) and 15 wt% (f) of Bioglass<sup>®</sup>-ceramic with 74% crystallinity. “P” represents the 45S5 Bioglass<sup>®</sup>-ceramic particles

As discussed, the hybrid GIC containing 5 wt% Bioglass<sup>®</sup>-ceramic with 74% crystallinity exhibits an overall improvement in mechanical properties compared to those of the commercial GICs as well as other hybrid GICs containing lower or higher amounts of Bioglass<sup>®</sup>-ceramic. In addition to the excellent interfacial adhesion between the Bioglass<sup>®</sup>-ceramic particles and the matrix (Fig. 4.7d), further characterization of the fracture surface of GIC specimens containing 5 wt% Bioglass<sup>®</sup>-ceramic revealed that there may be several mechanisms contributing to the

enhancement of their mechanical properties (Fig. 4.8). These mechanisms prevent crack formation and/or propagation hindering the failure of the GIC under stress.

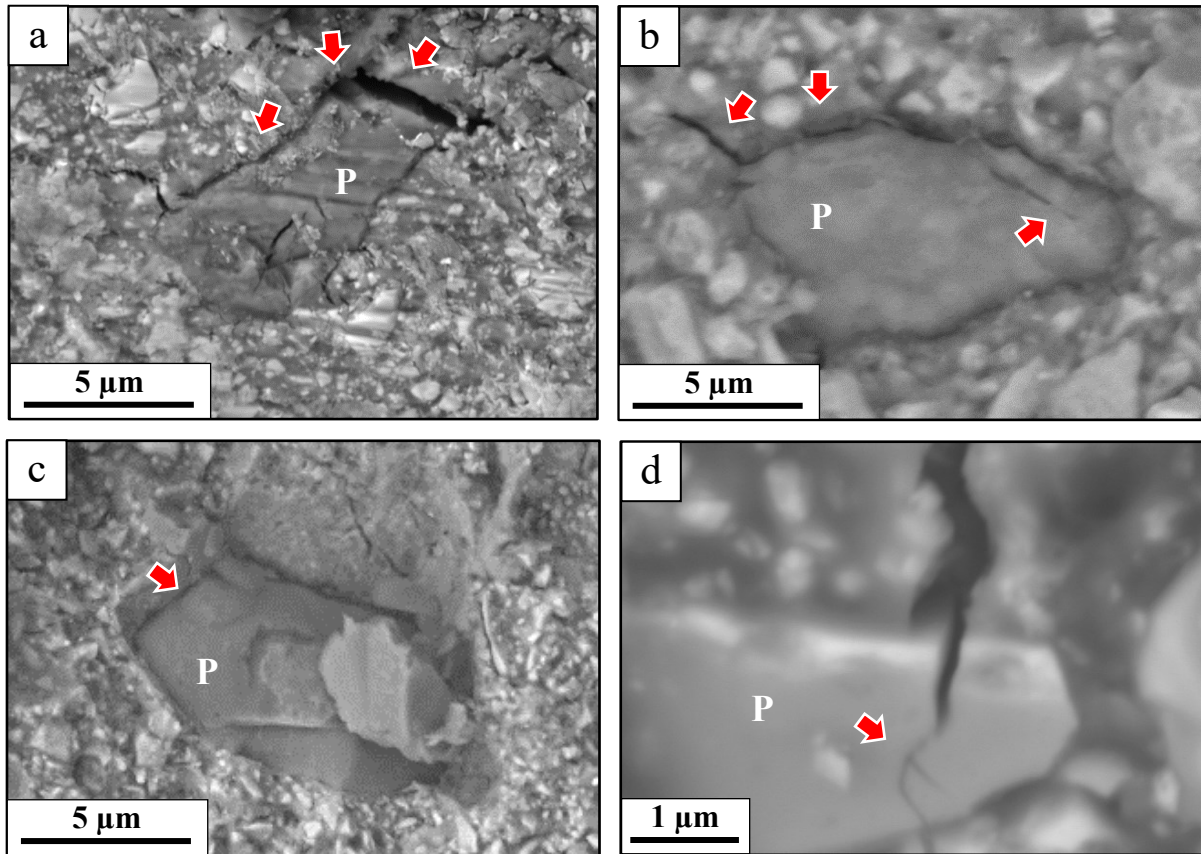


Fig. 4. 8. SEM images captured from the fracture surfaces of the hybrid GIC containing 5 wt% Bioglass<sup>®</sup>-ceramic with 74% crystallinity after the compression test. Various strengthening mechanisms induced by the incorporation of Bioglass<sup>®</sup>-ceramic particles are shown in these images (indicated by the arrows): crack deflection (a and b); particle pull-out (c), and crack branching (d). Note that, “P” represents the Bioglass<sup>®</sup>-ceramic particles.

The crack expansion along the interface of the matrix and a Bioglass<sup>®</sup>-ceramic particle, indicating the crack deflection mechanism, is observed in Fig. 4.8a. In this mechanism, the deviation of the crack increases its surface area which dissipates its energy and reduces the stress intensity at its tip [145, 153]. Fig. 4.8b shows a crack that was first deflected by the Bioglass<sup>®</sup>-ceramic particle and then entered through it where it was stopped from further propagation. This mechanism is known as crack-tip shielding which can effectively contribute to increase in the toughness of brittle materials [154]. In this mechanism, a dislocation cloud forms around the crack

tip, as dislocation mobility is constrained in a brittle Bioglass<sup>®</sup>-ceramic, which is effectively found to lower the stress at the crack tip [154]. Also, an example of the particle pull-out mechanism is shown in Fig. 4.8c where the absorbed energy due to the pull-out of the Bioglass<sup>®</sup>-ceramic particles can hinder or stop crack propagation. Fig. 4.8d shows the crack branching mechanism [155] where the main crack branches into smaller cracks dissipating its energy [155].

All these toughening mechanisms explained above can absorb considerable amounts of fracture energy, hindering crack propagation within this hybrid GIC containing 5 wt% Bioglass<sup>®</sup>-ceramic particles so improving its overall mechanical properties [154]. In our hybrid GICs, the mechanically stronger nature of the Bioglass<sup>®</sup>-ceramic particles (containing combeite crystals) compared to that of the Bioglass<sup>®</sup> particles, effectively demonstrates these strengthening mechanisms.

### **4.3.6 In vitro studies in SBF**

#### *4.3.6.1 pH measurements*

Fig. 4.9 presents the change in the pH of the SBF media as a function of immersion time for the commercial GIC as well as the hybrid GICs containing 5 wt% and 10 wt% Bioglass<sup>®</sup>-ceramic. The pH increases for all combinations after 1 d in SBF followed by a gradual decrease thereafter. The initial increase in pH can be related to the ion exchange of Ca<sup>2+</sup> in the GICs with H<sup>+</sup> in SBF resulting in the formation of a hydrated silica layer on the GICs [156]. This hydrated layer provides phosphate nucleation sites on the surface of the GICs followed by the formation of HA through incorporating OH<sup>-</sup> from SBF leading to decreasing pH over time [157]. Note that, during this period, the pH for GICs containing Bioglass<sup>®</sup>-ceramic decreases more than that of the commercial GIC which can be due to the formation of higher amount of HA, and is in agreement with the SEM, XRD and FTIR results presented in the following sections.



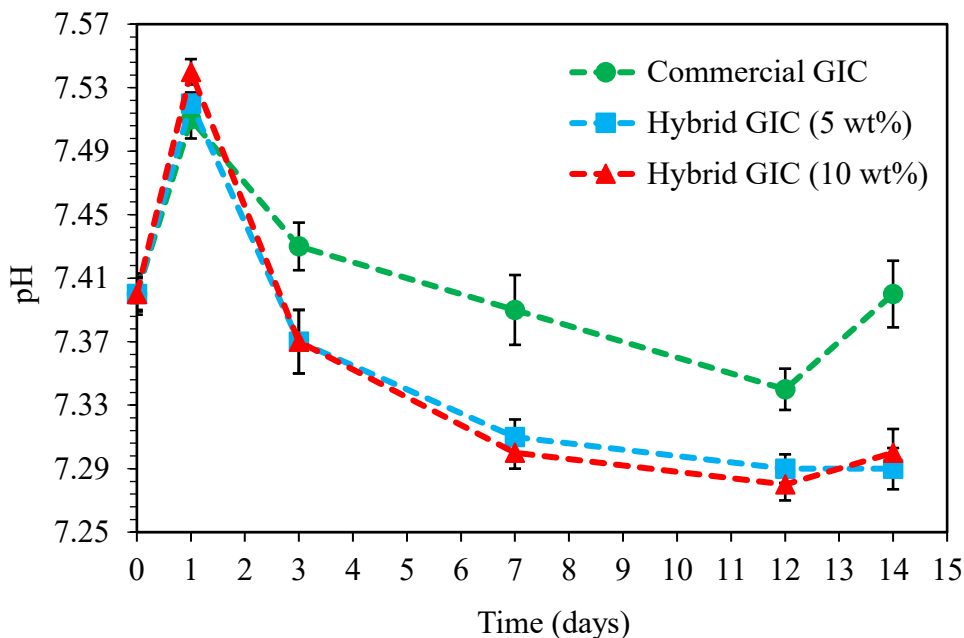


Fig. 4. 9. Change in pH of SBF as a function of immersion time for the commercial GIC ● as well as hybrid GICs containing 5 wt% ■ and 10 wt% ▲ Bioglass<sup>®</sup>-ceramic particles with 74% crystallinity (n = 3).

#### 4.3.6.2 FTIR

Hybrid GICs containing 5 wt% and 10 wt% Bioglass<sup>®</sup>-ceramic were also analyzed by FTIR to further study their structures before and after immersion in SBF (Fig. 4.10). The FTIR spectrum of the GIC containing 10 wt% Bioglass<sup>®</sup>-ceramic (Fig. 4.10c) exhibits a peak at  $1064\text{ cm}^{-1}$  corresponding to Si-O-Si stretching [63] which is stronger than that of the GIC containing 5 wt% Bioglass<sup>®</sup>-ceramic (Fig. 4.10a). This is due to the fact that, the 45S5 Bioglass<sup>®</sup>-ceramic composition has a higher silica content compared to that of the original glass of GICs; thus, incorporating more Bioglass<sup>®</sup>-ceramic leads to higher amounts of Si-O-Si bonds in the hybrid GICs. Also, the peak at  $\sim 1550\text{ cm}^{-1}$  (Fig. 4.10 a and c) corresponding to COO<sup>-</sup> stretching vibration, is related to the crosslinked polymeric acid chains [158].

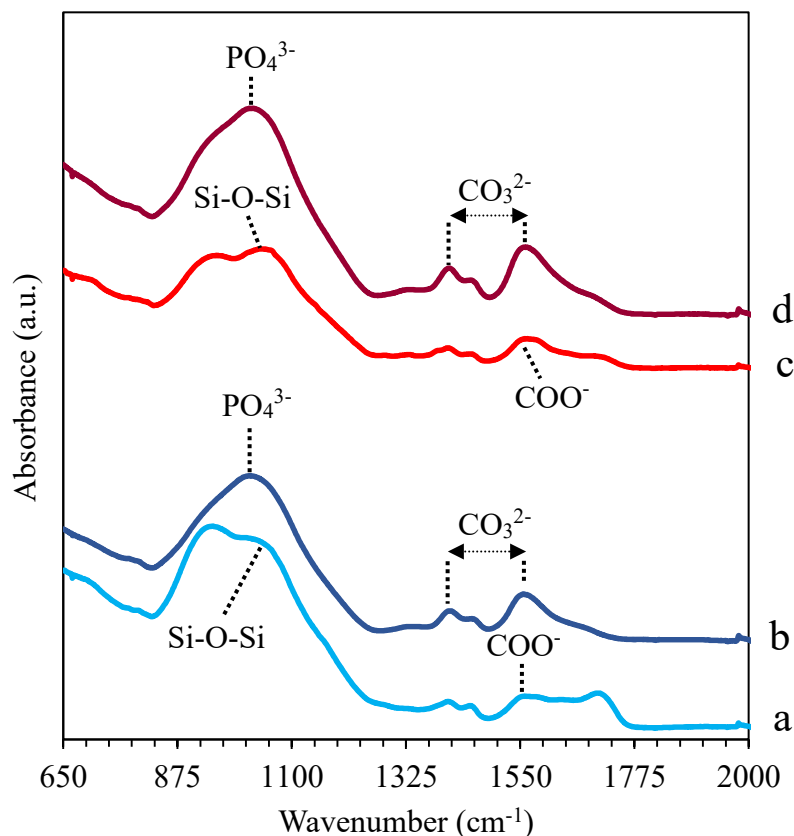


Fig. 4. 10. FTIR spectra of the hybrid GIC containing 5 wt% Bioglass<sup>®</sup>-ceramic before (a) and after (b) 14 d in SBF and the hybrid GIC containing 10 wt% Bioglass<sup>®</sup>-ceramic before (c) and after (d) 14 d in SBF.

After 14 d immersion in SBF, two significant changes can be observed in the FTIR spectra of the GICs. A peak at 1030 cm<sup>-1</sup> appeared in the spectra of both hybrid GICs after 14 d in SBF (Fig. 4.10 b and d) which is the characteristic peak of PO<sub>4</sub><sup>3-</sup> and is superimposed over the Si-O-Si peak at 1064 cm<sup>-1</sup>. The intensity of the PO<sub>4</sub><sup>3-</sup> peak increases by increasing the Bioglass<sup>®</sup>-ceramic content from 5 wt% (Fig. 4.10b) to 10 wt% (Fig. 4.10d), indicating more phosphate precipitation which is attributed to the PO<sub>4</sub> release from the Bioglass<sup>®</sup>-ceramic particles [159]. The second change for both GIC systems is the intensification of their absorption band at 1410-1550 cm<sup>-1</sup> after 14 d immersion which corresponds to the CO<sub>3</sub><sup>2-</sup> vibration mode [160]. Note that, the CO<sub>3</sub><sup>2-</sup> band shows higher intensity for the GIC containing higher amount of Bioglass<sup>®</sup>-ceramic (10 wt%), indicating greater CO<sub>3</sub><sup>2-</sup> formation.

These results suggest that the phase precipitated on the hybrid GICs containing Bioglass<sup>®</sup>-ceramic particles after immersion in SBF may be carbonated hydroxyapatite (CHA) which is very similar to the mineral phase of dentin. The formation of CHA is also verified by XRD which is presented and discussed in the following section.

#### 4.3.6.3 XRD Characterization

Based on the FTIR results, both hybrid GICs containing 5 wt% and 10 wt% Bioglass<sup>®</sup>-ceramic showed a similar behavior after 14 d immersion in SBF; thus, the former system (5 wt%), which also showed the best overall mechanical properties, was opted for further characterization by XRD.

The XRD patterns of the commercial GIC after 14 d in SBF and the hybrid GIC containing 5 wt% Bioglass<sup>®</sup>-ceramic after 7 d and 14 d in SBF are presented in Fig. 4.11. The XRD pattern of the commercial GIC after 14 d in SBF (Fig. 4.11a) reveals no sign of crystalline CHA; whereas, two low-intensity peaks related to combeite and CHA, were detected in the patterns of the hybrid GIC (Fig. 4.11 b and c) [161]. This verifies that within the timeframe of this *in vitro* testing (14 d), the commercial GIC does not remineralize, but with 5 wt% incorporation of Bioglass<sup>®</sup>-ceramic (i.e. the hybrid GIC), it exhibits remineralization. Considering the relatively low Bioglass<sup>®</sup>-ceramic content of the hybrid GIC (5 wt%) and the short *in vitro* studies in SBF (up to 14 d), low quantities of CHA was expected to form which is reflected by the low intensity of the CHA peaks (Fig. 4.11 b and c). Additionally, a small portion of the Bioglass<sup>®</sup>-ceramic content is on the surface of the GIC and effectively exposed to the SBF medium, which further contributes to the low amount of CHA formed.

This relatively low rate of CHA formation is due to not only the relatively small bioglass-ceramic content, but also their semi-crystalline nature resulting in a slower dissolution in SBF [98, 100]. This trend in hybrid GICs is beneficial since it allows the Bioglass<sup>®</sup>-ceramic particles to not only induce remineralization and convert to CHA via a controlled manner and time [142] but also serve their reinforcing role by maintaining their strength over time as they dissolve at a lower rate. As shown in the XRD patterns (Fig. 4.11 b and c), the peak corresponding to combeite (i.e. the reinforcing crystalline phase) remained unchanged indicating its slow dissolution. The appropriately low rate of our bioglass-ceramic dissolution and CHA formation can provide

sufficient time for the development of improved chemical bonding between the dentine tissue and the GIC while its mechanical support is maintained [142]. The Bioglass<sup>®</sup>-ceramic particles embedded inside the GIC, which are in less contact with the physiological fluids, continuously contribute to this mechanical support over a long time period. Thus, the hybrid GIC containing 5 wt% Bioglass<sup>®</sup>-ceramic not only exhibits improved mechanical (Figs. 4.4-4.6) and remineralizing properties, but also can potentially maintain its suitable mechanical properties *in vivo* serving as a reliable dental restorative.

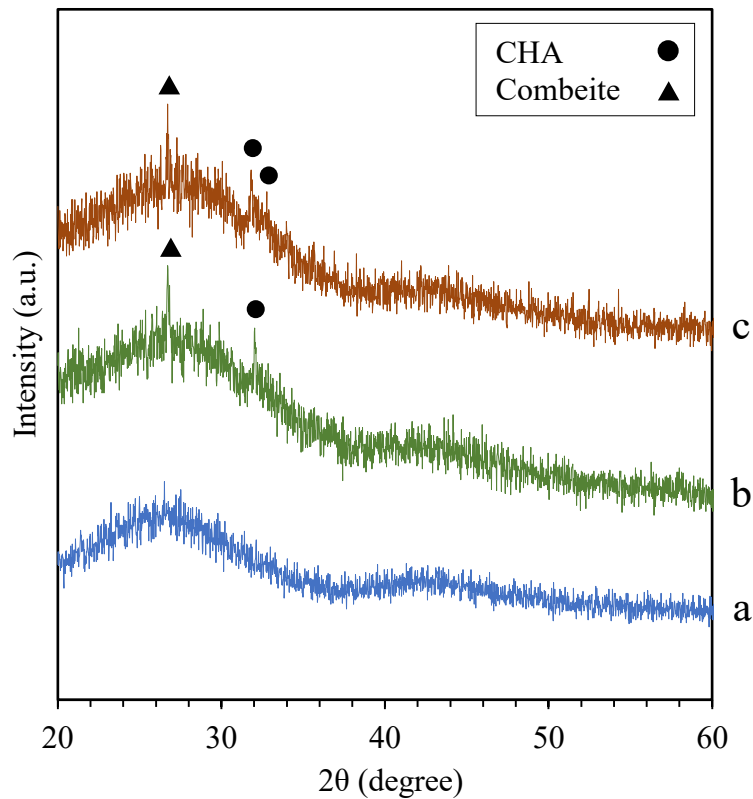


Fig. 4. 11. XRD results for the commercial GIC after 14 d in SBF (a) as well as the hybrid GIC containing 5 wt% Bioglass<sup>®</sup>-ceramic after 7 d (b) and 14 d (c) immersion in SBF.

#### 4.3.6.4 SEM Analysis

Fig. 4.12 presents the SEM images captured from the surface of the commercial GIC as well as hybrid GICs containing 5 wt% and 10 wt% Bioglass<sup>®</sup>-ceramic after immersion in SBF for 1 d, 3 d, 7 d and 14 d.

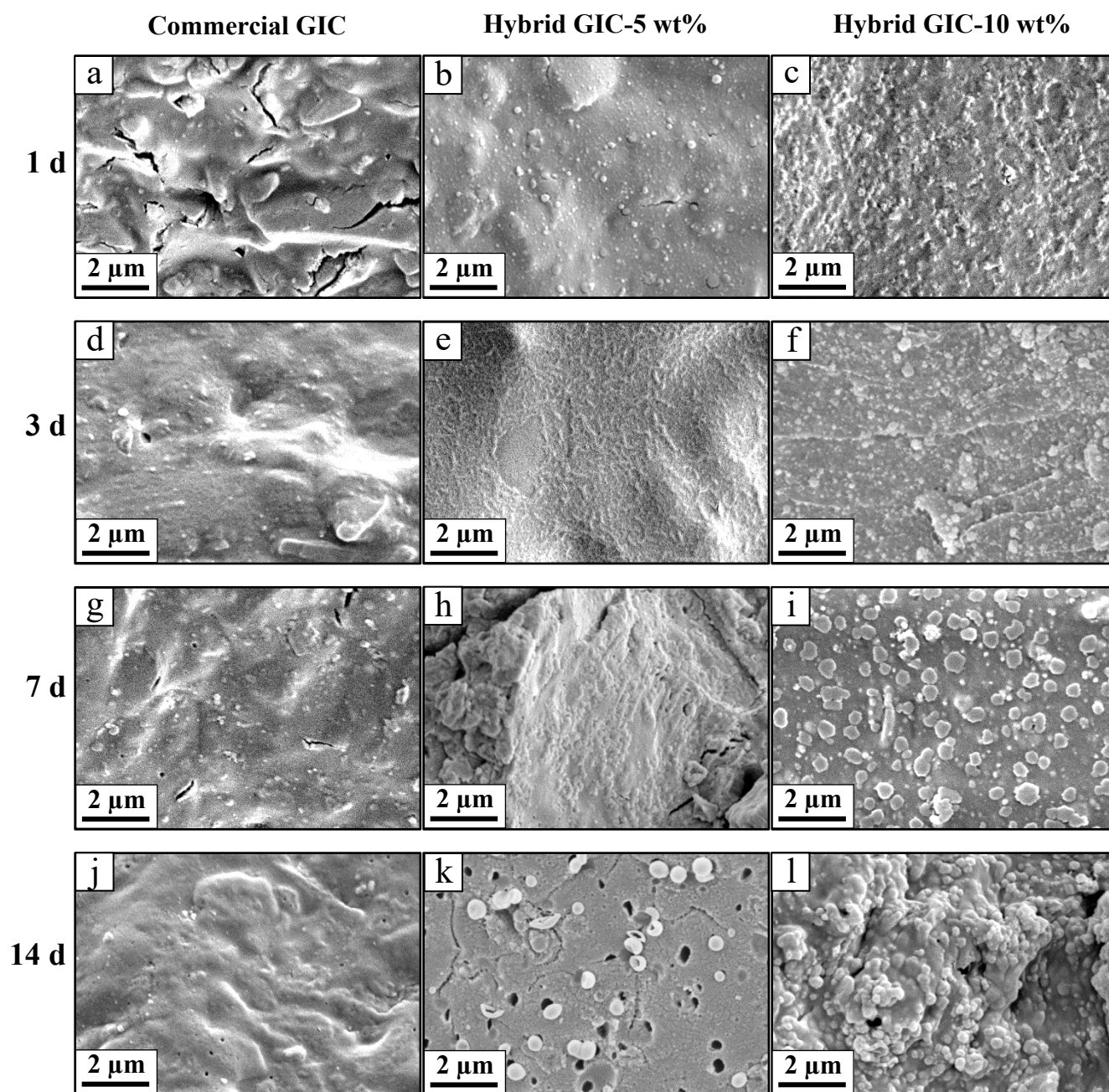


Fig. 4. 12. SEM images captured from the surfaces of the commercial GIC (left column) and hybrid GICs containing 5 wt% (middle column) and 10 wt% (right column) after 1 d (a-c), 3 d (d-f), 7 d (g-i) and 14 d (j-l) immersion in SBF.

As expected from the XRD results, no typical sign of CHA precipitation is observed on the commercial GIC after up to 14 d immersion in SBF (Fig. 4.12 a, d, g and j). On the other hand, apatite precipitation [62, 71, 169] is observed on the hybrid GICs containing 5 wt% and 10 wt% Bioglass<sup>®</sup>-ceramic after 1 d immersion in SBF (Fig. 4.12 b and c). Immersion in SBF for 3 d (Fig. 4.12 e and f) resulted in a smoother surface, which may be attributed to the formation of an incipient apatite coating [71]. These precipitates tend to grow into different apatite morphologies over various immersion times in SBF (Fig. 4.12 e, f, h, i, k, l) [61, 71] which can be partly due to the gradual incorporation of carbonate ions into the apatite structure [162]. Three-dimensional discrete islands of apatite appeared on the GIC surface with longer immersion times (Fig. 4.12 i, k and l).

#### 4.4 Conclusions

In this study we improved the mechanical and remineralizing properties of a commercially available GIC by the incorporation of 45S5 Bioglass<sup>®</sup>-ceramic particles containing a mechanically strong combeite phase ( $\text{Na}_2\text{Ca}_2\text{Si}_3\text{O}_9$ ). We showed that the hybrid GIC containing 5 wt% Bioglass<sup>®</sup>-ceramic with 74% crystallinity has the highest overall mechanical properties based on the results of the compression strength, diametral tensile strength and microhardness tests. For these samples, the average compressive strength and DTS values were respectively increased by 15% and 60% after 7 days immersion in distilled water, when compared to those of the corresponding commercial GIC.

Strengthening mechanisms including crack deflection, crack branching, crack-tip shielding and particle pull-out contributing to the mechanical performance enhancement were observed and discussed for this hybrid GIC. The overall mechanical properties of other hybrid GICs with higher Bioglass<sup>®</sup>-ceramic contents (e.g. 10 wt%) dropped due to the larger number of loosely attached particles acting as crack initiation sites. Furthermore, the results of the *in vitro* studies revealed that, hybrid GICs containing Bioglass<sup>®</sup>-ceramic particles can lightly mineralize in SBF.

## **Acknowledgment**

This research was funded by the Natural Sciences and Engineering Research Council of Canada (NSERC) under the Discovery Grants program and Concordia University. The authors thank Prof. Robert Hill (Barts and The London School of Medicine and Dentistry) and Dentsply DeTrey for kindly donating the 45S5 Bioglass<sup>®</sup> powder and the glass ionomer cements, respectively.

## Chapter 5

# Development of aluminum-free glass ionomer cements using 45S5 Bioglass<sup>®</sup> and its Bioglass<sup>®</sup>-ceramic <sup>1</sup>

Alireza Zandi Karimi <sup>a</sup>, Ehsan Rezabeigi <sup>b</sup>, and Robin A.L. Drew <sup>a</sup>

<sup>a</sup> *Department of Mechanical, Industrial and Aerospace Engineering, Concordia University, Montréal, Quebec H3G 1M8, Canada.*

<sup>b</sup> *Department of Mining and Materials Engineering, McGill University, Wong Building, 3610 Rue University, Montréal, Quebec H3A 0C5, Canada.*

**Abstract.** Although the incorporation of bioactive glasses into glass ionomer cements (GICs) has led to promising results, using a bioactive glass as the only solid component of GICs has never been investigated. In this study, we produced an Al-free GIC with standard compressive strength using various combinations of 45S5 Bioglass<sup>®</sup> and its glass-ceramic as the solid component. The glass-ceramic particles with 74% crystallinity were used for this purpose as they can best act as both remineralizing and reinforcing agents. Strengthening mechanisms including crack deflection and crack-tip shielding were activated for the GICs containing 50-50 wt% Bioglass<sup>®</sup> and Bioglass<sup>®</sup>-ceramic as the optimum ratio. We monitored and verified the progression of the GIC setting reaction at its early stages. We also discussed that our bimodal particle size distribution containing both micron- and nanosized Bioglass<sup>®</sup> and Bioglass<sup>®</sup>-ceramic particles may enhance the packing density and integrity of the structure of the cements after setting. In such GICs produced in this study, the toxic effects of Al are avoided while chemical bonds are expected to form between the cement and the surrounding hard tissue(s) through interfacial biomineralization and adhesion.

**Keywords:** Glass ionomer cements; Mechanical Properties; Bioactive; 45S5 Bioglass<sup>®</sup>; 45S5 Bioglass<sup>®</sup>-ceramic; Aluminum-free GIC

---

<sup>1</sup> This chapter is currently under review in *Journal of Advanced Engineering Materials*.



## 5.1 Introduction

Glass ionomer cements (GICs), also known as glass polyalkenoates, were developed and patented in 1969 at the Laboratory of the Government Chemist (London, UK) [14]. Since then, GICs have been extensively studied and used as luting, sealing and restorative materials in modern dentistry [171, 172]. GICs exhibit many clinical advantages compared to other restoratives including the ability to develop physicochemical bond to hard tissues, low coefficient of thermal expansion, desirable translucency and proper biocompatibility with the pulp tissue and primary cultures of bone cells – all of which can significantly promote their *in vivo* performance [16, 173].

GICs are classified as acid-base cements consisting of an aqueous solution of a polyalkenoic acid and a powdered calcium aluminosilicate glass component with a basic nature [150]. The polyalkenoic acid is a family of complex acids normally including polyacrylic acid (PAA) or an acrylic/maleic/itaconic acid copolymer. During the acid-base setting reaction, multivalent counterions (e.g.  $\text{Ca}^{2+}$  and  $\text{Al}^{3+}$ ) leach out from glass particles resulting in the crosslinking of polyalkenoic acid chains [16, 163], which leads to cement hardening.

In addition to the field of dentistry, GICs have been considered as a potential substitute for polymethylmethacrylate (PMMA) bone cements for orthopedic applications due to their ability to chemically bond to hydroxyapatite (HA) [164]. Unlike PMMA-based bone cements, GICs exhibit good adhesion to hard tissue, proper stability in aqueous environment, low shrinkage and low exothermic setting reaction [135, 165, 175]. Despite all the advantages, the reliance of GICs on the presence of Al has restricted their application in orthopedics and dentistry. Al ion is recognized as a neurotoxin which promotes cellular oxidation [69] and disrupts cellular homeostasis [70]. There have been reports of aluminum traces in the brain, cerebral spinal fluid, blood and urine up to 77 days after implanting an aluminum-containing bone cement [71]. This issue has also been implicated in and linked to the pathogenesis of many neurological disorders such as Parkinson's disease [72]. Due to the concerns about the release of Al ions from GICs, there has been a growing interest towards the development of Al-free glass ionomer cements for both dentistry and orthopedics applications [71]. Also, the existing formulations of conventional GIC suffer from poor mechanical properties limiting their applications in high stress-bearing areas of the body. Attempts have been made to overcome this drawback including the incorporation of glass fibers

[139] or metallic oxide (nano-) particles [140]; glass composition modification [70] and using novel polyacids [166]. In our previous work [64], it was shown that the incorporation of an optimum amount of 45S5 Bioglass<sup>®</sup>-ceramic with certain degree of crystallinity containing mechanically strong combeite ( $\text{Na}_2\text{Ca}_2\text{Si}_3\text{O}_9$ ) phase could improve the mechanical performance of GICs while enhancing their remineralizing properties [64].

GICs can be considered bioactive since they can release ions via dissolution of calcium aluminosilicate glass particles causing certain biomineralization within their clinical environment [142]. Improving GICs remineralizing properties can potentially lead to a stronger chemical bond between the native tissue(s) and the cement *in vivo*. Although the incorporation of various bioactive glass or ceramic fillers into GICs has been investigated for this purpose [61, 64, 65], utilizing bioactive glass particles as the whole solid powder component of the cement has never been previously studied. If the used bioactive glass in such a GIC transforms into HA in a controlled manner, the hard tissues surrounding the GIC can take advantage of the resulting interfacial biomineralization and adhesion [142].

45S5 Bioglass<sup>®</sup> (45 wt%  $\text{SiO}_2$ , 24.5 wt%  $\text{Na}_2\text{O}$ , 24.5 wt%  $\text{CaO}$ , 6 wt%  $\text{P}_2\text{O}_5$ ) is known to be the first commercial bioactive glass [77]. Developed by Hench in late 70's, this bioglass was the first material that was able to form a stable bond with tissues through the formation of an apatite layer [77, 107]. 45S5 Bioglass<sup>®</sup> has similar characteristics to the common GIC glass component. For instance, it contains high volume of network modifiers,  $\text{CaO}$  and  $\text{Na}_2\text{O}$ , that can break the continuous  $\text{Si-O-Si}$  structural units resulting in formation of non-bridging oxygens [1]. Upon incubation in an aqueous environment, 45S5 Bioglass<sup>®</sup> participates in cation exchange of  $\text{Na}^+$ ,  $\text{Ca}^{2+}$  with  $\text{H}^+$  from the solution [61]. When this bioglass is mixed with polyacid solution, the released  $\text{Ca}^{2+}$  ions may be able to react with the polyacrylate chains creating an ionically crosslinked polyacrylate matrix [1, 178], similar to the setting reaction in conventional GICs. Furthermore,  $\text{PO}_4^{3-}$  is released from the Bioglass<sup>®</sup> as a result of reacting with the polyacid [61]. It has been shown that the existence of phosphorous (along with Si) within the matrix results in formation of an inorganic network which interpenetrates with the aforementioned  $\text{Ca}^{2+}$  polyacrylate matrix [167]. Formation of this network contributes to insolubility of GICs as well as their gradual increase in compressive strength with time [168].

Due to its high bioactivity index [107], 45S5 Bioglass<sup>®</sup> can be overreactive with polyacid resulting in a premature setting. Alternatively, 45S5 glass-ceramic with appropriately lower bioactivity (i.e. reaction/dissolution rate) and superior mechanical properties compared to those of the 45S5 Bioglass<sup>®</sup> may be used as the GIC glass component [95].

Due to lack of Al, 45S5 Bioglass<sup>®</sup> might not have high basicity as other GIC glass compositions [61]. It has been reported that reducing the particle size of the glass component in GICs increases its reactivity [151], resulting in higher setting rates which can make up for the less reactivity caused by the lack of Al in the Bioglass<sup>®</sup> composition.

The main objective of this study was to develop a remineralizing, aluminum-free GIC consisting of an optimum ratio of 45S5 Bioglass<sup>®</sup> to its glass-ceramic as the glass component as well as polyacrylic acid aqueous solution. The new resulting GICs exhibited proper mechanical properties comparable to commercially available GICs. We also show that our 45S5 Bioglass<sup>®</sup>-based GIC not only meets the ISO compressive strength requirement but also may improve the remineralizing properties of cements.

## **5.2 Materials and methods**

### **5.2.1 Bioglass<sup>®</sup> synthesis, heat treatment and characterization**

The 45S5 Bioglass<sup>®</sup> used in this research was prepared and donated by Dr. Robert Hill from Queen Mary University of London. In short, calculated amounts of high-purity precursors were mixed and then melted in a platinum/rhodium crucible at 1380 °C for 1 h using an electric furnace. The resulting melt was then rapidly quenched in deionized water at room temperature. Next, the frit was dried and melted again for 30 min. followed by a grinding process using a vibratory mill [64, 95, 119].

To eliminate any internal stress created during grinding process, the as-received Bioglass<sup>®</sup> was annealed at 460 °C for 8 h under ambient atmosphere. X-ray diffraction (XRD; PANalytical X'Pert Pro) using Cu K $\alpha$  radiation ( $10^\circ < 2\theta < 90^\circ$ ) was used to confirm that the amorphous nature of the material was completely retained.

In order to prepare the 45S5 Bioglass<sup>®</sup>-ceramic containing combeite, the as-received 45S5 Bioglass<sup>®</sup> was heat treated through a controlled process [95] to induce 74% crystallinity in its structure which was previously reported to be the optimum crystallinity, leading to the highest mechanical performance when incorporated into GICs [64]. The heat treatment profiles used to obtain various degrees of combeite crystallinity in 45S5 Bioglass<sup>®</sup> are explained in detail in our previous study [95]. The heat-treated glass was then lightly ground using an agate mortar and pestle. Particle size distribution of the as-received glass and heat-treated glass-ceramic was measured via laser light scattering particle size distribution analysis (PSA; Horiba LA-920) using isopropyl alcohol as a dispersant and after 5 minutes in an ultrasonic bath. Note that the refractive indices of 1.55 and 1.08 were respectively used for the 45S5 Bioglass<sup>®</sup> and isopropyl alcohol. Also, morphology of the as-received glass and heat-treated glass-ceramic particles was examined using a scanning electron microscope (SEM; HITACHI, S-3400N).

### **5.2.2 Cement preparation**

The glass component of our cements was prepared by mixing of 45S5 Bioglass<sup>®</sup> and 45S5 Bioglass<sup>®</sup>-ceramics (74% crystallinity). In order to investigate the effect of incorporation of Bioglass<sup>®</sup>-ceramic, eleven powder mixtures containing 0, 10, 20, 30, 40, 50, 60, 70, 90 and 100 wt% Bioglass<sup>®</sup>-ceramic (C0, C10, C20, ..., C100; Table 5.1) were prepared using a Coulter mixer for 30 min. to reach homogeneity. Note that, the materials codes and details of the glass powder components are given in Table 5.1.

A 50 wt% aqueous solution of PAA,  $M_w = 240,000$  g/mol (Acros Organics) in deionized water was used as the liquid component of the cement. The glass powder components were hand-mixed with the liquid component on a watch glass at different ratios. The powder to liquid ratio (P:L) with the best working and handling properties (P:L = 1:0.8) was found by trial and error among ten tested ratios ranging from 1:0.4 to 1:2.2. Note that, all the samples were prepared at room temperature ( $21 \pm 2$  °C) throughout this process. Depending on the subsequent characterization technique, different setting procedures were followed as explained in the next section.

### 5.2.3 Cement properties

The setting time of each cement was recorded ( $n = 3$ ) according to ISO 9917-1: dentistry-water-based cements [51]. Compression tests were carried out according to the same standard [51]. Cylindrical-shaped cements were made at ambient temperature ( $21 \pm 2$  °C) by casting the mixed materials into silicone molds ( $D = 4$  mm and  $h = 6$  mm) followed by an hour incubation at  $37 \pm 1$  °C. Samples were then removed from the molds and incubated in distilled water at  $37 \pm 1$  °C for various durations of 1 h, 1 d, 3 d, 7 d, 14 d, 21 d and 42 d. After each timepoint, samples were tested using an Instron 3382 Universal Testing Machine with a 5 kN load cell at a crosshead speed of 0.5 mm/min. The compressive strength (CS) was calculated using the following equation ( $n = 6$ ):

$$CS = \frac{4P}{\pi D^2} \quad \text{eq (1)}$$

where P is the maximum applied load (N) and D is the diameter of the sample (mm). The fracture surface of the cements was examined by SEM.

A microhardness tester (Mitutoyo MVK-H1) was also used to measure the Vickers microhardness of all the cements by applying a 50 gf load on the surface of each cement for 30 s ( $n = 6$ ).

The resulting cements were characterized by Fourier transform infrared spectroscopy (FTIR, Thermo Scientific, Nicolet iS10) at room temperature over wavenumber range of 500 to 4000  $\text{cm}^{-1}$ . Each FTIR experiment was performed at the high resolution of 1  $\text{cm}^{-1}$  over 64 scans. However, only the portions of the FTIR spectra containing useful information are presented here. To examine the effect of the powder composition, the FTIR spectra of the C0, C50 and C100 cements after 7 d immersion in distilled water (DW) were obtained and studied. To study the effect of immersion time, the C50 cements, which exhibited the highest mechanical properties among all compositions, were examined by FTIR after 1 d, 7 d and 21 d immersion in DW. To investigate the early stages of setting, spectra were collected from the C50 composition at 1, 3, 5, 7, 10, 15, 20 and 25 minutes immediately post mixing ( $n = 3$ ). To monitor the setting progress of the C50 cement, the band

intensity ratios between the free carboxyls (COOH) absorption band at  $\approx 1650 \text{ cm}^{-1}$  to the Ca-polyacrylate ( $\text{COO}^- \text{Ca}^{2+}$ ) absorption bands at  $\approx 1550 \text{ cm}^{-1}$  and  $1410 \text{ cm}^{-1}$  [169, 174, 179, 183] were computed from each FTIR spectrum and the differences in the  $\text{COO}^- \text{Ca}^{2+}/\text{COOH}$  band intensity ratios as a function of setting time (1, 3, 5, 7, 10, 15, 20 and 25 min) were plotted.

## 5.3 Results and discussions

### 5.3.1 Bioglass<sup>®</sup> characterization

The XRD patterns, the PSA results (particle size distribution) and the SEM micrographs of both as-received Bioglass<sup>®</sup> and the heat treated Bioglass<sup>®</sup>-ceramic particles with 74% crystallinity are presented in Fig. 5.1. The XRD pattern of Fig. 5.1a confirms that the as-received Bioglass<sup>®</sup> has retained its amorphous nature after the stress-relief heat treatment at  $460 \text{ }^\circ\text{C}$  as explained in section 2.1. Also, the XRD pattern of Fig. 5.1b reveals that the Bioglass<sup>®</sup>-ceramic powder contains solely combeite crystalline phase. The particle size of Bioglass<sup>®</sup> powder (Fig. 5.1a) is in the range of  $0.3$  to  $90 \text{ }\mu\text{m}$  with an average of  $4.6 \text{ }\mu\text{m}$ . The wide bimodal distribution in this graph consists of two major populations of submicron and micron-sized particles. On the other hand, the particle size distribution of Bioglass<sup>®</sup>-ceramic particles (Fig. 5.1b) shows a slight shift to larger particle size (ranged from  $0.3$  to  $100 \text{ }\mu\text{m}$ ; mean size =  $6.3 \text{ }\mu\text{m}$ ) while maintaining a similar bimodal distribution. The shift to larger size and the decrease in intensity of submicron peak can be the result of heat treatment which might lead to slight agglomeration. These characterization results are important since particle size can significantly affect the mechanical properties of cements [151, 180]. GICs prepared by the powders with a bimodal particle size distribution, are shown to have higher fracture toughness and improved workability properties. This is due to the fact that, such distribution leads to a high packing density of the glass particles within the cement matrix in which fine particles mostly provide the reactive surface area required for setting reaction (i.e. faster setting times) whilst coarse particles may mainly contribute to the strengthening mechanisms (i.e. crack deflection) [160, 170, 180]. In the absence of Al as an important element in 3D polysalt formation and hardening of the cements [16], particle size distribution can play a significant role in tailoring the mechanical properties of aluminum-free cements.

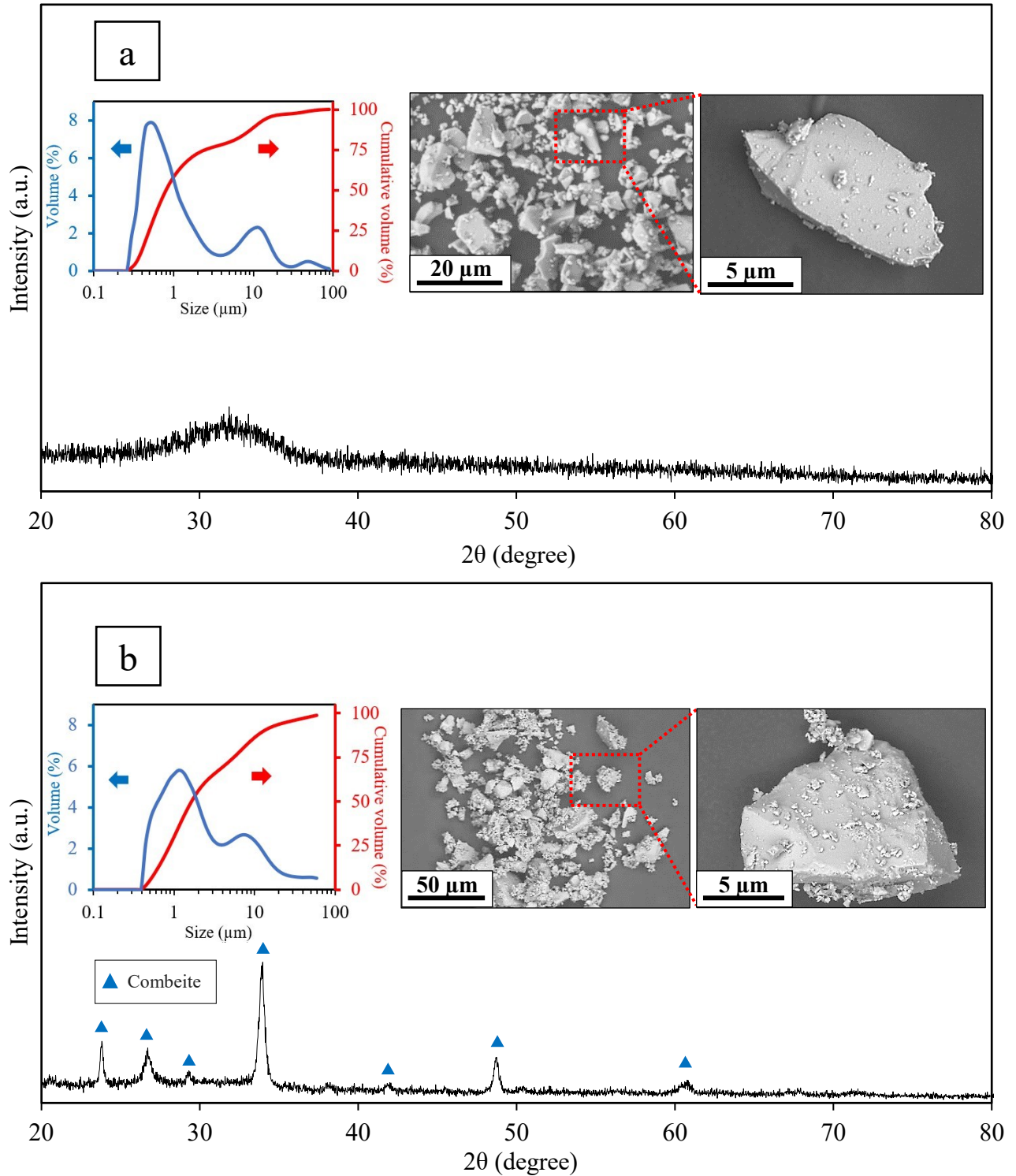


Fig. 5. 1. XRD patterns, particle size distributions and SEM micrographs of a) the as-received Bioglass<sup>®</sup> powder and b) heat treated Bioglass<sup>®</sup>-ceramic particles with 74% crystallinity. The XRD patterns are adapted with permission from [29]. Copyright 2014, Elsevier.

In the SEM images (Fig. 5.1), submicron and micron-sized glass particles can be observed in both as-received Bioglass<sup>®</sup> (Fig. 5.1a) and the Bioglass<sup>®</sup>-ceramic (Fig. 5.1b) powders which is consistent with the PSA results. The SEM images also show submicron particles which are agglomerated onto the micron-sized particles which seems to be more in the case of heat-treated powder (Fig. 5.1 b). This may happen due to the higher surface energy of sub-micron particles which increases their tendency to agglomerate [107].

### 5.3.2 Cement properties

The powder/liquid (P:L) ratios and setting times of all cements are presented in Table 5.1. The P:L of 1:0.8 which was the highest ratio that delivered the best working and handling properties, was obtained by trial and error. It has been shown that higher P:L can result in better mechanical performance in GICs due to the development of more polysalt bridges which results in higher degree of crosslinking [170]. According to this Table, the setting time increases with increasing the Bioglass<sup>®</sup>-ceramic content of the cements. This can be attributed to the lower reactivity of the Bioglass<sup>®</sup>-ceramic particles compared to that of the amorphous Bioglass<sup>®</sup> [100] resulting in slower reaction with polyacrylic acid (i.e. delayed setting process).

Table 5. 1. Bioglass<sup>®</sup> and Bioglass<sup>®</sup>-ceramic contents; powder to liquid ratios; and setting times (n=3) of the cements.

Cement group	Bioglass <sup>®</sup> -ceramic* (wt%)	Bioglass <sup>®</sup> (wt%)	P:L (g/g) **	Setting time (min.)
C0	0	100	1:0.8	6.5 ± 1.2
C10	10	90	1:0.8	6.8 ± 2.2
C20	20	80	1:0.8	7.9 ± 1.7
C30	30	70	1:0.8	8.7 ± 3.3
C40	40	60	1:0.8	8.6 ± 2.6
C50	50	50	1:0.8	9.1 ± 2.4
C60	60	40	1:0.8	10.6 ± 2.8
C70	70	30	1:0.8	10.8 ± 3.4
C80	80	20	1:0.8	15.4 ± 3.7
C90	90	10	1:0.8	18.1 ± 3.4
C100	100	0	1:0.8	22.7 ± 3.2

\* As mentioned, all Bioglass<sup>®</sup>-ceramics used in this study have 74% crystallinity.

\*\* Note that the liquid component consists of 0.4 g polyacrylic acid and 0.4 g water (50 wt%).



It has been reported that the metallic ions (e.g.  $\text{Ca}^{2+}$ ) in 45S5 Bioglass<sup>®</sup> glass network can be released upon reacting with PAA and take part in setting reaction [61]. The setting times of 45S5 Bioglass<sup>®</sup>-based GICs (Table 5.1) are longer than the range of 1.5 to 6 min. required by ISO 9917-1:2002 standard for GICs when used as restorative materials. The prolonged setting times may be resulted from the absence of Al component limiting the ability of the cements from forming polysalt bridges at higher rates upon mixing. Even though our GIC still can be considered for other glass ionomer cement applications [51], the resulted setting times can be reduced by manipulating different parameters such as particle size, polyacid composition, etc.

Fig. 5.2. shows the SEM micrographs for the C0, C20, C50 and C100 cements after setting. All micrographs show a high packing density in the cements structures which is partly due to the bimodal particle size distribution (Fig. 5.1). Such distribution of particle size is shown to have a two-fold effect on setting time and mechanical properties of the GICs as explained in section 3.1. In the structure of C0 and C20 cements (Fig. 5.2a and b), more loosely attached particles can be observed. The setting reaction rate for these systems may be too high such that a fraction of the glass particles were remained unreacted (i.e. loosely attached). Interestingly, the SEM images of C100 cement (Fig. 5.2d) show a similar microstructure containing many loosely attached particles. This is attributed to the fact that the Bioglass<sup>®</sup>-ceramic content of C100 cement is less reactive compared to the fully amorphous glass content of other cements [100] resulting in unreacted particles which are poorly attached to the matrix. On the other hand, in the C50 cement micrograph (Fig. 5.2c), the particles are shown to be more integrated and attached to the cement matrix. Thus, C50 cement containing 50 wt% Bioglass<sup>®</sup> and 50 wt% Bioglass<sup>®</sup>-ceramic with bimodal particle size distributions may present an optimum composition where the submicron Bioglass<sup>®</sup> particles have sufficient surface area to fully react with PAA, while the larger particles, in particular the less reactive glass-ceramic particles, are allowed to be embedded within the matrix during this setting process. This also explains the high mechanical properties of the C50 cement which is discussed in the next section.

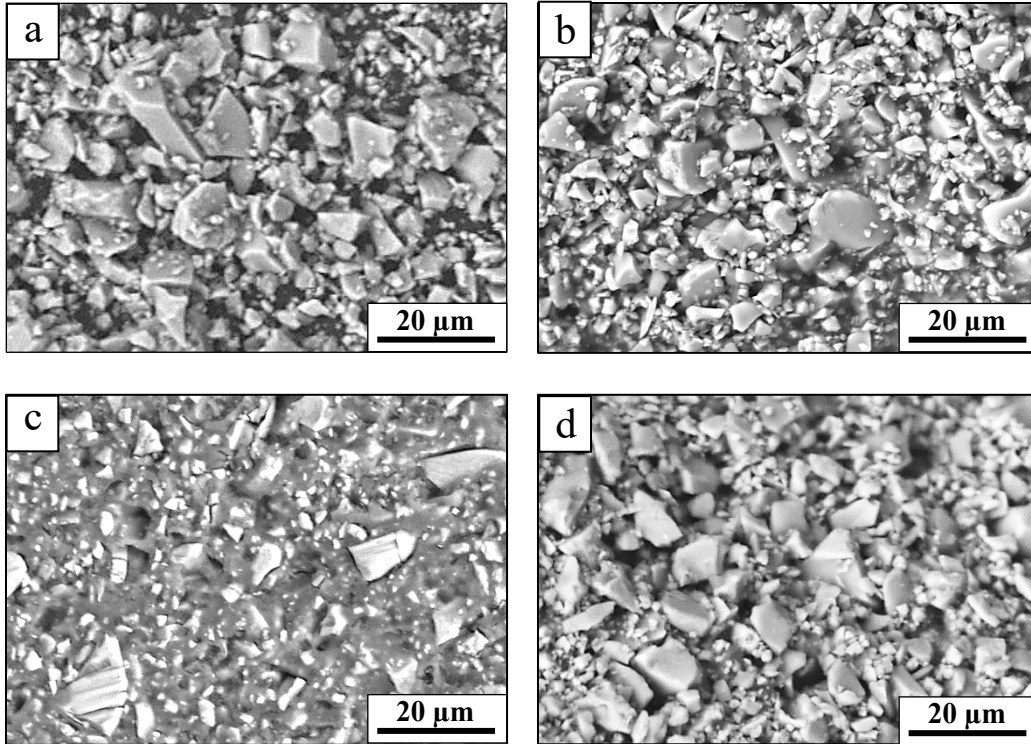


Fig. 5. 2. SEM images captured from the surface of a) C0, b) C20, c) C50 and d) C100 cements after setting.

### 5.3.2.1 Mechanical properties

The results of the compression and microhardness tests performed on the cements containing various amounts (Table 5.1) of Bioglass<sup>®</sup>-ceramic particles are presented in Fig. 5.3. Both compressive strength and microhardness have been improved for all cements containing Bioglass<sup>®</sup>-ceramic up to 60 wt% compared to those of C0 cement (i.e. the control cement containing no Bioglass<sup>®</sup>-ceramic). Note that, the C50 cement exhibits the highest combination of both compressive strength and microhardness among all cement compositions. The strengthening mechanisms that can contribute to the high mechanical properties of this cement are discussed at the end of this section based on SEM images. Higher mechanical properties of the C50 cements can be attributed to the higher strength of the Bioglass<sup>®</sup>-ceramic compared to that of the Bioglass<sup>®</sup> [99] making C50 a cement with stronger reinforcing agent than those with less Bioglass<sup>®</sup>-ceramic content. Besides, C50 was shown to have an optimum composition (50 wt% Bioglass<sup>®</sup>, 50 wt% Bioglass<sup>®</sup>-ceramic) leading to a high packing density (Fig. 5.2c). Cements containing more than

50 wt% Bioglass<sup>®</sup>-ceramic in their solid component, exhibit a constant decrease in their compressive strength and microhardness. The reactivity of bioactive glasses is known to decrease upon crystallization [100]. Therefore, Bioglass<sup>®</sup>-ceramic is considered less reactive with PAA compared to the Bioglass<sup>®</sup>. Incorporation of the excess amounts of Bioglass<sup>®</sup>-ceramic (50 wt% ≤) may interfere with the setting reaction which results in more unreacted particles remaining in the system (e.g. Fig. 5.2d).

According to ISO 9917-1:2002 standard, the minimum compressive strength for a clinically acceptable GIC as restoratives is 100MPa [19, 51] which reveals that C30, C40 and C50 cement groups are in compliance with the compressive strength requirements of this standard. A comparison between our GICs and a few commercially available GICs reveals that C50 has higher compressive strength (~114 MPa on the average) than Fuji IX (99 MPa) and Vitro Molar (70 MPa) [138, 181, 171]. Also, the microhardness of the C50 cement (~72 HV on the average) is comparable to that of the  $\alpha$ -Fil (87 HV), Fuji II (83 HV) and Ketac Molar Easymix (73 HV) [138, 181, 171]. Note that, all the aforementioned commercial GICs contain Al, whereas our GIC is Al-free. Even though the 45S5 Bioglass<sup>®</sup> composition lacks aluminum and it was not originally designed to be used in GICs, these results show that Al-free 45S5 Bioglass<sup>®</sup>-based cements are promising and can compete with commercially available GICs in terms of mechanical performance.

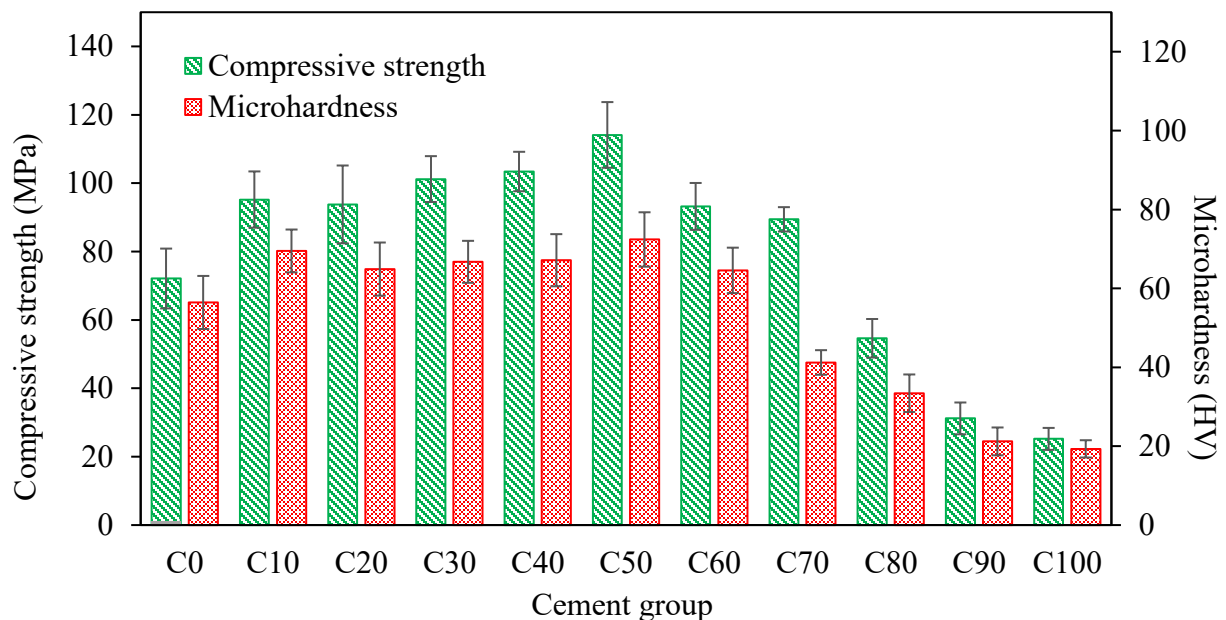


Fig. 5. 3. Compressive strength and microhardness of cements containing various amounts of Bioglass<sup>®</sup>-ceramic particles (Table 5.1) after 7 d immersion in distilled water. (n = 6).

To further investigate the active strengthening mechanisms, the fracture surface of the C50 cement, which demonstrated the highest mechanical performance, was analyzed using SEM (Fig. 5.4). Fig. 5.4a shows a crack that is entering into an embedded submicron particle where it is stopped from further propagation (denoted with a circle) which is known as crack-tip shielding mechanism that can effectively contribute to the improvement of toughness in brittle materials [154]. A similar mechanism can be also observed in Fig. 5.4b. In this mechanism, the stress at the crack tip is decreased by the formation of a dislocation cloud around the crack tip constraining the crack growth. Fig. 5.4c demonstrates another mechanism known as crack deflection mechanism where a crack deviates from its original path when it is encountered with a reinforcing agent (i.e. a Bioglass<sup>®</sup>-ceramic particle). In this mechanism, the increased crack surface due to the deflection, reduces the stress intensity at the crack tip and dissipates its energy [145, 172]. Fig. 5.4d and 4e show the fracture surface of the C50 cement and a commercial GIC (Chemfil Rock, Dentsply), respectively. It can be observed that the fracture surface of the C50 cement has a grainy, rough structure similar to that of the commercial GIC revealing the significant fracture surface energy consumed upon failure.

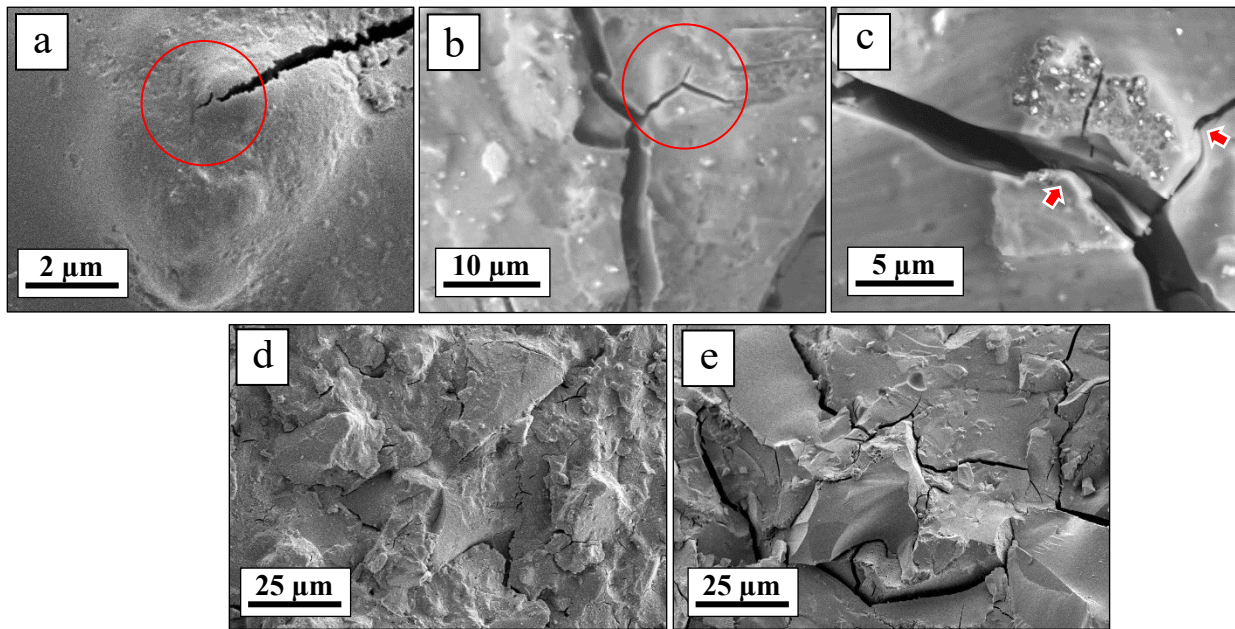


Fig. 5. 4. SEM images captured from the fracture surface of the C50 cement after the compression tests (a, b and c). The circles and arrows indicate crack-tip shielding (a and b) and crack deflection mechanisms (c), respectively. Fig. 5.4d and 4e show the fracture surface of the C50 cement and a commercial GIC (Chemfil Rock, Dentsply), respectively.

In Fig. 5.5 the effect of immersion time in DW on compressive strength and microhardness of the C50 cement, which exhibited the best mechanical properties (Fig. 5.3), is presented. Longer immersion in DW has been reported to improve the compressive strength of GICs [149]. During GIC setting, there is a progressive diffusion-controlled process that forms a hard phase due to the continuous crosslinking of the polyacrylate chains. The presence of Si and P within the matrix results in formation of an inorganic network interpenetrating with the metal (e.g.  $\text{Ca}^{2+}$ ) polyacrylate one. Formation of such inorganic network along with the aforementioned hard phase, leads to a gradual improvement in the strength, stiffness and insolubility of GICs over time, even after the setting [150]. This is consistent with our mechanical properties results (Fig. 5.5) for the C50 cement showing that immersion in DW up to 7 d increases the compressive strength and microhardness of this cement. However, the compressive strength and microhardness of the C50 cement gradually decrease for immersion times longer than 7 d and 14 d, respectively. This can be attributed to the presence of unreacted particles within the set cement (previously observed in Fig. 5.2). Such loosely attached particles may be detached more easily from the matrix over longer immersion times in DW, creating potential crack initiation sites which may result in lower mechanical properties.

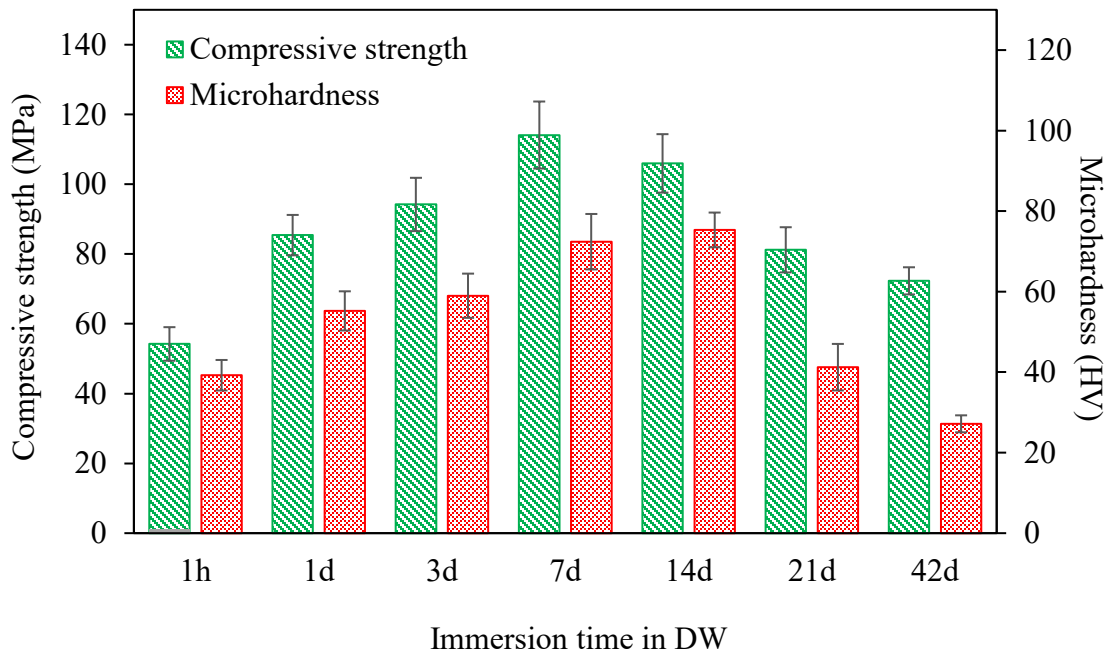


Fig. 5. 5. The effect of immersion time in DW on compressive strength and microhardness of the C50 cement (n = 6).

With applying some adjustments, even higher mechanical properties may be obtained for these cements. According to the PSA results (Fig. 5.1a and b), more than 70 vol% of the particles in both 45S5 Bioglass<sup>®</sup> and Bioglass<sup>®</sup>-ceramic particles are submicron. Since these particles provide a large surface area to react with PAA, there may be insufficient number of ionomer available to effectively hold the large amount of submicron particles resulting in those particles to remain unreacted and unattached to the matrix of the cements and lowering their strength. This might be also the reason for relatively low P:L ratio of the cements in this study (1:0.8) reported in Table 5.1. It has been previously shown that low P:L ratios, may lead to lower mechanical properties (e.g. decreased compressive strength values) [173]. Having a bimodal particle size distribution consist of two equally populated submicron and micron-sized ranges, may not only reduce the number of unreacted submicron particles, but also allow higher P:L ratios and potentially enhance the mechanical performance.

#### 5.3.2.2 FTIR analysis

The FTIR spectra showing the effects of powder composition and immersion time on the structure of our Bioglass<sup>®</sup>-based GICs are presented in Fig. 5.6. The absorption bands at 1410 cm<sup>-1</sup> and 1550 cm<sup>-1</sup> respectively correspond to the symmetric and asymmetric stretching vibration of Ca-polyacrylate complex (COO<sup>-</sup> Ca<sup>2+</sup>) and the peak at 1050 cm<sup>-1</sup> is assigned to silicic acid (H<sub>2</sub>SiO<sub>3</sub>) formation [170, 183, 184]. Ca-polyacrylate formation is the result of PAA ionic crosslinking which utilizes cations (i.e. Ca<sup>2+</sup>) leaching out of the glass particles [158]. Also, silicic acid is the result of the dissolution of SiO<sub>2</sub> glass network when attacked by PAA [73].

Fig. 5.6a presents the FTIR spectra of the C0, C50 and C100 cements. The spectrum of the C50 cement shows the highest peak intensity for both COO<sup>-</sup> Ca<sup>2+</sup> and H<sub>2</sub>SiO<sub>3</sub>, among the three spectra, which may indicate a higher degree of crosslinking that is in line with its superior mechanical properties (Fig. 5.3). The FTIR spectra of the C50 cement after 1 d, 7 d and 21 d immersion in DW are presented in Fig. 5.6b. It can be observed that by increasing the immersion time, the intensity of both COO<sup>-</sup> Ca<sup>2+</sup> and H<sub>2</sub>SiO<sub>3</sub> peaks increases which can be due to the continuous crosslinking of the polyacrylate chains and formation of the hard phase.

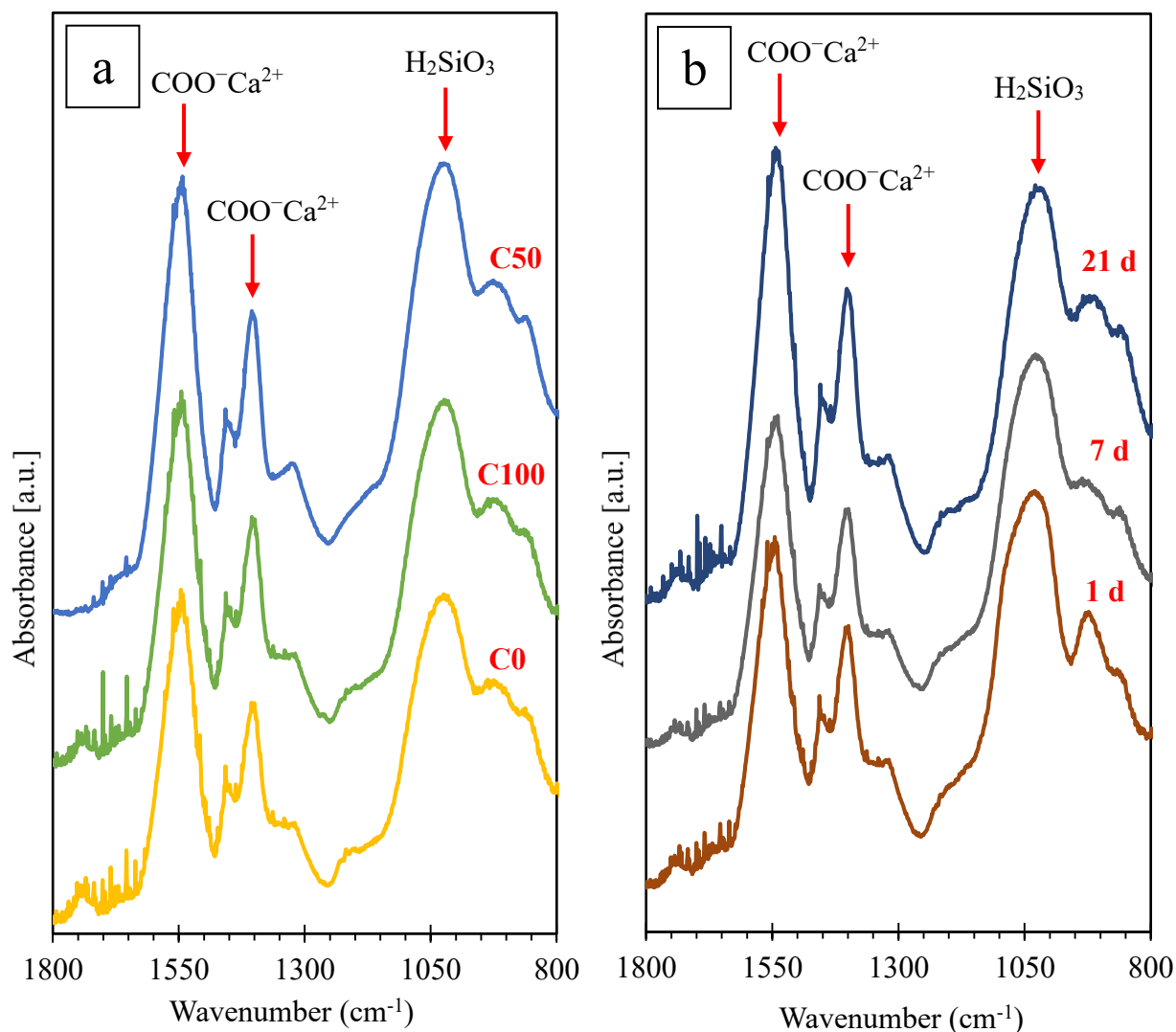


Fig. 5. 6. FTIR spectra of the C0, C50 and C100 cements after 7 d immersion in DW (a); and the C50 cement after 1, 10 and 20 days of immersion in DW (b).

Using FTIR, the complex formation process of our GICs is assessed in situ over the initial 25 minutes of setting (Fig. 5.7) through monitoring the changes in absorbance ratio of complexed to free carboxyls [183, 184]. Fig. 5.7 shows the change in the intensity of the COOH (1650 cm<sup>-1</sup>) and the COO<sup>-</sup>Ca<sup>2+</sup> (1550 cm<sup>-1</sup>) peaks for our Bioglass<sup>®</sup>-based GIC (C50) over time. It appears that, the intensity of the COO<sup>-</sup>Ca<sup>2+</sup> peak increases over time at the expense of the COOH peak. This gradual time-dependent change can be an indication for the progression of the acid-base reaction until the GIC sets [179, 183, 184]. The released Ca<sup>2+</sup> ions from the glass particles start to create salt bridges which crosslink the polyacrylate chains and lead to a decrease in COOH (1650 cm<sup>-1</sup>) peak intensity. Simultaneously, the intensity of peaks corresponding to the symmetric (1410

$\text{cm}^{-1}$ ) and asymmetric ( $1550 \text{ cm}^{-1}$ )  $\text{Ca-polyacrylate} (\text{COO}^- \text{Ca}^{2+})$  bonds increases. The progression of the GIC setting reaction is further assessed by plotting the  $\text{COO}^- \text{Ca}^{2+}/\text{COOH}$  ratios (i.e. the ratio of  $1550 \text{ cm}^{-1}$  to  $1650 \text{ cm}^{-1}$  and  $1410 \text{ cm}^{-1}$  to  $1650 \text{ cm}^{-1}$ ) over time (the subplot in Fig. 5.7). The  $\text{COO}^- \text{Ca}^{2+}/\text{COOH}$  ratio increases over time indicating the increase in concentration of the crosslinked carboxylates and the progressive nature of the setting reaction in our GICs [183, 184].

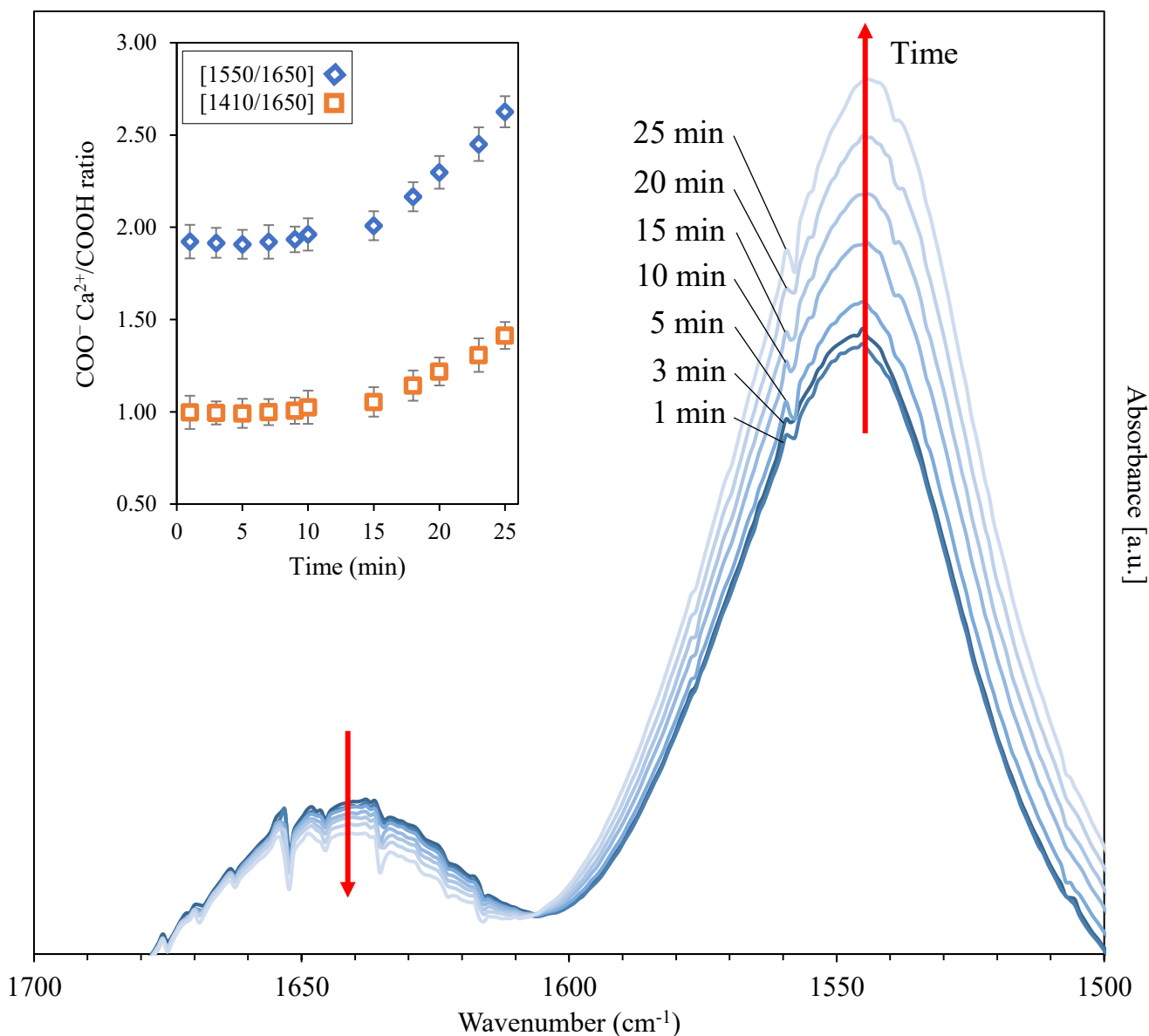


Fig. 5. 7. Change in intensity of the absorbance peaks of  $\text{COO}^- \text{Ca}^{2+}$  ( $1550 \text{ cm}^{-1}$ ) and  $\text{COOH}$  ( $1650 \text{ cm}^{-1}$ ) during FTIR analysis of the C50 system as a function of time. The subplots in the upper left of spectra depicts the ratio of  $1550 \text{ cm}^{-1}$  to  $1650 \text{ cm}^{-1}$  ( $\blacklozenge$ ) and  $1410 \text{ cm}^{-1}$  to  $1650 \text{ cm}^{-1}$  ( $\blacksquare$ ) band intensities ( $n = 3$ ). Note that the peak assigned to symmetric vibration band of  $\text{COO}^- \text{Ca}^{2+}$  ( $1410 \text{ cm}^{-1}$ ) which was used in the subplot is not presented here.



## 5.4 Conclusions

In this study, we produced an Al-free 45S5 Bioglass<sup>®</sup>-based GIC with standard compressive strength comparable to that of the commercially available GICs. We showed that the cements with the solid component containing 50 wt% Bioglass<sup>®</sup> and 50 wt% Bioglass<sup>®</sup>-ceramic (74% crystallinity) exhibited the highest combination of compressive strength and microhardness. Strengthening mechanisms such as crack deflection and crack-tip shielding were found to be activated enhancing the mechanical properties of this group of GICs. Also, cements with lower (e.g. 10 wt%) and higher (e.g. 100 wt%) Bioglass<sup>®</sup>-ceramic contents showed many loosely attached particles in their microstructure acting as crack initiation sites. It was also discussed that the bimodal particle size distribution of the solid component in these GICs may have contributed to their high packing density and structural integrity after setting where smaller particles mostly take part in the setting reaction while larger particles participate in strengthening mechanisms e.g. crack deflection. Supplementary *in vitro* and *in vivo* tests are required in the future to further study these 45S5 Bioglass<sup>®</sup>-based GICs and their performance as dental restorative and/or bone cements.

## Acknowledgment

Compliance with Ethical Standards: This research was funded by the Natural Sciences and Engineering Research Council of Canada (NSERC) under the Discovery Grants program and Concordia University. E. Rezabeigi is supported by the NSERC postdoctoral fellowship award. The authors thank Prof. Robert Hill (Barts and The London School of Medicine and Dentistry) for kindly donating the 45S5 Bioglass<sup>®</sup> powder.

## Conflict of Interest

The authors declare that they have no conflict of interest.

## Chapter 6

### 6.1 Summary of conclusions

In this study new hybrid GICs with improved mechanical and remineralizing properties were developed by incorporation of 45S5 Bioglass<sup>®</sup>-ceramic particles.

A comprehensive set of heat treatment regimes were presented providing the possibility of tailoring the crystallinity of 45S5 Bioglass<sup>®</sup> from 5% up to 100% by controlling the nucleation and growth of mechanically strong phase of combeite ( $\text{Na}_2\text{Ca}_2\text{Si}_3\text{O}_9$ ) as the only crystalline phase present in the system. Such heat treatments can be used to produce Bioglass<sup>®</sup>-ceramics with appropriate degree of crystallinity for specific applications such as bone regeneration and additives for dental restoratives.

The results of DSC and XRD analyses on a melt-derived 45S5 Bioglass<sup>®</sup> powder were used to develop the heat treatment profiles. The same results were used to calculate the crystallization energy ( $E = 192 \text{ kJ/mol}$ ) for and obtain the Avrami exponent ( $n = 0.71$ ) of combeite which were then used to explain its crystallization mechanism. The crystallization energy was calculated using three numerical methods namely the Kissinger, the Ozawa and the Yinnon methods. The enthalpy of crystallization ( $\Delta H$ ) was recorded as  $153 \pm 4 \text{ J/g}$  and it was shown to be independent of the heating rate.

The SEM/EDS results showed that the combeite crystallization mostly occurred on the surface of the particles. The microstructural analysis showed that the size of the combeite crystals increased up to 27 nm by increasing the heat treatment temperature from 650 °C and 800 °C. Two distinct elemental distribution patterns within and between the grains were reported by X-ray mapping analysis. The intergranular region between the combeite crystals was shown to be the P-rich amorphous phase which was preferentially dissolved during etching due to its lower chemical stability compare to that of combeite.

The mechanical and remineralizing properties of a commercially available GIC was enhanced through the incorporation of 45S5 Bioglass<sup>®</sup>-ceramic particles containing a

mechanically strong combeite phase ( $\text{Na}_2\text{Ca}_2\text{Si}_3\text{O}_9$ ). Based on the results of the compression, diametral tensile and microhardness tests, the 45S5 Bioglass<sup>®</sup>-ceramic with 74% crystallinity was shown to deliver the highest overall mechanical properties when incorporated into the GIC. The 45S5 Bioglass<sup>®</sup>-ceramic with 74% crystallinity was reported to contain an optimum balance of combeite and P-rich phase contributing to the improved mechanical properties of the particles and their interfacial adhesion with the GIC matrix, respectively.

It was shown that the hybrid GICs containing 5 wt% Bioglass<sup>®</sup>-ceramic with 74% crystallinity had higher compressive strength and diametral tensile strength compared to that of the commercial GIC. It was reported that after 7 days immersion in distilled water that the compressive strength and diametral tensile strength of these samples were improved by 15% and 60%, respectively, compared to those of the commercial GIC. Strengthening mechanisms including crack deflection, crack branching, crack-tip shielding, and particle pull-out were reported and discussed as contributing to the mechanical performance enhancement for this hybrid GIC. It was also shown that the longer soaking times of the GICs containing up to 5 wt% Bioglass<sup>®</sup>-ceramic in distilled water (7 days) improved their compressive strength. It was reported that the incorporation of excess Bioglass<sup>®</sup>-ceramic (10 wt%  $\leq$ ) resulted in a high number of loosely attached particles which detach easily from the GIC matrix, thus diminishing the compressive strength and diametral tensile strength by creating potential crack initiation sites.

The *in vitro* studies in SBF showed that the pH increased after 1 d immersion in SBF followed by a gradual decrease thereafter. The pH increase was shown to be due to ion exchange of  $\text{Ca}^{2+}$  in the GICs with  $\text{H}^+$  in SBF and formation of a hydrated silica layer on the GICs. The pH decrease was demonstrated to be the result of the formation of carbonated hydroxyapatite through incorporating  $\text{OH}^-$  from SBF which was later verified and confirmed by XRD results.

It was reported that the CHA was formed at a low rate which can be beneficial for the hybrid GIC containing 5 wt% Bioglass<sup>®</sup>-ceramic as it allows the Bioglass<sup>®</sup>-ceramic particles to not only provide sufficient time for the development of improved chemical bonding between the dentine tissue but also play their reinforcing role by maintaining their strength over time and serving as a reliable dental restorative. The apatite precipitation was observed by SEM analysis on the hybrid GICs containing 5 wt% and 10 wt% Bioglass<sup>®</sup>-ceramic after 1 d immersion in SBF

which was shown to grow into various apatite morphologies (e.g. three-dimensional discrete islands) by increasing the immersion times.

An Al-free 45S5 Bioglass<sup>®</sup>-based GIC with standard compressive strength comparable to that of the commercially available GICs was developed. The setting time of developed cements with the powder to liquid ratio (P:L) of 1:0.8 ranged from  $6.5 \pm 1.2$  to  $22.7 \pm 3.2$  min. It was reported that the GICs containing 50-50 wt% Bioglass<sup>®</sup> and Bioglass<sup>®</sup>-ceramic (C50) resulted in the highest mechanical performance with compressive strength of  $114 \pm 10$  MPa and microhardness of  $72 \pm 7$  HV. It was shown that the strengthening mechanisms such as crack deflection and crack-tip shielding were activated in C50 cements which was attributed to their optimum composition.

FTIR analysis showed that the C50 cements represented the highest peak intensity for both  $\text{COO}^- \text{Ca}^{2+}$  and  $\text{H}_2\text{SiO}_3$  indicating a higher degree of crosslinking in this GIC group compared to other compositions. The results of the in situ FTIR analysis on setting C50 cements showed that the intensity of the  $\text{COO}^- \text{Ca}^{2+}$  peak gradually increased over time at the expense of the COOH peak which was an indication of a well-performed acid-base reaction in this GIC.

It was also reported that the bimodal particle size distribution of the solid component in the C50 cements might have contributed to their high packing density and structural integrity after setting where smaller particles mostly take part in the setting reaction while larger particles participate in strengthening mechanisms e.g. crack deflection.

## 6.2 Contributions to Knowledge

Each stage of this study has produced novel contributions which all combine to allow for improvement of mechanical and biomineralizing properties of glass ionomer cements doped with 45S5 Bioglass<sup>®</sup>-ceramic particles. The idea of crystallization of the Bioglass<sup>®</sup> and incorporating it in glass-ceramic form can be usefully applied to other biomaterials e. g. bone cements, scaffolds, and implants. The results obtained from the Bioglass<sup>®</sup> thermal analysis can definitely help in understanding the Bioglass<sup>®</sup> crystallization behavior. The produced hybrid GIC with enhanced mechanical and remineralizing performance can potentially gain wide clinical interest. Being Al-free while acquiring the required standard mechanical properties, the novel 45S5 Bioglass<sup>®</sup>-based

GIC developed in the last chapter of this research can be a promising material as dental restorative and/or bone cement. The details of the contributions of the current research are explained below.

For the first time it was demonstrated that a comprehensive set of heat treatment regimes can be developed to accurately crystallize the Bioglass<sup>®</sup> to the desired degree of crystallization of combeite to obtain a mechanically strong yet bioactive phase. Depending on the target application, different levels of mechanical and remineralizing properties may be required. The crystallinity of 45S5 Bioglass<sup>®</sup> can be tailored from 5% to 95% by applying the appropriate heat treatment regime selected from the profiles developed in this study. Also, the detailed experimental methodology designed for studying the thermal and crystallization behavior of the Bioglass<sup>®</sup> can be used for similar bioactive glasses.

For the first time, a modified hybrid GIC with improved mechanical and remineralizing properties was produced by incorporation of an optimum amount (5 wt%) of 45S5 Bioglass<sup>®</sup>-ceramic containing optimum combeite crystallinity (74%). Based on the literature, previously developed GIC containing bioglasses, severely lack compressive strength and also cement integrity. The hybrid GIC produced in this study benefit from a compressive strength higher than the commercially available GIC. The understanding of the fact that sufficient amounts of crystallized phase (i.e. combeite) and the amorphous phosphorous-rich phase are both needed for the glass-ceramic to effectively partake in the setting process and form an excellent interfacial bond with the GIC matrix can help in the design of the microstructure and properties of the hybrid GICs produced. A widespread investigation on the *in vitro* behavior of the hybrid GICs as well as the effective strengthening mechanisms leading to their prominent mechanical performance were also described. Such hybrid GICs can potentially offer improved *in vivo* performance with broad clinical applications.

The development of an Al-free GICs using 45S5 Bioglass<sup>®</sup> and its corresponding Bioglass<sup>®</sup>-ceramic with standard mechanical properties is another major contribution of this study. For the first time additions of a bioactive glass as the only solid component of GICs was investigated. The 45S5 glass-ceramic particles with 74% crystallinity were used for this purpose as they can best act as both remineralizing and reinforcing agents. In these GICs, the neurotoxic effects of Al are avoided while chemical bonds are expected to form between the GIC and the surrounding hard tissue(s) through interfacial biomineralization and adhesion.

### 6.3 Future work

The following suggestions are proposed as future work to expand further the current study:

- ❖ The comprehensive set of heat treatment regimes presented in chapter 3 provides the possibility of producing mechanically strong Bioglass<sup>®</sup>-ceramics with appropriate degree of crystallinity suitable for various applications (e.g. bone cements). The same experimental approach used in this study can be employed to improve mechanical and remineralizing properties of bone cements.
- ❖ In vitro cell tests, in vivo tests and clinical studies should be performed on GICs developed in this research to further evaluate their biocompatibility as well as their mechanical performance in-service.
- ❖ It is suggested to study the adhesion properties (e.g. shear bond strength to dentin) of the GICs developed in this research.
- ❖ It would be interesting to conduct a similar research utilizing commercially available bioglasses other than 45S5 Bioglass<sup>®</sup> and compare the results.
- ❖ 45S5 Bioglass<sup>®</sup> and Bioglass<sup>®</sup>-ceramic used in this research were in the powder form. It would be interesting to see the result when they are used in other forms e.g. fiber, microfibers, nanoparticles, etc.
- ❖ Bimodal distribution of the Bioglass<sup>®</sup> and Bioglass<sup>®</sup>-ceramic was shown to affect the mechanical performance of the GICs. It is suggested to study the effect of particle size of the Bioglass<sup>®</sup>-ceramic on the mechanical and setting properties of the GICs developed in this study.
- ❖ It would be worth examining the addition of an optimized amount of a chelating agent to the liquid component of the Al-free GIC to better control the setting reaction and possibly lowering the setting time.

## REFERENCES

- [1] S. K. Sidhu, Ed., *Glass-ionomers in Dentistry*. London: Springer, 2015.
- [2] J. Graham and W. R. H. Mount, *Preservation and Restoration of Tooth Structure*, 2nd ed. Sandgate: Knowledge books and software, 2005.
- [3] M. S. Baig and G. J. P. Fleming, “Conventional glass-ionomer materials : A review of the developments in glass powder, polyacid liquid and the strategies of reinforcement,” *J. Dent.*, vol. 43, no. 8, pp. 897–912, 2015.
- [4] R. G. Craig and J. M. Power, “Restorative dental materials. Mosby-Year Book,” *Inc., Missouri*, p. 486, 1997.
- [5] C. L. Davidson, “Advances in glass-ionomer cements,” *J. Appl. Oral Sci.*, vol. 14, no. SPE, pp. 3–9, 2006.
- [6] S. J. Bonsor and G. Pearson, *A clinical guide to applied dental materials*. Elsevier Health Sciences, 2012.
- [7] S. Sorel, “Procedure for the formation of a very solid cement by the action of chloride on the oxide of zinc,” *CR Hebd Seances Acad Sci*, vol. 41, pp. 784–785, 1855.
- [8] E. E. Hill and J. Lott, “A clinically focused discussion of luting materials,” *Aust. Dent. J.*, vol. 56, pp. 67–76, 2011.
- [9] J. W. Nicholson, “The History and Background to Glass-Ionomer Dental Cements,” in *Glass-Ionomers in Dentistry*, Springer, 2016, pp. 1–24.

- [10] A. D. Wilson and J. W. Nicholson, *Acid-base cements: their biomedical and industrial applications*, vol. 3. Cambridge University Press, 2005.
- [11] A. Kakaboura and G. Vougiouklakis, “Cements in orthodontics,” in *Orthodontic Materials: Scientific and Clinical Aspects.*, Stuttgart: Thieme, 2001, pp. 221–240.
- [12] A. D. Wilson, “Acidobasicity of oxide glasses used in glass ionomer cements,” *Dent. Mater.*, vol. 12, no. 1, pp. 25–29, 1996.
- [13] A. D. Wilson, “The glass-ionomer cement, a new translucent cement for dentistry,” *J Appl Chem Biotechnol*, vol. 21, p. 313, 1971.
- [14] A. D. Wilson, “A new translucent cement for dentistry: the glass-ionomer cement,” *Br Dent J*, vol. 132, pp. 133–135, 1972.
- [15] V. Buerkle, J. Kuehnisch, M. Guelmann, and R. Hickel, “Restoration materials for primary molars—results from a European survey,” *J. Dent.*, vol. 33, no. 4, pp. 275–281, 2005.
- [16] A. D. Wilson and J. W. McLean, *Glass ionomer cement*. Chicago, IL, USA: Quintessence Publishing Co, 1988.
- [17] A. D. Wilson, S. Crisp, H. J. Prosser, B. G. Lewis, and S. A. Merson, “Aluminosilicate glasses for polyelectrolyte cements,” *Ind. Eng. Chem. Prod. Res. Dev.*, vol. 19, no. 2, pp. 263–270, 1980.
- [18] S. Crisp, B. G. Lewis, and A. D. Wilson, “Gelation of polyacrylic acid aqueous solutions and the measurement of viscosity,” *J. Dent. Res.*, vol. 54, no. 6, pp. 1173–



1175, 1975.

- [19] J. W. Nicholson, "Adhesion of glass-ionomer cements to teeth: A review," *Int. J. Adhes. Adhes.*, vol. 69, pp. 33–38, 2016.
- [20] J. W. Nicholson and B. Czarnecka, "The biocompatibility of resin-modified glass-ionomer cements for dentistry," *Dent. Mater.*, vol. 24, no. 12, pp. 1702–1708, 2008.
- [21] A. Valanezhad, T. Odatsu, K. Udoh, and T. Shiraishi, "Modification of resin modified glass ionomer cement by addition of bioactive glass nanoparticles," *J. Mater. Sci. Mater. Med.*, vol. 27, no. 1, pp. 1–9, 2016.
- [22] G. Palmer, H. M. Anstice, and G. J. Pearson, "The effect of curing regime on the release of hydroxyethyl methacrylate (HEMA) from resin-modified glass-ionomer cements," *J. Dent.*, vol. 27, no. 4, pp. 303–311, 1999.
- [23] W. D. Cook, "Degradative analysis of glass ionomer polyelectrolyte cements," *J. Biomed. Mater. Res.*, vol. 17, no. 6, pp. 1015–1027, 1983.
- [24] R. Zimehl and M. Hannig, "Non metallic restorative materials based on glass ionomer cements - Recent trends and developments," *Colloids Surfaces A Physicochem. Eng. Asp.*, vol. 163, no. 1, pp. 55–62, 2000.
- [25] S. Crisp and A. D. Wilson, "Reactions in glass ionomer cements: V. Effect of incorporating tartaric acid in the cement liquid," *J. Dent. Res.*, vol. 55, no. 6, pp. 1023–1031, 1976.
- [26] A. D. Wilson, "A hard decade's work: steps in the invention of the glass-ionomer

- cement,” *J. Dent. Res.*, vol. 75, no. 10, pp. 1723–1727, 1996.
- [27] S. Crisp and A. D. Wilson, “Cements comprising acrylic acid/itaconic acid copolymer and fluoroaluminosilicate glass powder.” Google Patents, 05-Apr-1977.
- [28] E. De Barra and R. Hill, “Influence of poly (acrylic acid) content on the fracture behaviour of glass polyalkenoate cements,” *J. Mater. Sci.*, vol. 33, no. 23, pp. 5487–5497, 1998.
- [29] A. H. Dowling and G. J. P. Fleming, “The influence of poly (acrylic) acid number average molecular weight and concentration in solution on the compressive fracture strength and modulus of a glass-ionomer restorative,” *Dent. Mater.*, vol. 27, no. 6, pp. 535–543, 2011.
- [30] S. Crisp, B. G. Lewis, and A. D. Wilson, “Characterization of glass-ionomer cements: 3. Effect of polyacid concentration on the physical properties,” *J. Dent.*, vol. 5, no. 1, pp. 51–56, 1977.
- [31] R. G. Hill and S. A. Labok, “The influence of polyacrylic acid molecular weight on the fracture of zinc polycarboxylate cements,” *J. Mater. Sci.*, vol. 26, no. 1, pp. 67–74, 1991.
- [32] S. F. Edwards, “The statistical mechanics of polymerized material,” *Proc. Phys. Soc.*, vol. 92, no. 1, p. 9, 1967.
- [33] P. Prentice, “The influence of molecular weight on the fracture of thermoplastic glassy polymers,” *J. Mater. Sci.*, vol. 20, no. 4, pp. 1445–1454, 1985.

- [34] R. Zimehl and M. Hannig, “Non metallic restorative materials based on glass ionomer cements — recent trends and developments,” vol. 163, pp. 55–62, 2000.
- [35] J. M. Paddon and A. D. Wilson, “Stress relaxation studies on dental materials 1. Dental cements,” *J. Dent.*, vol. 4, no. 4, pp. 183–189, 1976.
- [36] A. D. Wilson, J. M. Paddon, and S. Crisp, “The hydration of dental cements,” *J. Dent. Res.*, vol. 58, no. 3, pp. 1065–1071, 1979.
- [37] M. S. A. Earl, W. R. Hume, and G. J. Mount, “Effect of varnishes and other surface treatments on water movement across the glass-ionomer cement surface,” *Aust. Dent. J.*, vol. 30, no. 4, pp. 298–301, 1985.
- [38] R. C. Randall and N. H. F. Wilson, “Glass-ionomer restoratives: a systematic review of a secondary caries treatment effect,” *J. Dent. Res.*, vol. 78, no. 2, pp. 628–637, 1999.
- [39] L. Forsten, “Fluoride release and uptake by glass ionomers,” *Eur. J. Oral Sci.*, vol. 99, no. 3, pp. 241–245, 1991.
- [40] W. M. Tay and M. Braden, “Fluoride ion diffusion from polyalkenoate (glass-ionomer) cements,” *Biomaterials*, vol. 9, no. 5, pp. 454–456, 1988.
- [41] A. M. J. C. De Witte, E. A. P. De Maeyer, R. M. H. Verbeeck, and L. C. Martens, “Fluoride release profiles of mature restorative glass ionomer cements after fluoride application,” *Biomaterials*, vol. 21, no. 5, pp. 475–482, 2000.
- [42] J. W. Nicholson, A. Aggarwal, B. Czarnecka, and H. Limanowska-Shaw, “The rate

- of change of pH of lactic acid exposed to glass-ionomer dental cements,”  
*Biomaterials*, vol. 21, no. 19, pp. 1989–1993, 2000.
- [43] J. D. Scholtanus and M.-C. D. Huysmans, “Clinical failure of class-II restorations of a highly viscous glass-ionomer material over a 6-year period: a retrospective study,”  
*J. Dent.*, vol. 35, no. 2, pp. 156–162, 2007.
- [44] J. L. Moreau and H. H. K. Xu, “Fluoride releasing restorative materials: Effects of pH on mechanical properties and ion release,” *Dent. Mater.*, vol. 26, no. 11, pp. e227–e235, 2010.
- [45] A. Wiegand, W. Buchalla, and T. Attin, “Review on fluoride-releasing restorative materials — Fluoride release and uptake characteristics, antibacterial activity and influence on caries formation,” vol. 3, pp. 343–362, 2006.
- [46] X. Xu and J. O. Burgess, “Compressive strength, fluoride release and recharge of fluoride-releasing materials,” *Biomaterials*, vol. 24, no. 14, pp. 2451–2461, 2003.
- [47] A. J. Preston, E. A. Agalamanyi, S. M. Higham, and L. H. Mair, “The recharge of esthetic dental restorative materials with fluoride in vitro—two years’ results,” *Dent. Mater.*, vol. 19, no. 1, pp. 32–37, 2003.
- [48] J. W. Nicholson, “Adhesive dental materials - A review,” *Int. J. Adhes. Adhes.*, vol. 18, no. 4, pp. 229–236, 1998.
- [49] Y. E. Y. Aboush, “An evaluation of the bonding of glass ionomer restorative to dentine and enamel,” *Br Dent J*, vol. 161, pp. 179–184, 1986.

- [50] H. C. Ngo, G. Mount, J. Mc Intyre, J. Tuisuva, and R. J. Von Doussa, "Chemical exchange between glass-ionomer restorations and residual carious dentine in permanent molars: an in vivo study," *J. Dent.*, vol. 34, no. 8, pp. 608–613, 2006.
- [51] "ISO 9917-1 Dentistry--Water-based cements--Part 1: Powder/liquid acid based cements," *Geneva. Switz. Int. Organ. Stand.*, 2003.
- [52] M. Kobayashi, M. Kon, K. Miyai, and K. Asaoka, "Strengthening of glass-ionomer cement by compounding short fibres with CaO–P<sub>2</sub>O<sub>5</sub>–SiO<sub>2</sub>–Al<sub>2</sub>O<sub>3</sub> glass," *Biomaterials*, vol. 21, no. 20, pp. 2051–2058, 2000.
- [53] J. J. Simmons, "The miracle mixture. Glass ionomer and alloy powder.," *Tex. Dent. J.*, vol. 100, no. 10, p. 6, 1983.
- [54] J. J. Simmons, "Silver–alloy powder and glass ionomer cement," *J. Am. Dent. Assoc.*, vol. 120, no. 1, pp. 49–52, 1990.
- [55] D. Miller, V. A. Marker, T. Okabe, J. J. Simmons, and L. D. Zardiackas, "Formulation and evaluation of dental amalgam alloy added to glass ionomer," in *Journal of Dental Research*, 1984, vol. 63, p. 231.
- [56] Y. W. Gu, A. U. J. Yap, P. Cheang, and K. A. Khor, "Zirconia-glass ionomer cement - A potential substitute for Miracle Mix," *Scr. Mater.*, vol. 52, no. 2, pp. 113–116, 2005.
- [57] R. E. Kerby and R. F. Bleiholder, "Physical properties of stainless-steel and silver-reinforced glass-ionomer cements," *J. Dent. Res.*, vol. 70, no. 10, pp. 1358–1361,

1991.

- [58] J. W. Nicholson, S. J. Hawkins, and J. E. Smith, "The incorporation of hydroxyapatite into glass-polyalkenoate ('glass-ionomer') cements: a preliminary study," *J. Mater. Sci. Mater. Med.*, vol. 4, no. 4, pp. 418–421, 1993.
- [59] A. Moshaverinia, S. Ansari, M. Moshaverinia, N. Roohpour, J. A. Darr, and I. Rehman, "Effects of incorporation of hydroxyapatite and fluoroapatite nanobioceramics into conventional glass ionomer cements (GIC)," *Acta Biomater.*, vol. 4, no. 2, pp. 432–440, 2008.
- [60] K. Arita *et al.*, "Hydroxyapatite particle characteristics influence the enhancement of the mechanical and chemical properties of conventional restorative glassionomer cement," *Dent. Mater. J.*, vol. 30, no. 5, pp. 672–683, 2011.
- [61] T. De Caluwé *et al.*, "Addition of bioactive glass to glass ionomer cements: Effect on the physico-chemical properties and biocompatibility," *Dent. Mater.*, vol. 33, no. 4, pp. 186–203, 2017.
- [62] M. E. Lucas, K. Arita, and M. Nishino, "Toughness, bonding and fluoride-release properties of hydroxyapatite-added glass ionomer cement," *Biomaterials*, vol. 24, no. 21, pp. 3787–3794, 2003.
- [63] D. A. Kim, J. H. Lee, S. K. Jun, H. W. Kim, M. Eltohamy, and H. H. Lee, "Sol–gel-derived bioactive glass nanoparticle-incorporated glass ionomer cement with or without chitosan for enhanced mechanical and biomineralization properties," *Dent. Mater.*, vol. 33, no. 7, pp. 805–817, 2017.

- [64] A. Zandi Karimi, E. Rezabeigi, and R. A. L. Drew, "Glass ionomer cements with enhanced mechanical and remineralizing properties containing 45S5 bioglass-ceramic particles," *J. Mech. Behav. Biomed. Mater.*, vol. 97, pp. 396–405, 2019.
- [65] H. Yli-Urpo, L. V. J. Lassila, T. Närhi, and P. K. Vallittu, "Compressive strength and surface characterization of glass ionomer cements modified by particles of bioactive glass," *Dent. Mater.*, vol. 21, no. 3, pp. 201–209, 2005.
- [66] J. E. Frencken, "The ART approach using glass-ionomers in relation to global oral health care," *Dent. Mater.*, vol. 26, no. 1, pp. 1–6, 2010.
- [67] J. E. Frencken, M. A. Van 't Hof, W. E. Van Amerongen, and C. J. Holmgren, "Effectiveness of single-surface ART restorations in the permanent dentition: A meta-analysis," *J. Dent. Res.*, vol. 83, no. 2, pp. 120–123, 2004.
- [68] S. Mickenautsch, V. Yengopal, and A. Banerjee, "Atraumatic restorative treatment versus amalgam restoration longevity: A systematic review," *Clin. Oral Investig.*, vol. 14, no. 3, pp. 233–240, 2010.
- [69] P. Zatta, T. Kiss, M. Suwalsky, and G. Berthon, "Aluminium(III) as a promoter of cellular oxidation," *Coord. Chem. Rev.*, vol. 228, no. 2, pp. 271–284, 2002.
- [70] B. A. Khader, O. Rodriguez, and M. R. Towler, "The effect of Mg<sup>2+</sup> incorporation into the glass phase of zinc-based glass polyalkenoate cements," *J. Non. Cryst. Solids*, vol. 483, no. October 2017, pp. 106–117, 2018.
- [71] J. Nourmohammadi, S. K. Sadrnezhad, and A. Behnamghader, "In vitro bioactivity

- of novel cured ionomer cement based on iron oxide,” *Ceram. Int.*, vol. 36, no. 5, pp. 1645–1651, 2010.
- [72] D. A. Kim, H. A. Abo-Mosallam, H. Y. Lee, G. R. Kim, H. W. Kim, and H. H. Lee, “Development of a novel aluminum-free glass ionomer cement based on magnesium/strontium-silicate glasses,” *Mater. Sci. Eng. C*, vol. 42, pp. 665–671, 2014.
- [73] M. N. Rahaman *et al.*, “Bioactive glass in tissue engineering,” *Acta Biomater.*, vol. 7, no. 6, pp. 2355–2373, 2011.
- [74] T. Kokubo and H. Takadama, “How useful is SBF in predicting in vivo bone bioactivity?,” *Biomaterials*, vol. 27, no. 15, pp. 2907–2915, 2006.
- [75] M. Cerruti, D. Greenspan, and K. Powers, “Effect of pH and ionic strength on the reactivity of Bioglass<sup>®</sup> 45S5,” *Biomaterials*, vol. 26, no. 14, pp. 1665–1674, 2005.
- [76] D. Arcos and M. Vallet-Regí, “Sol–gel silica-based biomaterials and bone tissue regeneration,” *Acta Biomater.*, vol. 6, no. 8, pp. 2874–2888, 2010.
- [77] L. L. Hench, “The story of Bioglass<sup>®</sup>,” *J. Mater. Sci. Mater. Med.*, vol. 17, no. 11, pp. 967–978, 2006.
- [78] J. R. Jones, “New trends in bioactive scaffolds: The importance of nanostructure,” *J. Eur. Ceram. Soc.*, vol. 29, no. 7, pp. 1275–1281, 2009.
- [79] S. M. Best, A. E. Porter, E. S. Thian, and J. Huang, “Bioceramics: past, present and for the future,” *J. Eur. Ceram. Soc.*, vol. 28, no. 7, pp. 1319–1327, 2008.



- [80] K. Rezwan, Q. Z. Chen, J. J. Blaker, and A. R. Boccaccini, “Biodegradable and bioactive porous polymer/inorganic composite scaffolds for bone tissue engineering,” *Biomaterials*, vol. 27, no. 18, pp. 3413–3431, 2006.
- [81] V. Rajendran, A. N. Begum, M. A. Azooz, and F. H. El Batal, “Microstructural dependence on relevant physical–mechanical properties on SiO<sub>2</sub>–Na<sub>2</sub>O–CaO–P<sub>2</sub>O<sub>5</sub> biological glasses,” *Biomaterials*, vol. 23, no. 21, pp. 4263–4275, 2002.
- [82] J. R. Jones, “Reprint of : Review of bioactive glass : From Hench to hybrids,” *Acta Biomater.*, vol. 23, pp. S53–S82, 2015.
- [83] S. Jung, D. Day, T. Day, W. Stoecker, and P. Taylor, “Treatment of non-healing diabetic venous stasis ulcers with bioactive glass nanofibers,” *Wound Repair Regen.*, vol. 19, no. 2, 2011.
- [84] L. L. Hench, R. J. Splinter, W. C. Allen, and T. K. Greenle, “Bonding mechanisms at the interface of ceramic prosthetic materials,” *J. Biomed. Mater. Res. Symp.*, vol. 5, no. 6, pp. 117–141, 1971.
- [85] A. E. Clark Jr, C. G. Pantano Jr, and L. L. Hench, “Auger spectroscopic analysis of bioglass corrosion films,” *J. Am. Ceram. Soc.*, vol. 59, no. 1-2, pp. 37–39, 1976.
- [86] L. L. Hench, “Bioceramics: From Concept to Clinic,” *J. Am. Ceram. Soc.*, vol. 74, no. 7, pp. 1487–1510, 1991.
- [87] E. A. A. Neel, T. Mizoguchi, M. Ito, M. Bitar, V. Salih, and J. C. Knowles, “In vitro bioactivity and gene expression by cells cultured on titanium dioxide doped

- phosphate-based glasses,” *Biomaterials*, vol. 28, no. 19, pp. 2967–2977, 2007.
- [88] I. Elgayar, A. E. Aliev, A. R. Boccaccini, and R. G. Hill, “Structural analysis of bioactive glasses,” *J. Non. Cryst. Solids*, vol. 351, no. 2, pp. 173–183, 2005.
- [89] P. Sepulveda, J. R. Jones, and L. L. Hench, “In vitro dissolution of melt-derived 45S5 and sol-gel derived 58S bioactive glasses,” *J. Biomed. Mater. Res. An Off. J. Soc. Biomater. Japanese Soc. Biomater. Aust. Soc. Biomater. Korean Soc. Biomater.*, vol. 61, no. 2, pp. 301–311, 2002.
- [90] R. G. Hill and D. S. Brauer, “Predicting the bioactivity of glasses using the network connectivity or split network models,” *J. Non. Cryst. Solids*, vol. 357, no. 24, pp. 3884–3887, 2011.
- [91] R. Li, A. E. Clark, and L. L. Hench, “An investigation of bioactive glass powders by sol-gel processing,” *J. Appl. Biomater.*, vol. 2, no. 4, pp. 231–239, 1991.
- [92] D. Bellucci, V. Cannillo, A. Sola, F. Chiellini, M. Gazzarri, and C. Migone, “Macroporous Bioglass<sup>®</sup>-derived scaffolds for bone tissue regeneration,” *Ceram. Int.*, vol. 37, no. 5, pp. 1575–1585, 2011.
- [93] T. Waltimo, T. J. Brunner, M. Vollenweider, W. J. Stark, and M. Zehnder, “Antimicrobial effect of nanometric bioactive glass 45S5,” *J. Dent. Res.*, vol. 86, no. 8, pp. 754–757, 2007.
- [94] L. L. Hench, D. L. Wheeler, and D. C. Greenspan, “Molecular control of bioactivity in sol-gel glasses,” *J. Sol-Gel Sci. Technol.*, vol. 13, no. 1–3, pp. 245–250, 1998.

- [95] A. Zandi Karimi, E. Rezabeigi, and R. A. L. Drew, “Crystallization behavior of combeite in 45S5 Bioglass<sup>®</sup> via controlled heat treatment,” *J. Non. Cryst. Solids*, vol. 502, pp. 176–183, 2018.
- [96] L. Lefebvre *et al.*, “Structural transformations of bioactive glass 45S5 with thermal treatments,” *Acta Mater.*, vol. 55, no. 10, pp. 3305–3313, 2007.
- [97] L. Lefebvre, L. Gremillard, J. Chevalier, R. Zenati, and D. Bernache-Assolant, “Sintering behaviour of 45S5 bioactive glass,” *Acta Biomater.*, vol. 4, no. 6, pp. 1894–1903, 2008.
- [98] Q. Z. Chen, I. D. Thompson, and A. R. Boccaccini, “45S5 Bioglass<sup>®</sup>-derived glass-ceramic scaffolds for bone tissue engineering,” *Biomaterials*, vol. 27, no. 11, pp. 2414–2425, 2006.
- [99] Q. Chen and A. R. Boccaccini, “Coupling mechanical competence and bioresorbability in bioglass<sup>®</sup>-derived tissue engineering scaffolds,” *Adv. Eng. Mater.*, vol. 8, no. 4, pp. 285–289, 2006.
- [100] O. P. Filho, G. P. Latorre, and L. L. Hench, “Effect of crystallization on apatite-layer formation of bioactive glass 45S5,” *J. Biomed. Mater. Res.*, vol. 30, no. 4, pp. 509–514, 1996.
- [101] D. F. Williams, *Fundamental Aspects of Biocompatibility*. Boca Raton, Florida: CRC Press, 1981.
- [102] L. L. Hench and J. K. West, “Biological applications of bioactive glasses,” *Life*

- Chem. Reports*, vol. 13, pp. 187–241, 1996.
- [103] L. L. Hench, “Bioceramics,” *J. Am. Ceram. Soc.*, vol. 81, no. 7, pp. 1705–1728, 1998.
- [104] S. Hattar, A. Asselin, D. Greenspan, M. Oboeuf, A. Berdal, and J. M. Sautier, “Potential of biomimetic surfaces to promote in vitro osteoblast-like cell differentiation,” *Biomaterials*, vol. 26, no. 8, pp. 839–848, 2005.
- [105] E. Rezabeigi, P. M. Wood-Adams, and R. A. L. Drew, “Morphological examination of highly porous polylactic acid/Bioglass® scaffolds produced via nonsolvent induced phase separation,” *J. Biomed. Mater. Res. Part B Appl. Biomater.*, vol. 105, no. 8, pp. 2433–2442, 2017.
- [106] D. C. Clupper and L. L. Hench, “Crystallization kinetics of tape cast bioactive glass 45S5,” *J. Non. Cryst. Solids*, vol. 318, no. 1–2, pp. 43–48, 2003.
- [107] E. Rezabeigi, P. M. Wood-Adams, and R. A. L. Drew, “Synthesis of 45S5 Bioglass® via a straightforward organic, nitrate-free sol-gel process,” *Mater. Sci. Eng. C*, vol. 40, pp. 248–252, 2014.
- [108] K. Rezwan, Q. Z. Chen, J. J. Blaker, and A. Roberto, “Biodegradable and bioactive porous polymer / inorganic composite scaffolds for bone tissue engineering,” vol. 27, pp. 3413–3431, 2006.
- [109] Y. W. Gu and Y. Q. Fu, “Heat treatment and thermally induced crystallization of glass for glass ionomer cement,” *Thermochim. Acta*, vol. 423, no. 1–2, pp. 107–112, 2004.

- [110] L. L. Hench, A. E. Clark, and H. F. Schaake, "Effects of microstructure on the radiation stability of amorphous semiconductors," *J. Non. Cryst. Solids*, vol. 8–10, no. C, pp. 837–843, 1972.
- [111] L. L. Hench and H. A. Paschall, "Histochemical responses at a biomaterial's interface," *J. Biomed. Mater. Res. Part A*, vol. 8, no. 3, pp. 49–64, 1974.
- [112] R. H. Doremus, *Glass science*. New York: Wiley, 1994.
- [113] H. Rawson, *Inorganic glass forming systems*. New York: Academic Press, 1967.
- [114] H. A. ElBatal, M. A. Azooz, E. M. A. Khalil, A. Soltan Monem, and Y. M. Hamdy, "Characterization of some bioglass-ceramics," *Mater. Chem. Phys.*, vol. 80, no. 3, pp. 599–609, 2003.
- [115] A. El-Ghannam, E. Hamazawy, and A. Yehia, "Effect of thermal treatment on bioactive glass microstructure, corrosion behavior  $\zeta$  potential, and protein adsorption," *J. Biomed. Mater. Res.*, vol. 55, no. 3, pp. 387–395, 2001.
- [116] O. Peitl, E. Dutra Zanotto, and L. L. Hench, "Highly bioactive P<sub>2</sub>O<sub>5</sub>-Na<sub>2</sub>O-CaO-SiO<sub>2</sub> glass-ceramics," *J. Non. Cryst. Solids*, vol. 292, no. 1–3, pp. 115–126, 2001.
- [117] J. M. Gomez-Vega, E. Saiz, A. P. Tomsia, G. W. Marshall, and S. J. Marshall, "Bioactive glass coatings with hydroxyapatite and Bioglass<sup>®</sup> particles on Ti-based implants. 1. Processing," *Biomaterials*, vol. 21, no. 2, pp. 105–111, 2000.
- [118] F. Barandehfard *et al.*, "The addition of synthesized hydroxyapatite and fluorapatite nanoparticles to a glass-ionomer cement for dental restoration and its effects on

- mechanical properties,” *Ceram. Int.*, vol. 42, no. 15, pp. 17866–17875, 2016.
- [119] K. Fujikura, N. Karpukhina, T. Kasuga, D. S. Brauer, R. G. Hill, and R. V. Law, “Influence of strontium substitution on structure and crystallisation of Bioglass<sup>®</sup> 45S5,” *J. Mater. Chem.*, vol. 22, no. 15, pp. 7395–7402, 2012.
- [120] Höhne, Günther, Hemminger, W. F., Flammersheim, and H.-J., *Differential Scanning Calorimetry*, 2nd ed. Springer-Verlag Berlin Heidelberg, 2003.
- [121] I. Avramov and I. Gutzow, “HEATING RATE AND GLASS TRANSITION TEMPERATURE,” *J. Non. Cryst. Solids*, vol. 104, pp. 148–150, 1988.
- [122] A. L. Patterson, “The Scherrer formula for X-ray particle size determination,” *Phys. Rev.*, vol. 56, pp. 978–982, 1939.
- [123] H. E. Kissinger, “Reaction Kinetics in Differential Thermal Analysis,” *Anal. Chem.*, vol. 29, no. 11, pp. 1702–1706, 1957.
- [124] T. Ozawa, “A New Method of Analyzing Thermogravimetric Data,” *Bull. Chem. Soc. Jpn.*, vol. 38, no. 11, pp. 1881–1886, 1965.
- [125] H. Yinnon and D. R. Uhlmann, “Applications of thermoanalytical techniques to the study of crystallization kinetics in glass-forming liquids, part I: Theory,” *J. Non. Cryst. Solids*, vol. 54, no. 3, pp. 253–275, 1983.
- [126] H. E. Kissinger, “Variation of Peak Temperature With Heating Rate In Differential Thermal Analysis,” vol. 57, no. 4, pp. 217–221, 1956.
- [127] V. C. S. Reynoso, K. Yukimitu, T. Nagami, C. L. Carvalho, J. C. S. Moraes, and E.

- B. Araújo, "Effect of PbS impurity on crystallization mechanism of phosphate glasses studied by differential scanning calorimetry," *Mater. Lett.*, vol. 56, no. 4, pp. 424–428, 2002.
- [128] S. M. OHLBERG and D. W. STRICKLER, "Determination of Percent Crystallinity of Partly Devitrified Glass by X-Ray Diffraction," *J. Am. Ceram. Soc.*, vol. 45, no. 4, pp. 170–171, 1962.
- [129] W. H. Zachariasen, "The atomic arrangement in glass," *J. Am. Chem. Soc.*, vol. 54, no. 10, pp. 3841–3851, 1932.
- [130] K. B. Wilson AD, "A new translucent cement for dentistry. The glass ionomer cement.," *Br Dent J*, vol. 132, pp. 133–135, Feb. 1972.
- [131] J. H. Berg, "Glass ionomer cements," *Pediatr. Dent.*, vol. 24, no. 5, pp. 430–8, 2002.
- [132] J. Berg, *Glass Ionomer Cement*, vol. 5, no. 24. Chicago, IL, USA: Quintessence Publishing Co, 2002.
- [133] J. W. Nicholson, S. J. Hawkins, and J. E. Smith, "The incorporation of hydroxyapatite into glass-polyalkenoate ('glass-ionomer') cements: a preliminary study," *J. Mater. Sci. Mater. Med.*, vol. 4, no. 4, pp. 418–421, 1993.
- [134] S. G. Griffin and R. G. Hill, "Influence of glass composition on the properties of glass polyalkenoate cements. Part I: Influence of aluminium to silicon ratio," *Biomaterials*, vol. 20, no. 17, pp. 1579–1586, 1999.
- [135] S. K. Sidhu and T. F. Watson, "Resin-modified glass ionomer materials. A status

- report for the American Journal of Dentistry.," *Am. J. Dent.*, vol. 8, no. 1, pp. 59–67, 1995.
- [136] A. Wiegand, W. Buchalla, and T. Attin, "Review on fluoride-releasing restorative materials-Fluoride release and uptake characteristics, antibacterial activity and influence on caries formation," *Dent. Mater.*, vol. 23, no. 3, pp. 343–362, 2007.
- [137] L. M. Jonck and C. J. Grobbelaar, "Ionos bone cement (glass-ionomer): An experimental and clinical evaluation in joint replacement," *Clin. Mater.*, vol. 6, no. 4, pp. 323–359, 1990.
- [138] D. Xie, W. A. Brantley, B. M. Culbertson, and G. Wang, "Mechanical properties and microstructures of glass-ionomer cements," *Dent. Mater.*, vol. 16, no. 2, pp. 129–138, 2000.
- [139] U. Lohbauer, R. Frankenberger, A. Clare, A. Petschelt, and P. Greil, "Toughening of dental glass ionomer cements with reactive glass fibres," *Biomaterials*, vol. 25, no. 22, pp. 5217–5225, 2004.
- [140] S. E. Elsaka, I. M. Hamouda, and M. V. Swain, "Titanium dioxide nanoparticles addition to a conventional glass-ionomer restorative: Influence on physical and antibacterial properties," *J. Dent.*, vol. 39, no. 9, pp. 589–598, 2011.
- [141] J. E. Frencken, S. C. Leal, and M. F. Navarro, "Twenty-five-year atraumatic restorative treatment (ART) approach: A comprehensive overview," *Clin. Oral Investig.*, vol. 16, no. 5, pp. 1337–1346, 2012.



- [142] P. K. Vallittu, A. R. Boccaccini, L. Hupa, and D. C. Watts, “Bioactive dental materials — Do they exist and what does bioactivity mean?,” *Dent. Mater.*, vol. 34, no. 5, pp. 693–694, 2018.
- [143] H. Yli-Urpo, L. V. J. Lassila, T. Närhi, and P. K. Vallittu, “Compressive strength and surface characterization of glass ionomer cements modified by particles of bioactive glass,” *Dent. Mater.*, vol. 21, no. 3, pp. 201–209, 2005.
- [144] H. Yli-Urpo, T. Närhi, and E. Söderling, “Antimicrobial effects of glass ionomer cements containing bioactive glass (S53P4) on oral micro-organisms in vitro,” *Acta Odontol. Scand.*, vol. 61, no. 4, pp. 241–246, 2003.
- [145] T. Waltimo, T. J. Brunner, M. Vollenweider, W. J. Stark, and M. Zehnder, “Antimicrobial Effect of Nanometric Bioactive Glass 45S5,” *J. Dent. Res.*, vol. 86, no. 8, pp. 754–757, 2007.
- [146] L. L. Hench and H. A. Paschall, “Direct chemical bond of bioactive glass-ceramic materials to bone and muscle,” *J. Biomed. Mater. Res.*, vol. 7, no. 3, pp. 25–42, Oct. 1973.
- [147] “DENTSPLY Wissenschaftliches Kompendium ChemFil Rock. [www.dentsply.de](http://www.dentsply.de).” .
- [148] T. Kokubo and H. Takadama, “How useful is SBF in predicting in vivo bone bioactivity?,” *Biomaterials*, vol. 27, no. 15, pp. 2907–2915, 2006.
- [149] S. Mitra and B. Kedrowski, . “Long-term mechanical properties of glass ionomers,” *Dent Mater*, vol. 10, no. 2, pp. 78–82, 1994.

- [150] J. W. Nicholson, J. H. Braybrook, and E. A. Wasson, “The biocompatibility of glass-poly(alkenoate) (Glass-Ionomer) cements: A review,” *J. Biomater. Sci. Polym. Ed.*, vol. 2, no. 4, pp. 277–285, 1991.
- [151] B. Brandt, U. Lohbauer, M. Goken, and K. Durst, “The Influence of Particle Size on the Mechanical Properties of Dental Glass Ionomer Cements,” *Adv. Eng. Mater.*, vol. 12, no. 12, pp. 684–689, 2010.
- [152] D. Khvostenko, J. C. Mitchell, T. J. Hilton, J. L. Ferracane, and J. J. Kruzic, “Mechanical performance of novel bioactive glass containing dental restorative composites,” *Dent. Mater.*, vol. 29, no. 11, pp. 1139–1148, 2013.
- [153] S. Tkachenko *et al.*, “Strength and fracture mechanism of iron reinforced tricalcium phosphate cermet fabricated by spark plasma sintering,” *J. Mech. Behav. Biomed. Mater.*, vol. 81, pp. 16–25, 2018.
- [154] R. W. Hertzberg, R. P. Vinci, and J. L. Hertzberg, *Deformation and fracture mechanics of engineering materials*, vol. 89. Wiley New York, 1996.
- [155] C. Shuai, J. Zhou, D. Gao, C. Gao, P. Feng, and S. Peng, “Functionalization of calcium sulfate/bioglass scaffolds with zinc oxide whisker,” *Molecules*, vol. 21, no. 3, pp. 1–11, 2016.
- [156] X. Chen *et al.*, “Synthesis and characteristics of monticellite bioactive ceramic,” *J. Mater. Sci. Mater. Med.*, vol. 19, no. 3, pp. 1257–1263, 2008.
- [157] W. Zhao and J. Chang, “Sol – gel synthesis and in vitro bioactivity of tricalcium

- silicate powders,” *Mater. Lett.*, vol. 58, no. 19, pp. 2350–2353, 2004.
- [158] F. O. Gomes, R. A. Pires, and R. L. Reis, “Aluminum-free glass-ionomer bone cements with enhanced bioactivity and biodegradability,” *Mater. Sci. Eng. C*, vol. 33, no. 3, pp. 1361–1370, 2013.
- [159] C. Wang, Y. Xie, A. Li, H. Shen, D. Wu, and D. Qiu, “Bioactive nanoparticle through postmodification of colloidal silica,” *ACS Appl. Mater. Interfaces*, vol. 6, no. 7, pp. 4935–4939, 2014.
- [160] A. Aminian *et al.*, “Synthesis of silicon-substituted hydroxyapatite by a hydrothermal method with two different phosphorous sources,” *Ceram. Int.*, vol. 37, no. 4, pp. 1219–1229, 2011.
- [161] A. Ślósarczyk, Z. Paszkiewicz, and C. Paluszkiwicz, “FTIR and XRD evaluation of carbonated hydroxyapatite powders synthesized by wet methods,” *J. Mol. Struct.*, vol. 744–747, no. SPEC. ISS., pp. 657–661, 2005.
- [162] S. Sarig, “Aspartic acid nucleates the apatite crystallites of bone: A hypothesis,” *Bone*, vol. 35, no. 1, pp. 108–113, Jul. 2004.
- [163] G. Mount, “Making the most of glass ionomer cements: 1.,” *Dent. Update*, vol. 18, no. 7, pp. 276–9, 1991.
- [164] L. Kiri and D. Boyd, “Predicting composition-property relationships for glass ionomer cements: A multifactor central composite approach to material optimization,” *J. Mech. Behav. Biomed. Mater.*, vol. 46, pp. 285–291, 2015.

- [165] I. M. Brook and P. V. Hatton, "Glass-ionomers: Bioactive implant materials," *Biomaterials*, vol. 19, no. 6, pp. 565–571, 1998.
- [166] A. Moshaverinia, N. Roohpour, J. A. Darr, and I. U. Rehman, "Synthesis and characterization of a novel N-vinylcaprolactam-containing acrylic acid terpolymer for applications in glass-ionomer dental cements," *Acta Biomater.*, vol. 5, no. 6, pp. 2101–2108, 2009.
- [167] E. A. Wasson and J. W. Nicholson, "Studies on the setting chemistry of glass-ionomer cements," *Clin. Mater.*, vol. 7, no. 4, pp. 289–293, 1991.
- [168] J. W. Nicholson, "Chemistry of glass-ionomer cements: A review," *Biomaterials*, vol. 19, no. 6, pp. 485–494, 1998.
- [169] A. C. A. Wan, A. U. J. Yap, and G. W. Hastings, "Acid – Base Complex Reactions in Resin-Modified and Conventional Glass Ionomer Cements," *J. Biomed. Mater. Res.*, vol. 119260, pp. 700–704, 1999.
- [170] S. Matsuya, T. Maeda, and M. Ohta, "IR and NMR Analyses of Hardening and Maturation of Glass-ionomer Cement," *J. Dent. Res.*, vol. 75, no. 12, pp. 1920–1927, 1996.
- [171] E. Bresciani, T. Barata, T. C. Fagundes, A. Adachi, M. M. Terrin, and M. F. Navarro, "Compressive and diametral tensile strength of glass ionomer cements," *J. Minim. Interv. Dent.*, vol. 1, no. 2, pp. 102–111, 2008.
- [172] S. Tkachenko *et al.*, "Strength and fracture mechanism of iron reinforced tricalcium phosphate cermet fabricated by spark plasma sintering," *J. Mech. Behav. Biomed.*

*Mater.*, vol. 81, pp. 16–25, 2018.

- [173] M. A. McKenzie, R. W. A. Linden, and J. W. Nicholson, “The physical properties of conventional and resin-modified glass-ionomer dental cements stored in saliva, proprietary acidic beverages, saline and water,” *Biomaterials*, vol. 24, no. 22, pp. 4063–4069, 2003.
- [174] B. Dickey, R. Price, and D. Boyd, “Evidence of a complex species controlling the setting reaction of glass ionomer cements,” *Dent. Mater.*, vol. 32, no. 4, pp. 596–605, 2016.
- [175] G. J. Pearson, “Effect of ultrasound on the setting characteristics of glass ionomer cements studied by Fourier Transform Infrared Spectroscopy,” *J. Mater. Sci. Mater. Med.*, pp. 405–411, 2009.
- [176] D. F. Williams, *Definitions in biomaterials*, vol. 4. Amsterdam: Elsevier Science Limited, 1987.

## Appendix A

Parts of the preliminary results of Chapters 3 and 4 of this research have been accepted as extended abstracts in the following conferences:

1. A. Zandi Karimi, and R. A.L. Drew, "Compressive strength of glass-ionomer cements containing 45S5 Bioglass<sup>®</sup>-ceramic", The 27<sup>th</sup> Canadian Materials Science Conference (CMSC), Dalhousie University, Halifax, Canada, June 2015.

2. A. Zandi Karimi, and R. A.L. Drew, " Effects of incorporation of partially crystallized 45S5 Bioglass<sup>®</sup> on glass-ionomer Cements (GIC)", The 40<sup>th</sup> International Conference and Exposition on Advanced Ceramics and Composites (ICACC), ACerS, Daytona Beach, Florida, USA, Jan 2016.